Project Number:	720270	Project Title:	Human Brain Project SGA1

Document Title:	D4.7.2 - Theoretical Neuroscience – Results for SGA1 Period 2
Document Filename:	D4.7.2 (D25.2 D33) SGA1 M24 ACCEPTED 180907
Deliverable Number:	SGA1 D4.7.2
Deliverable Type:	Report
Work Package(s):	WPs 4.1, 4.2, 4.3, 4.4, 4.5
Dissemination Level:	PU = Public
Planned Delivery Date:	SGA1 M30 / 30 March 2018
Actual Delivery Date:	RESUBMITTED: 25 July 2018 with new Addendum, accepted 7 Sep 2018

Abstract:	This deliverable is the annual compound of HBP deliveries and results (outputs and outcomes) from Sub-Project SP4 – Theoretical Neuroscience. The live complete catalogue of HBP deliveries is accessible on-line from the HBP model catalog app. The main deliveries from April-2017 to March-2018 have been: Models and softwares
Keywords:	Theoretical neuroscience models

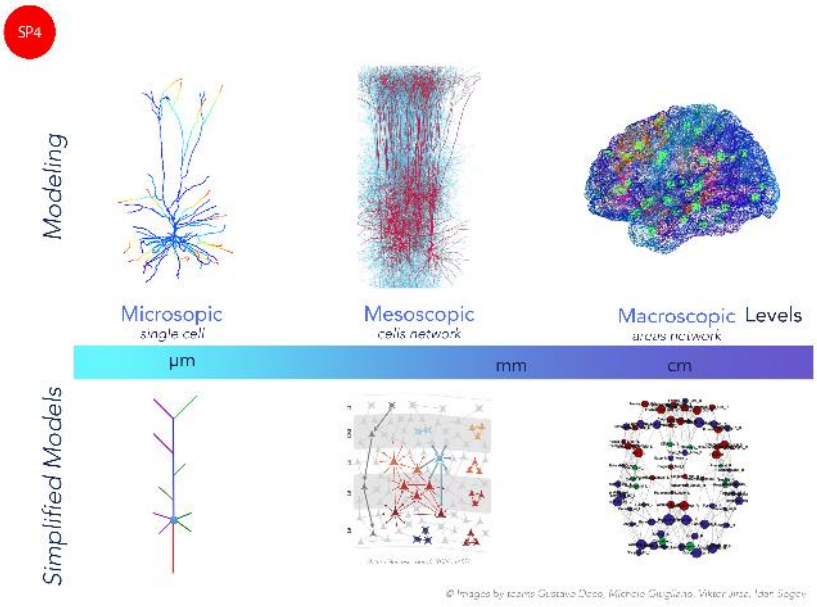

Figure 1 HBP SP4 theoretical neuroscientists' models investigate all scales of the brain

Authors:	Alain DESTEXHE, CNRS (P10)
Compiling Editors:	Morgane BOURDONNAIS, CNRS (P10) Katherine FREGNAC, CNRS (P10)
Contributors:	Neil BURGESS, UCL (P82) Marc DE KAMPS, ULEEDS (P104) Gustavo DECO, UPF (P77) Alain DESTEXHE, CNRS (P10) Markus DIESMANN, JUELICH (P20) Gaute EINEVOLL, NMBU (P44) Olivier Faugeras, INRIA (P33) Wulfram GERSTNER, EPFL (P1) Michele GIUGLIANO, UA (P80) Sonja GRÜN, JUELICH (P20) André GRÜNING, SURREY (P102) Jeanette HELGREN KOTALESKI, KTH (P39) Viktor JIRSA, AMU (P78) Marja-Leena LINNE, TUT (P103) Olivier MARRE, UPMC (P105) Idan SEGEV, HUJI (P60) Walter Senn, UBERN (P71) Misha TSODYKS, WEIZMANN (P84) Shimon ULLMAN, WEIZMANN (P84)

Table of Contents

List of Figures

1. Introduction

SP4 occupies an important position in the HBP, bridging experimental neuroscience with the platforms, where SP4 serves as a "first user". SP4 formulates theoretical and computational models from the biological principles, and implements these models in the HBP platforms, thus bridging biology and technology. One of the main goals of SP4 is to contribute models to understand key aspects of brain function, which requires investigation at different scales, as detailed in all of SP4 work.

At the cellular level, the goal is to understand how single neurons (and their dendrites) process synaptic inputs, and to generate simplified models of those. Such simplified models can be implemented in HBP platforms, typically neuromorphic circuits. At larger scales, such as circuits, population-level or the whole-brain, the goal is to understand how neuronal properties combine with specific patterns of connectivity to account for collective behavior of neuronal populations. Models are designed in SP4 for each one of these levels. This also includes the genesis of models of the different brain signals recorded experimentally, such as single units, local field potentials, voltage-sensitive dye up to electroencephalogram (EEG) or magnetoencephalogram (MEG) recordings. This modeling of brain signals connects naturally to the different levels of modeling, and is thus multiscale, but most importantly, it provides an important bridge to experimental data. The comparison between models and experimental data is a priority for SP4, and is at the heart of most of our computational models.

SP4 also investigates a number of brain mechanisms and key cognitive processes. The study of synaptic plasticity and its integration in computational models is central to understand how networks of neurons can learn and adapt to the changing environment. Plasticity can also lead to the emergence of various network phenomena, which are under study in SP4. The recent success of deep learning techniques is also a motivation for such studies, which could contribute to the design of biologically plausible deep learning strategies and models. Such models are also aimed at being implemented on HBP platforms, and SP4 plays a key role in the perspective of implementing learning strategies on neuromorphic computers.

Finally, SP4 aims at contributing to understanding of key cognitive processes, such as vision, sensorimotor coordination, and spatial navigation as examples. Here, computational models are designed with very specific sensory- or motor-driven goals, and such models naturally connect to different HBP platforms, such as neuro-robotics or neuro-informatics. The design of whole-brain models of the mouse, and later for the human brain, will also provide knowledge important to the understanding of normal brain activity, as well as various brain pathologies. This research thus naturally connects to the medical informatics platform, and we expect such connections to grow in the next years with the maturation of our computational models.

In the second year of SGA1, SP4 had the important objective of implementing nearly all of its models to the HBP platforms. The different models developed in this period, as well as their platform implementation, are described here, successively for each task, starting from the cellular level, circuits, networks, up to whole-brain levels.

2. Results

2.1 Bridging scales (WP 4.1)

2.1.1 Simplified models of neurons (T4.1.1)

The major task of the HUJI partner is to develop a systematic, analytical, (and public domain) method for reducing complex neuron model into simplified models, while preserving the I/O properties of the full model and saving significant computational time and memory. In the previous period we have developed such a method (schematically represented in Figure 2). The reduction method starts with the passive “skeleton” of a detailed model (Figure 2A and explained in the respective legend). In this period, we have expended the model to include NMDA spike – which typically occur at distal dendritic branches of cortical pyramidal cells. We have generated refined

models of the NMDA-spike based on recent experiments (Figure 3) and examined the impact of local dendritic inhibition on the NMDA-spike as well as on the neuron's spiking output (Figure 4).

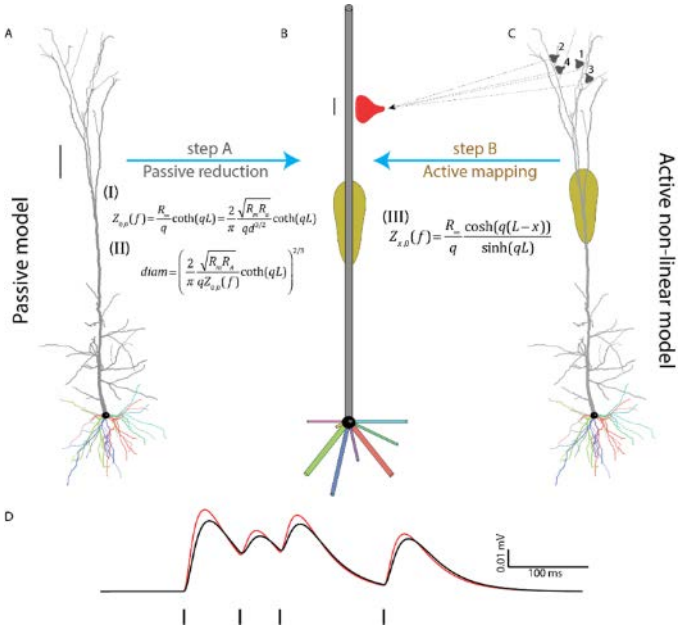

Figure 2 An analytic reduction scheme for reducing neuron model complexity (NeuronReduce).

A. Detailed passive model of 3D reconstructed L5 pyramidal cell from the rat neocortex. B. Each stem dendrite in the full model is reduced to a single cylinder that preserves the specific cable properties (R_m, C_m and R_i) of the original tree. The diameter and length of the respective cylinders are computed analytically such that they preserve both the transfer resistance from the most distal dendritic tip to the soma ($Z_{L,0}$) as well the input resistance ($Z_{0,0}$) at the soma end of the corresponding stem dendrite. C. Synapses (black numbered triangles on the full tree) all with identical transfer resistance to the soma, $Z_{x,0}$; they are all mapped to the respective reduced cylinder so that $Z_{x,0}$ is preserved in the two models. In the reduced model, these synapses are merged into one "Neuron" process (red synapses in B). The same mapping holds also for active conductances (schematic yellow region). D. Comparison of the composite somatic EPSP resulting from sequential activation of the four synapses shown in C for the full model (black trace) and the reduce model (red trace). The synapses were activated in temporal order 1, 2, 3, 4. Modified from Eyal et al., (in preparation)

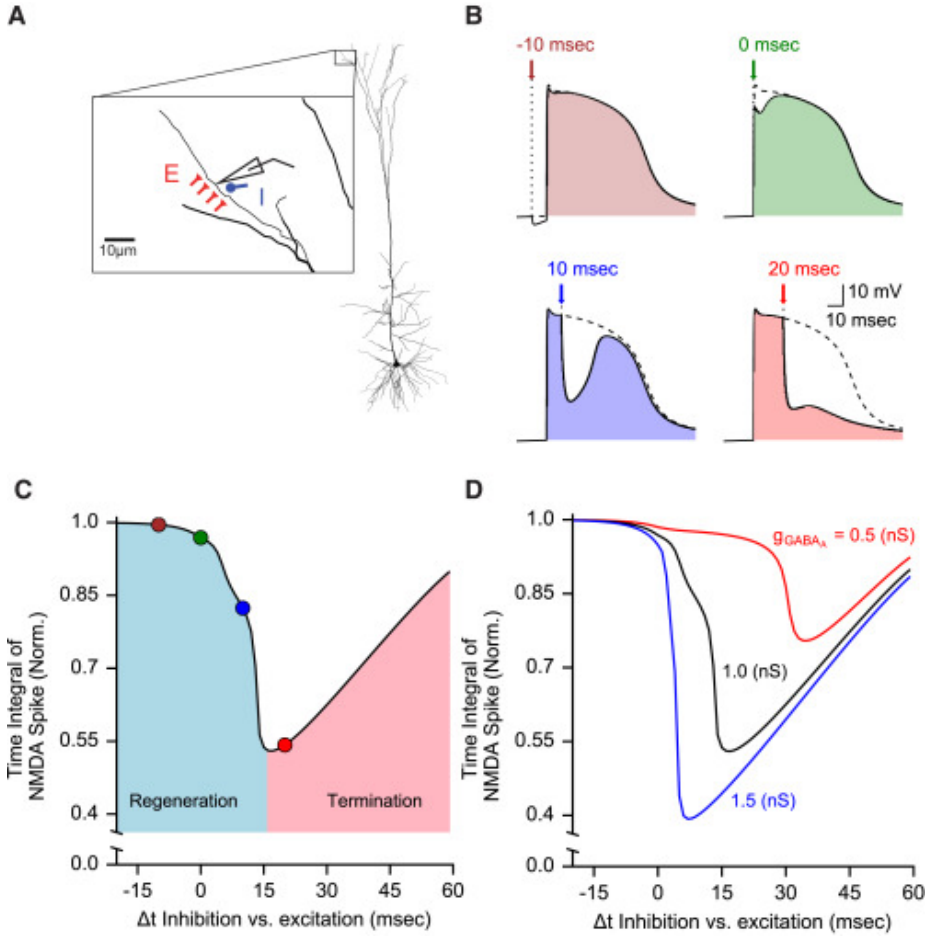

Figure 3 Dendritic NMDA spikes are susceptible to timed synaptic inhibition.

(A) Reconstructed L5 pyramidal neuron model. Twenty synchronously activated AMPA- and NMDA-based excitatory synapses (red) and a single GABAA synapse (blue) were distributed around the center of a distal apical dendritic branch from which the membrane voltage was recorded (schematic electrode). (B) NMDA spikes generated in the modeled dendritic branch shown in (A); arrows point to the inhibition activation time. NMDA spike in the presence of inhibition (colored area); dashed trace without inhibition. (C) Normalized time integral of the NMDA spike for different activation times of the inhibitory synapse (the "vulnerability function"). Colored dots on the black curve correspond to the respective traces in (B). The blue and red areas respectively denote the regeneration and termination phases of the NMDA spike. (D). As in (C), with different GABAA peak conductance values.

In addition to highlighting the impact of inhibition on the local NMDA spike we also explored the effect of inhibition on the global output of the cell; this is exemplified in Figure 4 below.

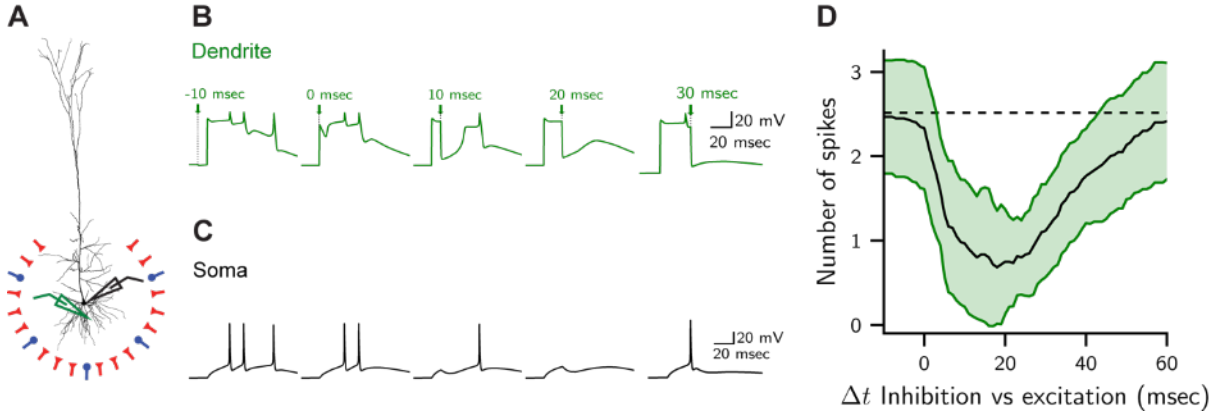

Figure 4 Interaction of timed dendritic inhibition with dendritic NMDA spikes finely modulates the neuron's output.

(A) Sixteen basal dendritic terminals synchronously activated, each by 20 excitatory and 2 inhibitory synapses. Voltage was recorded from the soma (black electrode) and from one of the activated branches (green electrode). (B) Local NMDA spike modulated by local timed inhibition. Arrows indicate the timing of inhibition with respect to excitation. Voltage was recorded from the green electrode in (A)). (C) Somatic spikes for the respective cases shown in (B). (D) Mean (black line) and standard deviation (green lines) of 60 possible combinations of 16 activated terminal basal branches as in (C). The dashed line is the average number of spikes in the control condition without inhibition.

Contributions to platforms

The new work on the NMDA spike (nonlinear dendritic properties) and its control by dendritic inhibition, adds a significant facet to our understanding of the I/O properties of neurons and provide principles for how to incorporate the interaction between dendritic excitability and synaptic inhibition. These principles will be next used for incorporating NMDA-spikes intoi Neuron_Reduce (Figure 4 above). This advanced reduced neuron models, in luding 3-types of spikes (NMDA, Ca and Na – dependent spikes) will serve in SP6 as building block for large scale network simulations and in SP9 for reduced Neuromorphic neurons.

Publications

Guy Eyal, Oren Amsalem, Noa Rogozinski and Idan Segev. NeuronReduce: An accurate and computationally-efficient analytical method for reducing complex neuron models (in preparation).

Doron M, Chindemi G, Muller E, Markram H, Segev I (2017). Timed Synaptic Inhibition Shapes NMDA Spikes, Influencing Local Dendritic Processing and Global I/O Properties of Cortical Neurons, Cell Reports, Nov 7;21(6):1550-1561. doi: 10.1016/j.celrep.2017.10.035.

Component Dependencies

Summarized links to components this key result depends on.

Component ID	Component Name	HBP Internal	Comment
959	*3D reconstructions of 200 cells in human neocortex (temporal, cingulate and frontal)*	*Yes*	*This morphological data on human cells served for the basis on modelling on human neurons*
955	*3D reconstructions of 300 pyramidal neurons from the mouse somatosensory cortex across layers II-IV*	*Yes*	*This morphological data on mouse cells served for the basis on modelling on mouse neurons*
1729	*Comparative physiology of Mouse and human*	yes	*The data on excitatory synapses is used for developing the reduced model (merging synapses)*
1730	*Comparative physiology of mouse and human neocortical pyramidal neurons and interneurons*	yes	This data is used to reduce model complexity of both human and mouse cortical neuron
759	*Morphological and physiological data from the same neurons in adult human*	yes	This data is used to first build detailed model of adult human neurons which are then used by the Neuron_reduce algorithm
757	*Morphological and physiological data from the same neurons in adult mouse*	*yes*	*This data is used to first build detailed model of adult mouse neurons which are the used by the Neuron_reduce algorithm*

84	*Detailed models of human cortical neurons*	*yes*	*These models of human neurons are used to reduce model complexity*

2.1.2 Simplified model of dendritic integration under in vivo conditions (T4.1.1)

This model, developed at the UNIC, is a continuation of the model reported last year which is aimed at understanding dendritic integration in neurons with nonlinear excitable dendrites.

Achieved Impact

We considered the case of dendrites endowed with Na spikes, as shown experimentally by recent in vivo work. We designed a multi-compartmental model where dendritic excitability was modelled by the AdEx mechanism, while in vivo conditions were simulated by correlated synaptic activity. We systematically compared the firing responses of three models: point neuron, neuron with passive dendrite and neuron with active dendrite [Figure 5].

In this comparison, we adjusted the output firing rate to be in the same range of values for all three models. We checked the responses for different input firing rates, refractory periods and synaptic weights. The neuron with active dendrite was predominantly processing synaptic correlation inversely compared to neurons with passive dendrites and to point neurons.

To check how biologically realistic are the firing rate responses to correlated synaptic activity for multicompartmental AdEx model, we compared these simulations to a Hodgkin-Huxley model [Figure 6].

We used the same morphology as for the multicompartmental AdEx model. To make our model more biologically realistic we also adjusted its morphology by tapering a dendrite, such that the EPSPs at soma, and local EPSPs as a function of distance from soma are now in the range of values measured experimentally.

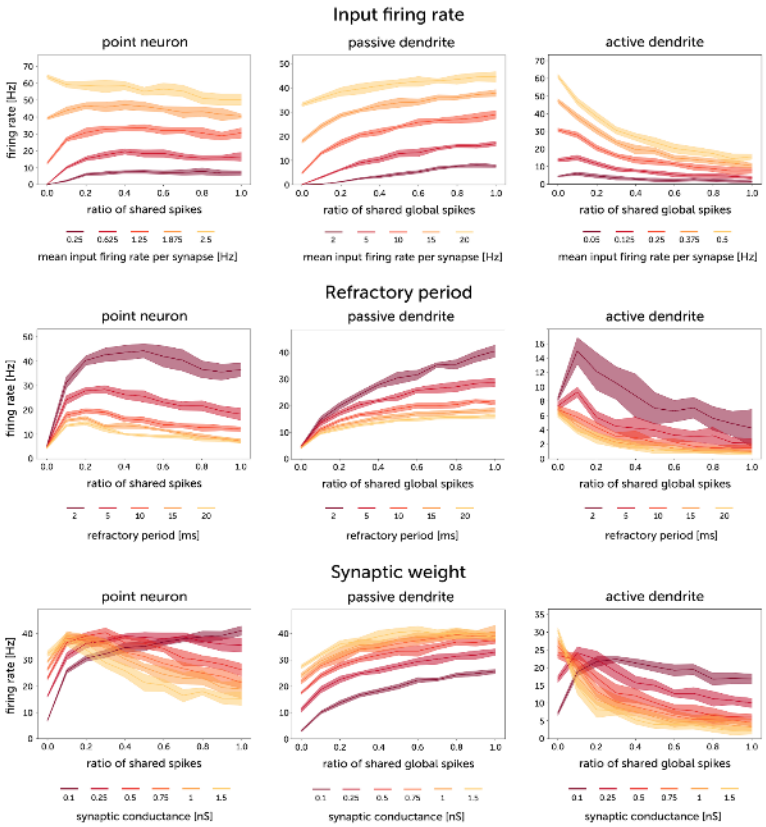

Figure 5 input for three different AdEx models.

The three models shown are the point neuron model (left), a neuron with passive dendrite (middle), and a neuron with active dendrite (right). We compared the responses of models for different input firing rates (first row), for different refractory periods (second row) and for different synaptic weights (third row).

In Fig. 6 we can see propagations and collisions of sodium dendritic spikes in the Hodgkin-Huxley model. Increasing the density of voltage-dependent ion channels in the dendrite changed the somatic firing rate response to correlation of synaptic input. For low densities of voltage-dependent channels, the response to correlation was mainly positive, but for higher densities the response became inverse [Figure 7].

This behavior of the Hodgkin-Huxley model is in accordance with the behavior of simpler multicompartmental AdEx models. This shows that inverse processing of correlation can be present independently on the type of model, and is a consequence of the presence of excitable dendrites. more realistic models

Figure 6 Propagation and collision of dendritic spikes in a Hodgkin-Huxley model of a dendrite.

(a) Sodium spike is created near the center of dendrite and propagates toward soma and distal dendritic end. (b) The correlated synaptic bombardment (c_G = 0.1, τ_j = 5 ms) creates two sodium spikes (600 μm and 1200 μm from soma) which

wavefronts collide and cancel due to refractory period.

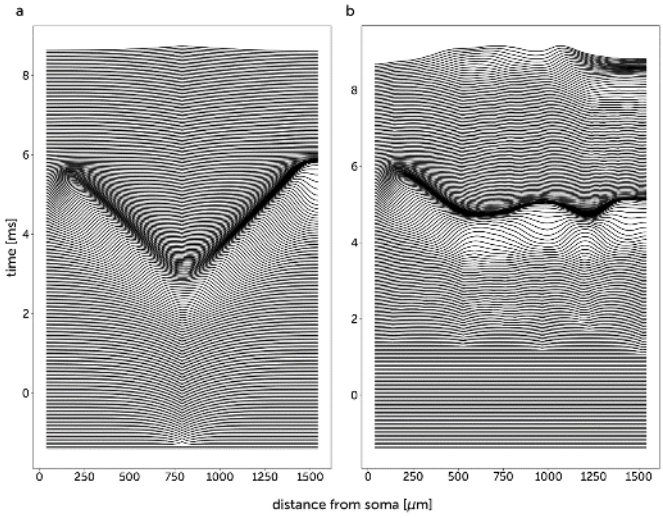

Figure 7 Somatic firing rate responses to correlated synaptic activity for Hodgkin-Huxley model of neuron with dendrite with synapses of weights: 0.5 nS and 1.5 nS.

First row : The responses of the neuron for different densities of fast sodium and potassium channels in dendrite. While changing dendritic densities the somatic densities were left unchanged (12 mS/cm2 for Na conductance and 7 mS/cm2 for K conductance).

Second row : The responses of the neuron with active dendrite for different input firing rates.

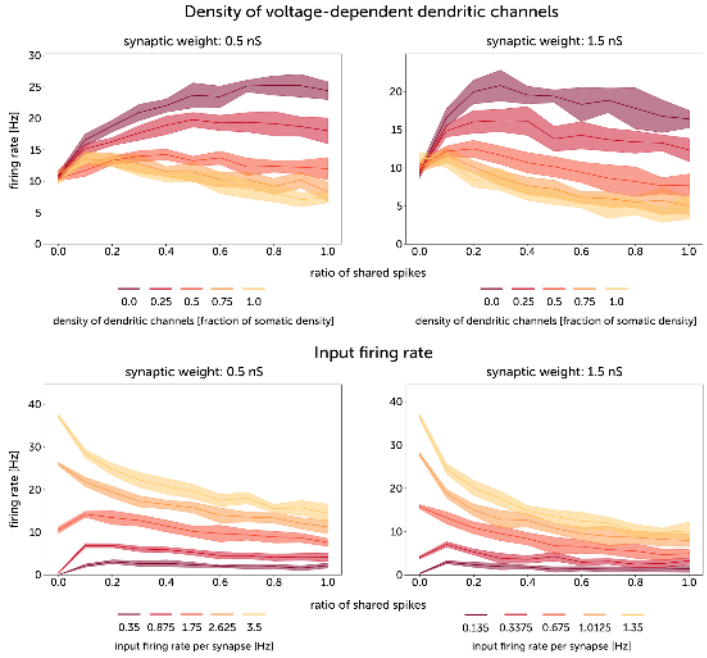

Contributions to platforms

Our model is now accessible in the HBP Collaboratory for further testing and usage. The multi-compartmental AdEx neuron is also in principle implementable on the BRAINSCALES neuromorphic hardware developed by Heidelberg University and Dresden University within the SP9 platform.

Publications

Górski T, Veltz R, Galtier M, Fragnaud H, Goldman J, Teleńczuk B and Destexhe A. (2017) Sodium spikes endow dendrites with inverse firing rate response to correlated synaptic activity. (under review)

bioRxiv preprint: https://www.biorxiv.org/content/early/2017/05/14/137984

Conclusion & Outlook

This study shows that different models of nonlinear excitable dendrites can lead to inverse correlation processing in neurons. This was seen in the Hodgkin-Huxley model, as well as in a simpler model, where dendritic excitability was accounted by the AdEx model. In all cases, the propagation of dendritic spikes and their collision is responsible for the observed effect.

In the future, we would like to extend this model by considering network simulations of neurons endowed with such inverse correlation dependence. Here, the neuromorphic platform may turn to be a very efficient tool to perform such network simulations. This work is planned in SGA2.

Component Dependencies

Summarized links to components this key result depends on.

Component ID	Component Name	HBP Internal	Comment
N/A	N/A	*N/A*	*N/A*

2.1.3 Discrete model of dendritic spike propagation in dendrites (T4.1.1 - T4.1.3)

Description of the model

T.4.1.3 "*Mean-field models of interacting spiking neurons with dendritic compartment ", prelude a un model mean-field.*

The INRIA partner has worked on a simplified description of the propagation of dendritic spikes in dendrite under the assumption that whenever two such spikes collide, they annihilate. Indeed, a detailed model was studied in [Gorski *et al.* 2017] but it is very computationally expensive and too detailed to be (easily) incorporated in a neural network.

Hence, we designed a mathematical model, called *discrete-state model*, aiming at grasping the core mechanisms of spike propagation / annihilation. The simulation is exact in that it is not based on a (time) discretization of the propagation of dendritic fronts. Finally, it allows to see whether the annihilation of spikes is enough to explain decrease of mean somatic spikes number.

More precisely, suppose that we are given a set of spatio-temporal synaptic inputs $S = \{(t_i, x_i)\}_{i=1}^{N}$ and assume that each input (t_i, x_i) produces two contra-propagating fronts (*e.g.* dendritic spikes). Starting from s, we build the set of fronts and annihilation events recursively. The complexity is $O(N \log(N))$ whereas the cost of adding a dendritic spike is $O(\log(N))$ making it suitable for incorporation in a network of spiking neurons with dendritic compartments (preliminary work has been done toward this end).

In Figure 8, the synaptic inputs are the blue dots and the lines, the propagating fronts. It shows the networks of propagating fronts for different propagating speeds but same inputs s drawn from a realistic distribution. One can see that increasing speed increases the dendritic spikes reaching the soma ($x = 0$). Intuitively, this occurs because a front has less chance to meet another front for higher propagation speeds. Finally, in Figure 9, we present the dependency of the mean number of spikes reaching the soma as a function of the ratio of shared spikes. In this scenario, each synaptic input triggers a dendritic spike, so the results correspond to the case of large synaptic weights of the multi-compartmental AdEx model, see [Gorski *etal.* 2017].

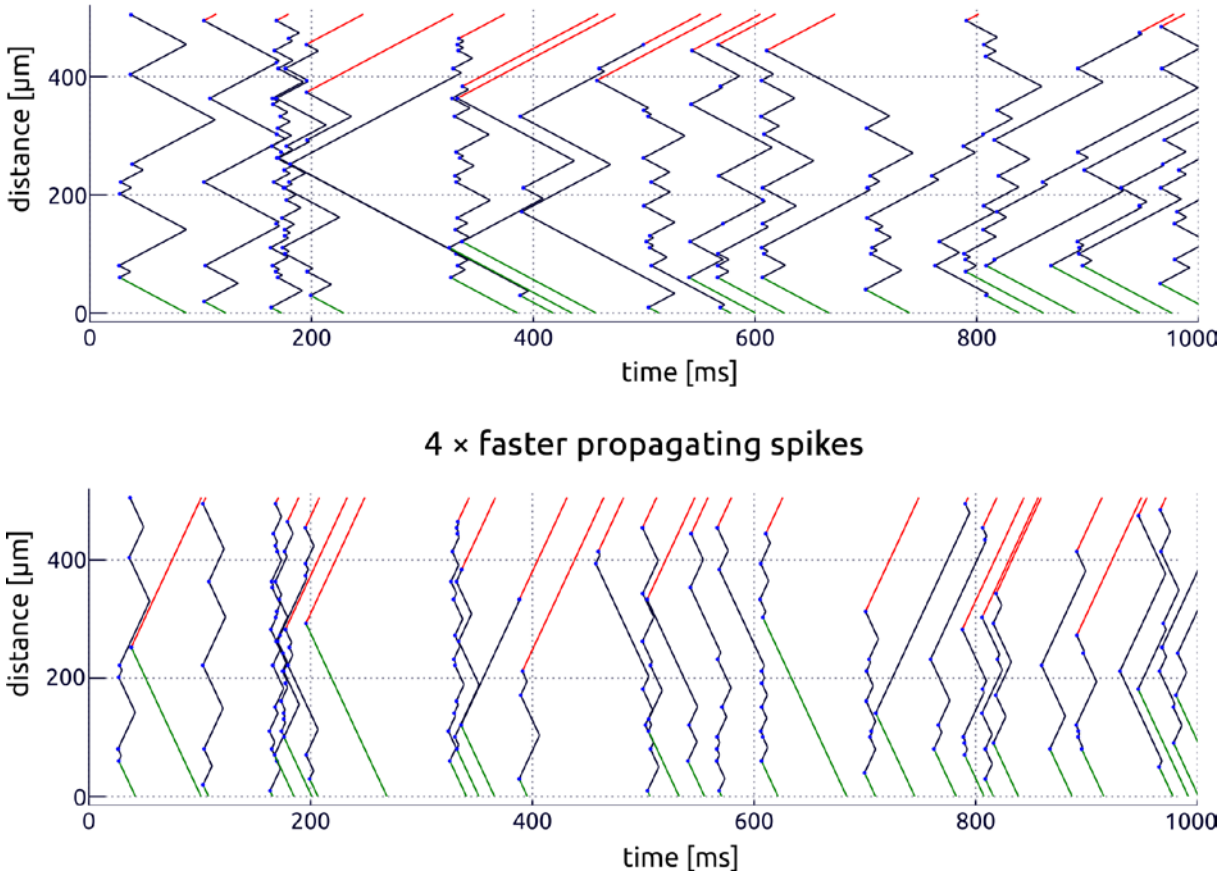

Figure 8

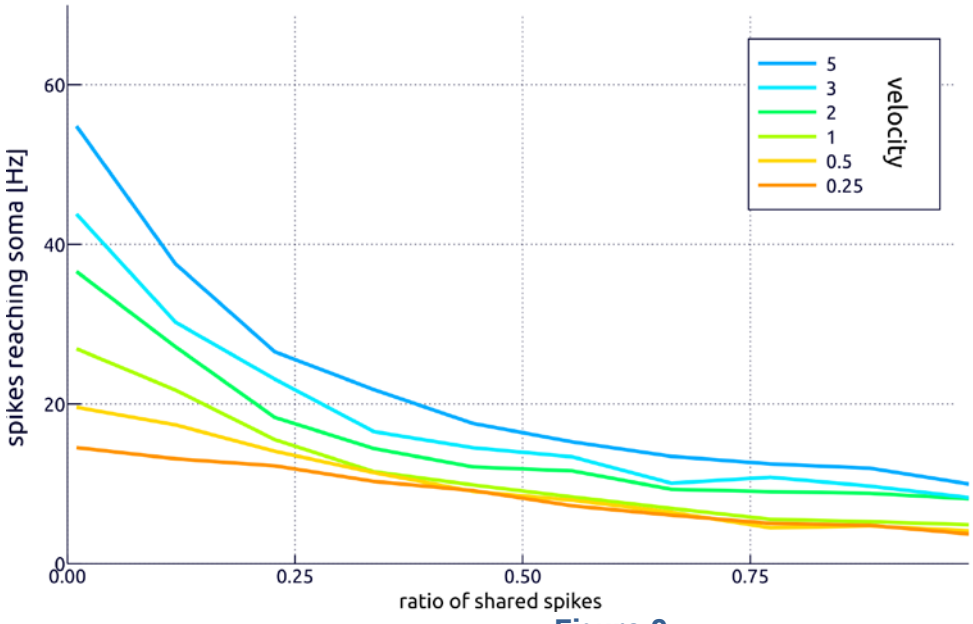

Figure 9

Publications

Gorski Tomasz, Veltz Romain, Galtier Mathieu , Fragnaud Hélissande, Goldman Jennifer , Teleńczuk Bartosz , Destexhe Alain (2017)

Achieved Impact

This model is now continued in different directions, including its incorporation into a network of spiking neurons, and extending its biological relevance without sacrifying simplicity.

Component Dependencies

Summarized links to components this key result depends on.

Component ID	Component Name	HBP Internal	Comment
N/A	Simplified model of dendritic integration under in vivo conditions	*Yes*	*Used to build a simplified model to study the effects of the parameters on the average dendritic spikes number*

2.1.4 Information encoding in Reconstructed Human Neurons (T4.1.2)

Description of the model

The UA partner has collaborated with Dr. H. Mansvelder (SP1) and received 50 3-dimensional morphological reconstructions of L2/3 cortical pyramidal neurons. Morphologies were obtained from resective neurosurgery in T1.2.2, 2.2.2, and 2.2.6, and were used by UA to build conductance-based spiking neuron models. Models were simulated using NEURON (Carnevale and Hines, 2006) and probed for their dynamical transfer properties, as in the experiments of Köndgen et al. (2008) and Testa-Silva et al., (2014) (but see also Linaro et al., 2017). Briefly, sinusoidally oscillating input currents were injected in the soma, allowing us to temporally modulate the instantaneous output firing rate of the model and quantify its output 'transfer gain' (Figure 10a, inset). When studied in this way, the neuronal transfer properties resemble those of electronic filters, whose low-pass performances in the Fourier domain (Figure 10a) define how fast can they encode inputs. We also systematically measured AP slope at its onset (Figure 10b)

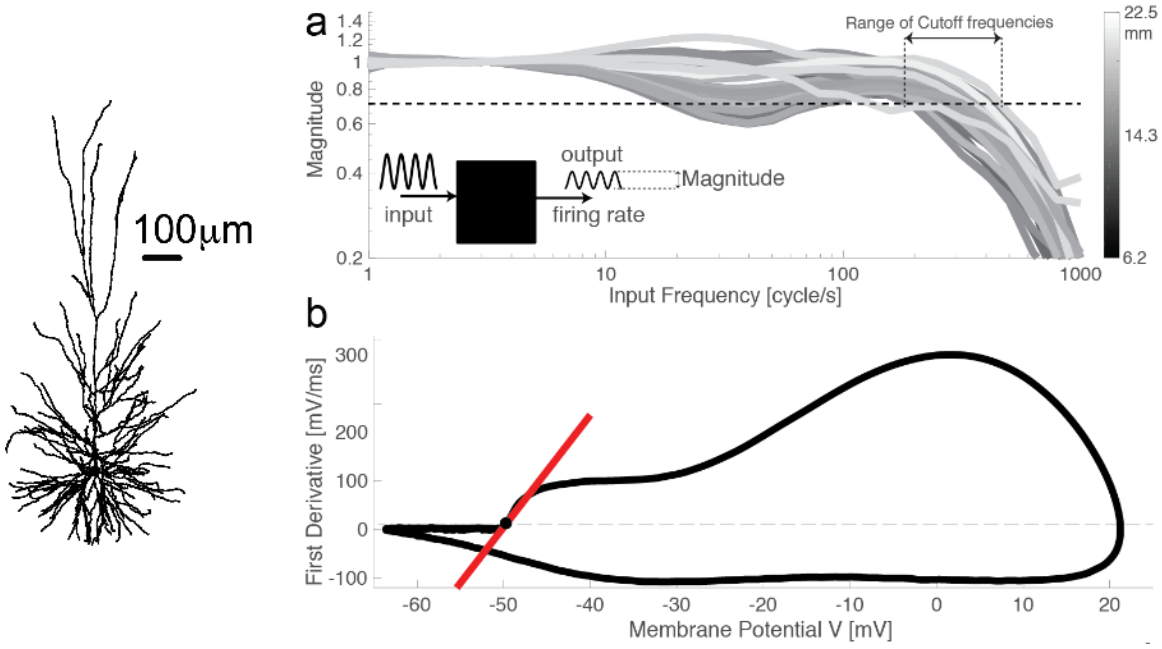

Figure 10 Reconstructed human cortical cells (left) display very broad bandwidth, when probed as transfer information channels.

We asked whether the total dendritic length played any role, in terms of those biophysical properties potentially relevant for information processing and cognition. HUJI (Etay et al. 2014) in fact previously suggested in silico that the size of dendrite migth be responsible for the enhanced encoding capability (Testa-Silva et al., 2014). We found that i) the total dendritic length is sufficient to justify a broader bandwidth of neuronal dynamical transfer properties, as there is a significant direct correlation (Pearson's r = 0.4, p < 0.01) between the "cutoff frequency" and the dendritic length (Figure 10b); ii) the total dendritic length is sufficient to justify a "kinkier" AP in the model, as there is a very significant direct correlation (Pearson's r = 0.55, p < 0.0005) between the "phase slope" of AP shape and the dendritic length (Figure 11c); iii) larger neurons track better rapidly changing temporal information, when compared to smaller cells - for the exact same input (Figure 11d);

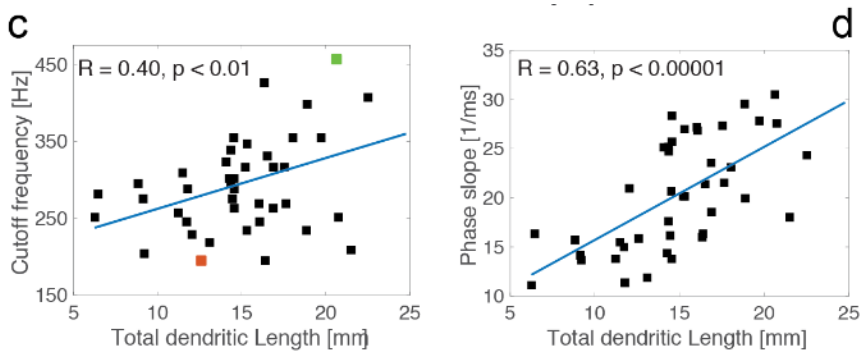

Figure 11 Both the bandwidth (quantified as its cutoff frequency) and the AP onset velocity significantly correlated to the dendrite total length, as predicted by the theory developed by HUJI.

Dynamical transfer properties. The dynamical transfer properties of each model neuron were probed by emulating a somatic time-varying input current injection, as in the experiments of Köndgen *et al.* (2008) (see also Linaro *et al.*, 2017). This allowed us to temporally modulate the instantaneous output firing rate of each model neuron and quantify the output 'transfer gain' (or the normalized 'response magnitude') of the cell, at each Fourier frequency component of the input (Figure 10a, inset). Briefly, rapidly varying sinusoidal inputs, with amplitude I_1 and frequency F (1–1'000 cycle/s) were injected simultaneously to a DC baseline I_0 and a randomly fluctuating waveform:

$$I(t) = I_0 + I_1 \sin(2\pi F\, t) + I_{noise}(t) \quad (1)$$

$I_{noise}(t)$ was synthesized as an exponentially filtered realization of a Gaussian white-noise process, to mimic at the soma a barrage of balanced background excitatory and inhibitory irregular synaptic inputs (Arsiero *et al.*, 2007): *it* had zero-mean, variance s^2 and correlation length τ_I = 5 ms, and was generated iterating the following expression,

$$I_{noise}(t + dt) = (1 - dt/\tau_I) I_{noise}(t) + s\sqrt{2dt/\tau_I}\,\xi_t \quad (2)$$

where $\{\xi_t\}$ is a sequence of independent pseudo-random numbers, with Gaussian distribution (Press et al., 2007). The variance s^2 of the fluctuating component was chosen by hyperpolarizing the membrane of each model cell at -75mV and iteratively searching (by the *regula falsi* algorithm; Press *et al.*, 2007) for the value of s that resulted in subthreshold membrane potential fluctuations of ~3mV. After s was fixed, the DC baseline I_0 was chosen iteratively by the same strategy to lead, at *F = 0 cycle/s*, to a mean firing rate of ~10 spike/s. Such an iterative algorithmic parameters search replaced the preliminary characterisation of the model's stationary *F-I* curve, required to elect the 'working point' for probing the dynamical response properties. I_1 was chosen as 1/6 of I_0 and each stimulation lasted 120 s.

The firing times $\{t_k\}$ were measured at the soma and collected for each model neuron across all values of *F*. The output 'transfer gain' (or the normalized 'response magnitude') at each frequency *F* was computed by taking the magnitude of the following complex number

$$r_1(F) = abs\{\sum_{j=1}^{N} \exp(j2\pi F t_k)\}/N \quad (3)$$

where N is the number of spikes and j is the imaginary unit. This was further normalised to the $r_1(F_0)$, with $F_0 = 3$ cycle/s. The cutoff was finally defined as the highest frequency F_c at which $r_1(F_c) = r_1(F_0)/\sqrt{2}$ (Figure 10a).

Achieved Impact

See 2.5.1 ***The impact of Axon Initial Segment on Information encoding (T4.1.2)***

Component Dependencies

Summarized links to components this key result depends on.

Component ID	Component Name	HBP Internal	Comment
759	*Morphological and physiological data from the same neurons in adult mouse*	*Yes*	*Data provided was necessary for model building*

2.1.5 The impact of Axon Initial Segment on Information encoding (T4.1.2)

Description of the model

The UA partner has made significant progress on simplified as well as morphologically detailed models of neurons, including the axon initial segment at variable distance from the soma (Figure 12, sketch). The same current-based probing protocol described in the previous section has been applied first to simplified "ball-and-stick" models and then to the detailed reconstructed L5 rat pyramidal cells (Figure 13), released by the group of Dr. H. Markram. The dynamical transfer function of these models was investigated and found to unexpectedly depend on (i) the distance between the soma and the Axon Initial Segment (AIS) and on (ii) the total dendritic length. At the same time, the relationship between the slope of the action potential in the phase plane and the transfer bandwidth was explored and found to be direct.

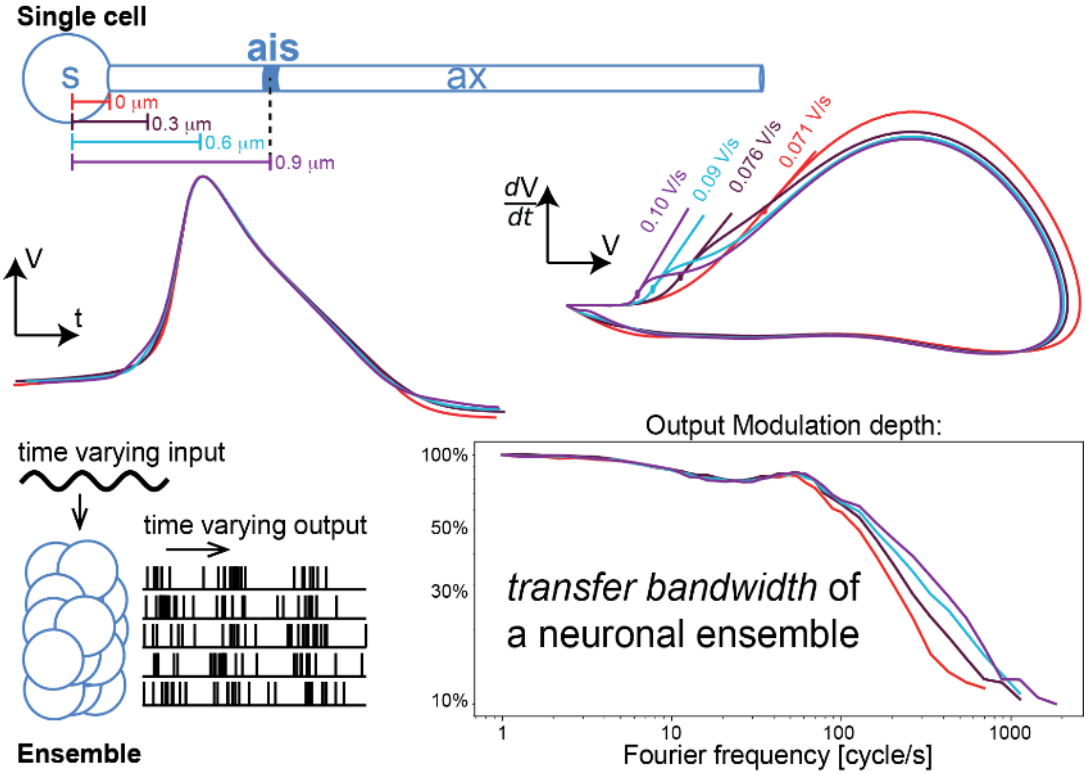

Figure 12 Modulation of the action potential slope

Modulation of the action potential slope in the phase-plane (top right) by the distance between the Axon Initial Segment and soma (top). The transfer function is affected only at high frequency (bottom right).

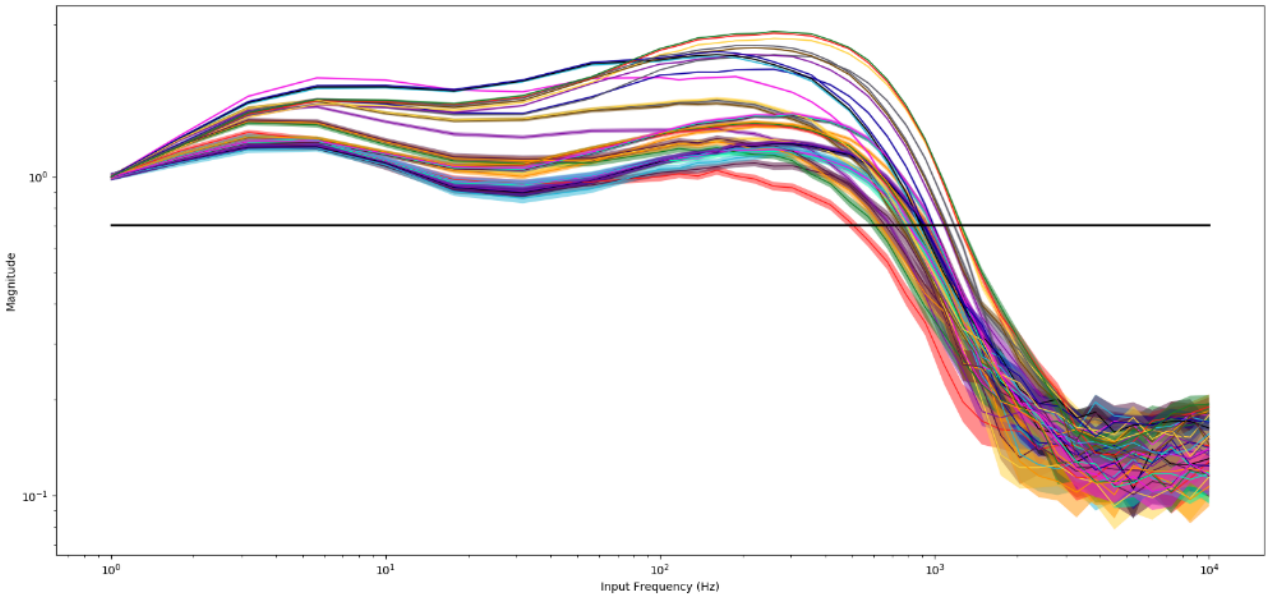

Figure 13 Modulation of the bandwidth of the dynamical transfer properties of reconstructed L5 thick tufted rat cortical pyramidal cells by the distance between the axon initial segment and the soma.

Implementation to platforms

Component 1008 contributes to CDP2-UC-001-single cell modeling

Implementation to platforms

Within the Brain Simulation Platform (WP6.4) and in collaboration with Dr. M. Migliore (T 6.4.5-6), we contributed an online "Collab" named "Dynamical response properties". It features a

Jupiter notebook interacting with the NEURON simulation platform. It receives several neuronal model as an input and it demonstrates the injection of *ad hoc* stimuli, required for characterizing the model's dynamical transfer properties.

Publications

Linaro D, Biró I, Giugliano M (2018) Dynamical response properties of neocortical neurons to conductance-driven time-varying inputs, European Journal of Neuroscience 47(1):17–32, https://doi.org/10.1111/ejn.13761

Goriounova NA, Heyer DD, Wilbers R, Verhoog MB, Giugliano M, Verbist C, Obermayer J, Kerkhofs A, Smeding H, Verberne M, Idema S, Baayen JC, Pieneman AW, de Kock CPJ, Klein M, Mansvelder HD (2018) A cellular basis of human intelligence (submitted)

Verbist C, Giugliano M (2018) The location of the Axon Initial Segment determines neuronal encoding properties of the axon. (in preparation)

Achieved Impact

These models are now continued in different directions, including correlation transfer and self-consistent sparse rhythms generation in collaboration with SP6 (Migliore) and SP1 (Mansvelder).

Conclusion & Outputs (UA)

These models aim at bridging the subcellular and the cellular scales, and ultimately to offer an actual phenomenological component to be included in mean-field models: theoretical descriptions at the population models should not only include an equivalent of the frequency-current curve and of the spike-frequency adaptation but also the high-frequency signal encoding properties revealed by the present study. These models will be continued in the next period, where they will challenged with respect to the correlation transfer properties upon controlling the fraction of common inputs.

Component Dependencies

Summarized links to components this key result depends on.

Component ID	Component Name	HBP Internal	Comment
N/A	*The basis of sharp spike onset in standard biophysical models (Telenczuk et al.2017)*	no	This paper inspired the model

2.1.6 Mean-field Models of GIM networks (T4.1.3)

The INRIA partner has worked on a mean-field model of neuronal population activity as prelude to the addition of dendritic compartments for the Component 1031 in T.4.1.3..

Description of the model

The INRIA partner has worked on a mean-field model of neuronal population activity, for networks of Generalised (GIM) integrate and fire neurons. This has been published recently [Drogoul etal. 2017]. The network was based on a single population of excitatory neurons with chemical synapses and gap junctions. The mean field model is based on recent work on stochastic spiking neural network [De Masi et al. 2015] and reads:

$$\begin{cases} \dfrac{\partial}{\partial t} g(t,v) = [\lambda v - a(g)]\partial_v g(t,v) + [\lambda - f(v)]g(t,v) \\ g(t,0) = \dfrac{p(g)}{a(g)} \\ g(0,\cdot) = g_0 \in L^1_+(\mathbb{R}_+), \quad \int_0^\infty g_0 = 1 \end{cases}$$

where g(t,v) is the distribution of membrane potentials in the population, lambda controls the time constant of the membrane potential dynamics and f is the instantaneous firing rate function.

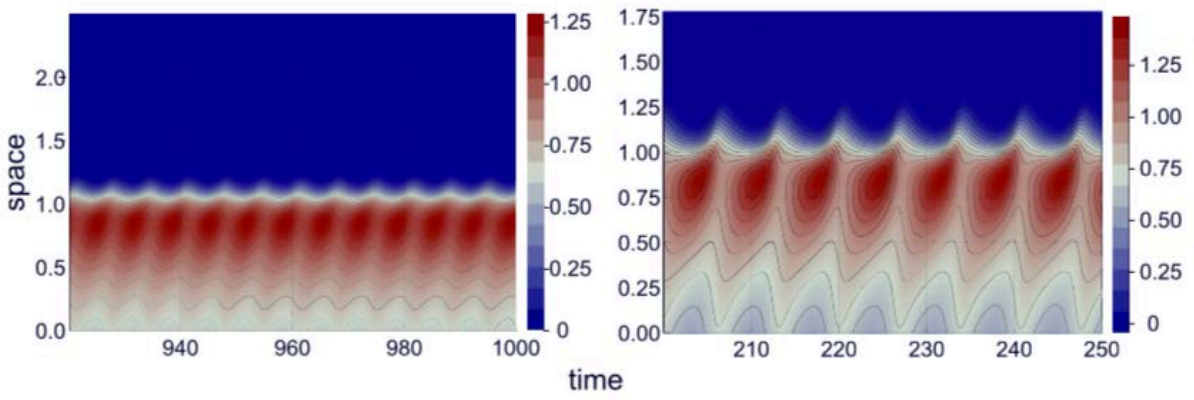

Figure 14 Simulations of f(v) = v8 for values of lambda close to the dynamical instability.

Is shown the contour plot of the membrane potential probability density (t,v) -> g(t,v)

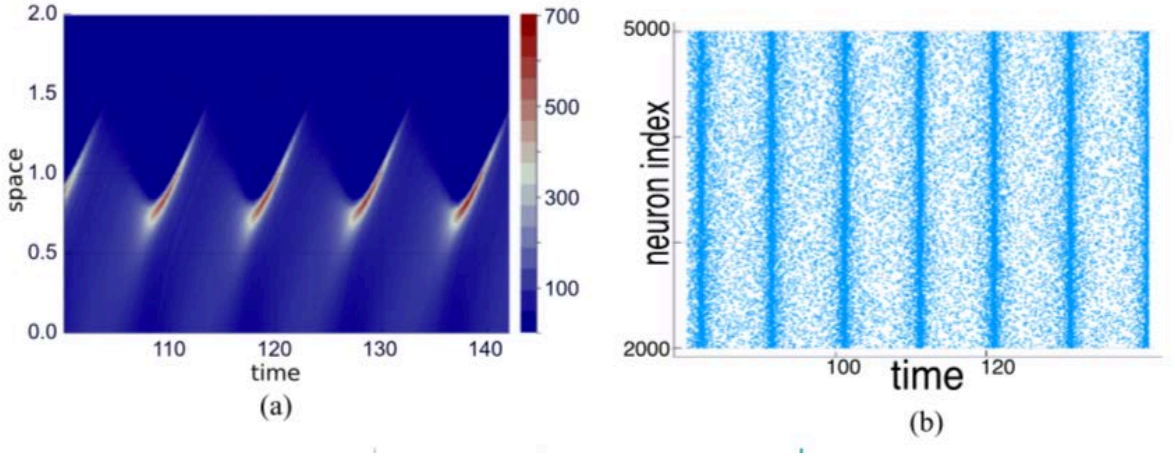

Figure 15 Simulations of f(v) = v8 for values of lambda far from the dynamical instability.

Left: plot of the membrane potential probability density (t,v) -> g(t,v). Right: raster plot.

We report here the effect of noise on the transition from asynchronous activity to partial synchronisation in excitatory globally pulse-coupled networks. We are able to predict numerically, the critical connectivity strength that leads to synchronisation as function of the noise level. This is done thanks to the mean field formulation (see equations above) which greatly simplifies the study. An example of oscillatory behaviour at the level of the mean field is shown in Figure 14.

In Figure 15. Left, we show that for larger connection strengths, the synchronisation improves compared to Figure 14. Figure 15 right shows that finite size effects are captured by the finite size network as the spikes of each neurons occur in precisely timed windows.

Implementation to platforms

(indicate here the components related to this model)

Component 1030, "Mean-field models of interacting populations of rate and spiking neurons " (T4.1.3).

Component 1031,"Mean-field models of interacting spiking neurons with dendritic compartment" (T4.1.3)

Implementation to platforms

This model was integrated to the collaboratory and the Model Catalog in SP5.

Publications

Drogoul, Audric, and Romain Veltz. "Hopf Bifurcation in a Nonlocal Nonlinear Transport Equation Stemming from Stochastic Neural Dynamics." *Chaos: An Interdisciplinary Journal of Nonlinear Science* 27, no. 2 (February 2017): 021101. https://doi.org/10.1063/1.4976510.

Achieved Impact

This model is now continued in different directions, including the addition of dendritic compartments.

Conclusion & Outlook

This model aims at brigding two scales, from cellular (spiking neurons) to population-level aspects. The model will be continued in the next period, in particular with the addition of dendritic compartments (preliminary work already done).

Component Dependencies

Summarized links to components this key result depends on.

Component ID	Component Name	HBP Internal	Comment
N/A	*N/A*	*N/A*	*N/A*

2.1.7 Long range dependence in Integrate and Fire models (T4.1.3)

Description of the model

INRIA: Long-range dependence (LRD) has been observed for several years in the spiking activity of neurons. Often, this is interpreted as originating from a non-Markovian system. In this model, we show that a purely Markovian integrate-and-fire (IF) model, with a noisy slow adaptation term, can generate interspike intervals (ISIs) that appear as having LRD. We compare it For comparison with a new model of individual IF neuron with fractional (non-Markovian) noise. The correlations of its spike trains are studied and proven to have LRD, unlike classical IF models.

The mathematical models write

$$\mathrm{d}V_t = (\mu_V - \lambda_V V_t + \gamma Z_t)\,\mathrm{d}t + \sigma \mathrm{d}B_t^\alpha$$
$$\mathrm{d}Z_t = (\mu_{Z,t} - \lambda_Z Z_t)\,\mathrm{d}t + \sigma' \mathrm{d}\tilde{B}_t^\alpha.$$

Where Z contains the adaptation part ($\gamma = 0$ stands for the model without adaptation). the noises and B_t^α are $\tilde{B}_t^\alpha$ fractional Brownian motions (fBm) of scaling parameter $\alpha \in (0,1)$

The spike trains are modeled as the successive times where the membrane potential variable V cross a fixed deterministic threshold. At such times, V is reset to a fixed value.

We have compared two fundamentally different cases:

(Markov case) $\alpha = 0.5$ and $\gamma \neq 0$

$\alpha \neq 0.5$ and $\gamma = 0$

For each model, we use the detrended fluctuation analysis and the Rescaled Range Statistics to evaluate the Hurst parameter (see Figure)

The main conclusion is that for a fixed (and small) number of Interspike intervals, it is impossible to discriminate if the data have been simulated with the Markov or the non Markov setting. However, the evolution of the curves as a function of the size of the spikes train give better results.

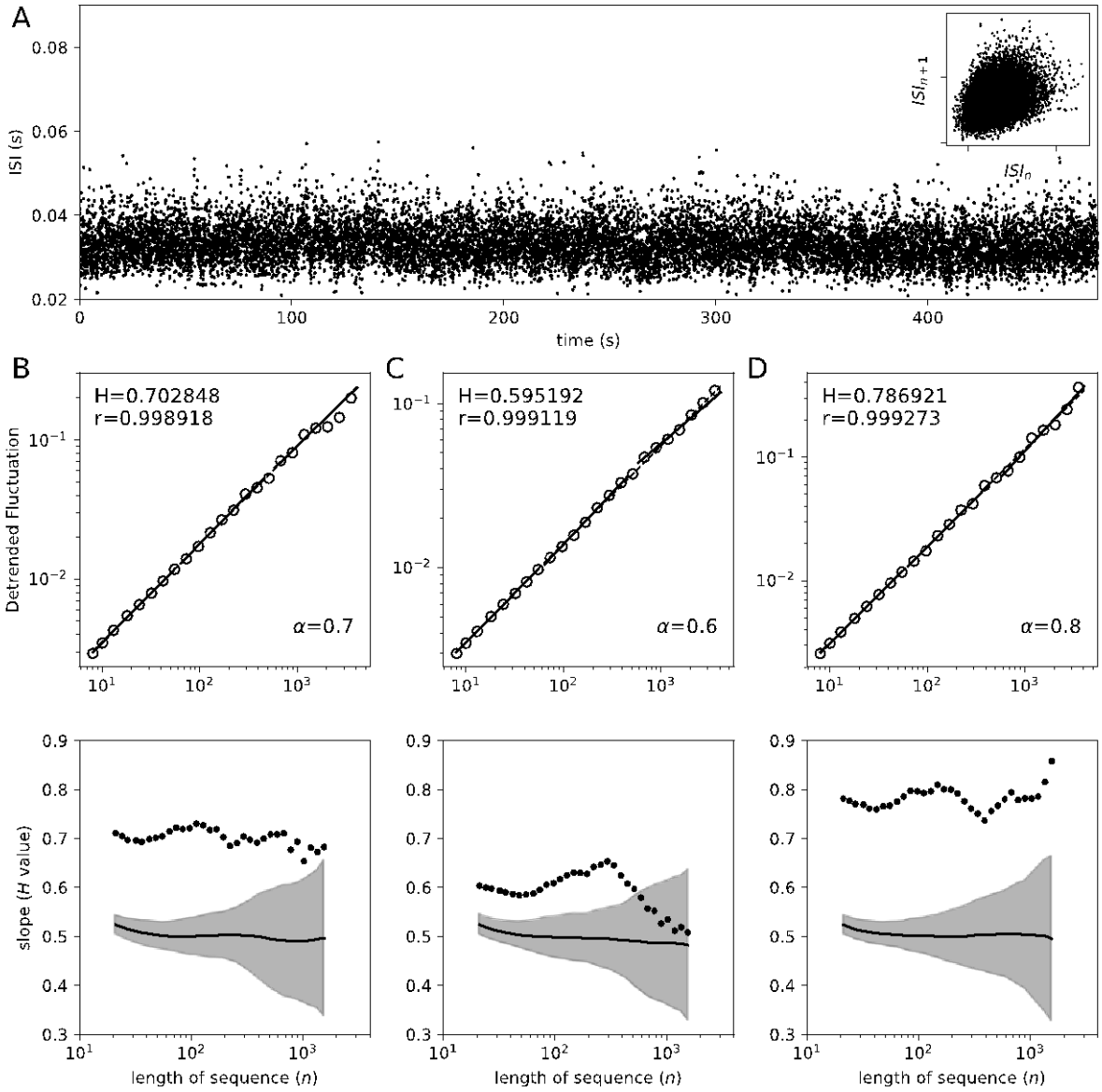
A
ISI (s)
time (s)
ISI_{n+1}
ISI_n
B
C
D
Detrended Fluctuation
H=0.702848
r=0.998918
α=0.7
H=0.595192
r=0.999119
α=0.6
H=0.786921
r=0.999273
α=0.8
slope (H value)
length of sequence (n)

Figure 16

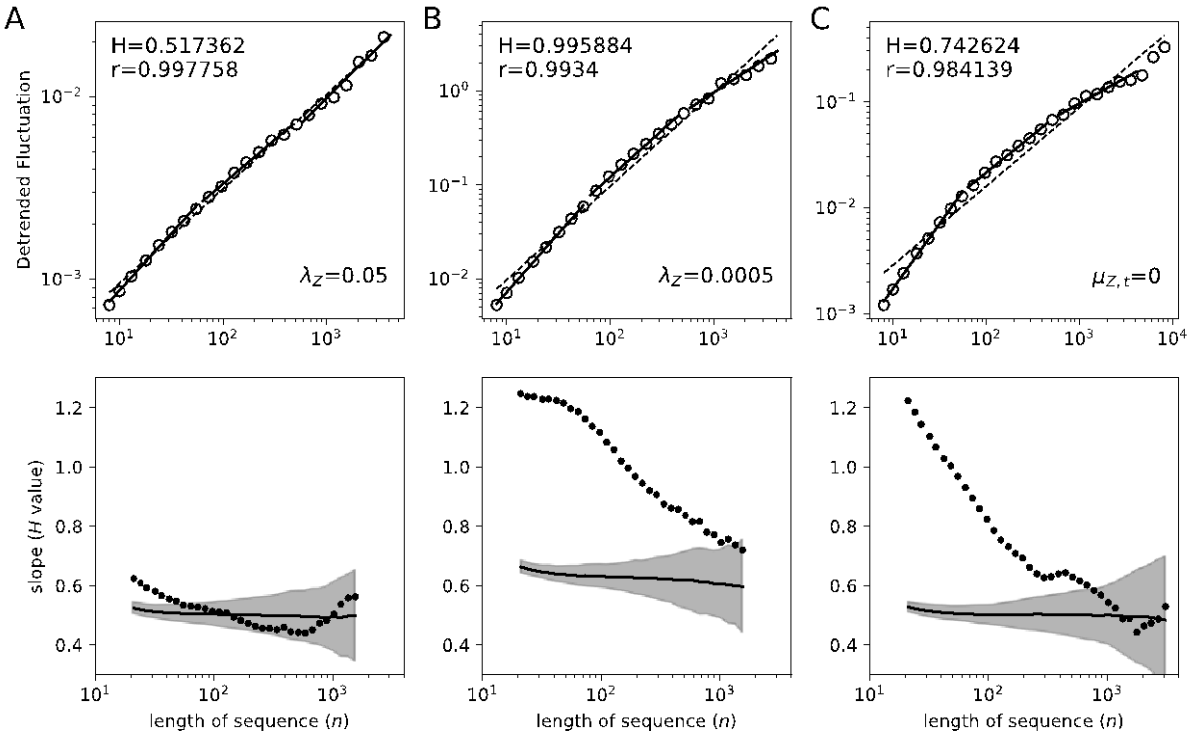

Figure 17

Publications

Richard A., Orio P. and Tanré E. (2018) An integrate-and-fire model to generate spike trains with long-range dependence. (to appear in Journal of Computational Neuroscience)

ArXiv preprint: https://arxiv.org/abs/1702.03762

Achieved Impact

This neuronal model is now used as the elementary part in a network. These neurons are connected with synapses modeled by (stochastic) synaptic weights. The behavior of large networks is studied (mean-field limit).

Conclusion & Outlook

This model aims at understanding deeply the nature of noise in individual neurons and the effect on the associated mean-field network. Understanding the best noise model at each scale of brain area is a big challenge.

Component Dependencies

Summarized links to components this key result depends on.

Component ID	Component Name	HBP Internal	Comment
N/A	*N/A*	*N/A*	*N/A*

2.1.8 Stability of Synchronization under stochastic perturbations in LIF neural network (T4.1.3)

Description of the model

INRIA: We consider a finite network of leaky integrate and fire neurons with independent additive Gaussian noises. We study the synchronization of the network, that is we evaluate the probability

that every neurons spike precisely at the same time. We both obtain results if the initial state of the network is already synchronized or not.

Implementation to platforms

Component 1030, "Mean-field models of interacting populations of rate and spiking neurons" (T4.1.3).

Publications

Guiraud P. and Tanré E. (2017) Stability of synchronization under stochastic perturbations in leaky integrate and fire neural networks of finite size.

ArXiv preprint: https://arxiv.org/abs/1609.07103

Achieved Impact

This model is being extended to the thermodynamic/mean-field limit.

Conclusion & Outlook

This model gives us a good comprehension of the effect of small adative noise in a network of LIF neurons. We prove the persistence of the synchronization phenomenon similarly to the deterministic model. Moreover, for some values of the parameters the noise increase the spiking rate of the network in addition to the synchronization.

Component Dependencies

Summarized links to components this key result depends on.

Component ID	Component Name	HBP Internal	Comment
N/A	*N/A*	*N/A*	*N/A*

2.1.9 Transient firing rates are a function of the geometry of the neural model (T4.1.3)

Description of the model

ULEEDS: We consider a population as the distribution of neurons over the state space of individual neurons. Because we consider the state space of two dimensional (2D) neural models, we are able to study models with adaptation, or other variables in a way that has not been done before. Our basis is the differential Chapman-Kolmogorov equation:

$$\frac{\partial \rho}{\partial t} + \frac{\partial}{\partial \vec{v}} \cdot \left(\frac{\vec{F}\rho}{\tau}\right) = \int_M d\vec{v'} \left\{ W(\vec{v} \mid \vec{v'})\rho(\vec{v'}) - W(\vec{v'} \mid \vec{v})\rho(\vec{v}) \right\} \quad (1)$$

Here, ρ is the density, v a two dimensional vector representing the state variables, F the neural model and W the transition matrix for the stochastic process.

Because we can simulate a large number of models in comparable condition, not just two dimensional ones, such AdExp or conductance-based, but also one dimensional models such as LIF, QIF, EIF, etc, we can observe broader patterns of behaviour.

For conductance based neurons the model is given by:

$$\begin{aligned} \tau \frac{dV}{dt} &= -g_l(V - E_L) - g_e(t)(V - E_e) \\ \tau_e \frac{dg_e}{dt} &= -g_e + I_{syn}(t) \end{aligned} \quad (2)$$

and the transition probability for shot noise:

$$W(v' \mid v) = \nu\delta(v' - v - h) + (1 - \nu)\delta(v - v') \quad (3)$$

Some populations produce a strong transient respons ("ringing"), some don't. Conductance based models converge calmly to their steady state output, LIF, QIF, but also AdExp neurons produce pronounced rining. Of the 1D models, the effect is stronger in QIF than in LIF.

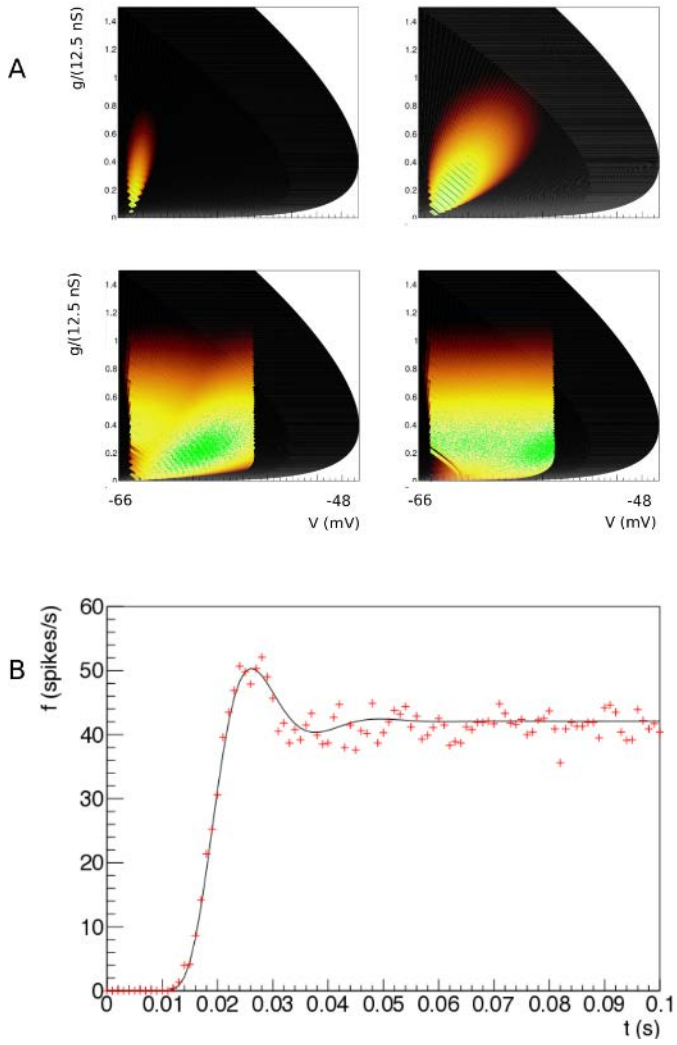

Figure 18 The evolution of the population density for neurons without a maximum conductance, neurons disperse in the g-direction, well before reaching threshold

So far, this effect has been explained as filtering by the synapses. We propose a complementary geometrical interpretation. For space reasons, we restrict ourselves to one example: conductance based neurons.

For conductance based neurons without maximum conductance the stochastic process pushes neurons into a direction where they are not restrained, and the population disperses well before reaching threshold boundary. When they reach the threshold boundary – which is not in the direction of the stochastic process, but reached under endegenous neural dynamics they pass as a group and drift toward equilibrium, leaving barely a blip in the firing rate.

Let us contrast this with a simulation where we introduce a maximum conductance $g_{max} = 0.8$, which for simplicity we assume to voltage independent. This then introduces a reflecting boundary at $g = g_{max}$, and therefore introduces a scale by which an efficacy can be judged to be large. As expected, probability mass is squashed against this boundary (Figure 19A))and has nowhere to go but laterally, in the direction of the threshold. Interestingly, the mass has not dispersed and clear groupings of mass huddled against the boundary can be observed. The traversal of the threshold by these groupings produces clear oscillations in the firing rate: a ``ringing" effect. The firing rate jump response reflects the effect of the presence of a maximum conductance in state space.

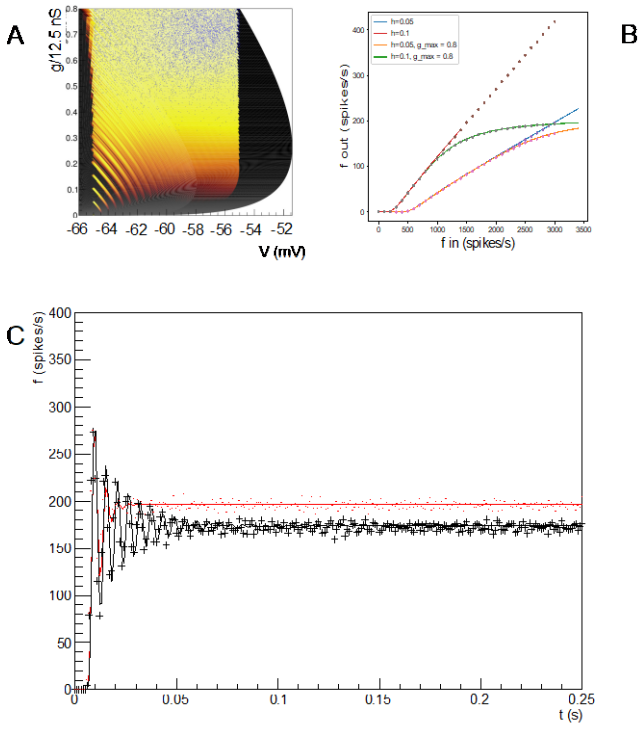

Figure 19 If there is a maximum conductance, neurons group against this boundary and do not disperse before reaching threshold. This is visible in the firing rate

We run two simulations: one with and one without maximum conductance, but otherwise identical, and repeat this experiment for two different synaptic efficacies: J = 1, 3 mV. Both simulations show a simulation with an input rate of 3 kHz. In case of no maximum conductance, probability mass can disperse in the g direction and mostly does so before arriving at the threshold. In Figure 19 one sees that the introduction of a maximum conductance leads to a reduced response firing rate for high inputs. This can be interpreted as the population unable to respond to an increase of input once the majority of its ion channels are already open. Such an effect has been proposed as the explanation of the experimentally observed sublinear addition of two cortical waves originating from different positions. Figure 19 shows that the firing rates of Monte Carlo simulations and our method agree over the entire range of input.

Even when the effects on the response firing rate are moderate, the transient dynamics can be radically different. For an efficacy J = 1 mV and and input rate $f_{in} = 3$ KHz, the firing rates for maximum conductance, compared to no maximum come out as 175 Hz vs 195 Hz. In Figure 19 C we show the response firing rate as a function of time. The result for the unrestrained conductance is given by the red line, which despite the high output firing rate still almost produces no overshoot. When we restrict the maximum conductance we see a somewhat reduced firing rate but a pronounced transient response (“ringing'”) which persists much longer than for an unrestrained conductance. It is striking to see that the reintroduction of a barrier in state space results in pronounced transients. In both cases, the calculated firing rates agree well with Monte

Carlo sin. We attribute this ringing to a geometrical effect: the introduction of a barrier in the direction of where the stochastic process is pushing neurons.

Implementation to platforms

(indicate here the components related to this model)

Component 1030, "Mean-field models of interacting populations of rate and spiking neurons" (T4.1.3).

Implementation to platforms

This model was integrated to the collaboratory (8740). Here the matrix, model and XML files are stored that can be used in conjunction with MIIND. MIIND is in the software catalogue and is available on the Simulator Platform since 16/02/2018

Publications

Computational Geometry for Modeling Neural Populations: from Visualization to Simulation

Marc de Kamps, Mikkel Elle Lepperød, Yi Ming Lai

bioRxiv 275412; doi: https://doi.org/10.1101/275412

Achieved impact

This model was important as part of the validation of the 2D method, and is part of the methods paper. The observation that a visualization of state space can lead to predictions about transient dynamics may be of benefit to the neuroscience community as a whole.

Achieved Impact

Short list, or narrative, outlining which impact has been achied to-data based on this result.

Component Dependencies

Summarized links to components this key result depends on.

Component ID	Component Name	HBP Internal	Comment
64 & 1034	*MIIND*	*Yes*	*Explain the qualitative difference in transient firing rate of population of neuron, based on differences the geometry on underlying neuron model. Validation of MIIND*

2.1.10 Stochastic Input Probes Subthreshold Dynamics of the AdExp Neuron (T4.1.3)

See HBP SGA1 M24 D472_ANNEX_restricted – 2.1 Stochastic Input Probes Subthreshold Dynamics of the AdExp Neuron (T4.1.3).

Achieved Impact

This model was important as part of the validation of the 2D method, but is too detailed to include in the methods paper.

Component Dependencies

Summarized links to components this key result depends on.

Component ID	Component Name	HBP Internal	Comment
64 & 1034	*MIIND*	*Yes*	We modeled how sub threshold stimulation of AdExp can lead to peaks in a response

			spectrum when the population is subjected to noise, despite the stimulus being weak.

2.1.11 Non-Markov processes in population density techniques (T4.1.3)

ULEEDS : Using random network theory, it is possible to model random walks that are subject to events that are not Poisson distributed. The righthand side of Eq 1 then generalizes to a so-called generalized Master equation:

$$\frac{d\mathcal{P}}{dt} = \frac{\nu}{\alpha}(M - I)\,(K_{norm}(t) * \mathcal{P}(t))$$

For gamma distributed spike intervals the solution entails a convolution of a kernel dependent on shape factor α with the recent history of the density. The difference between Poisson distributed and non-Markovian gamma distributed interspike intervals is profound:

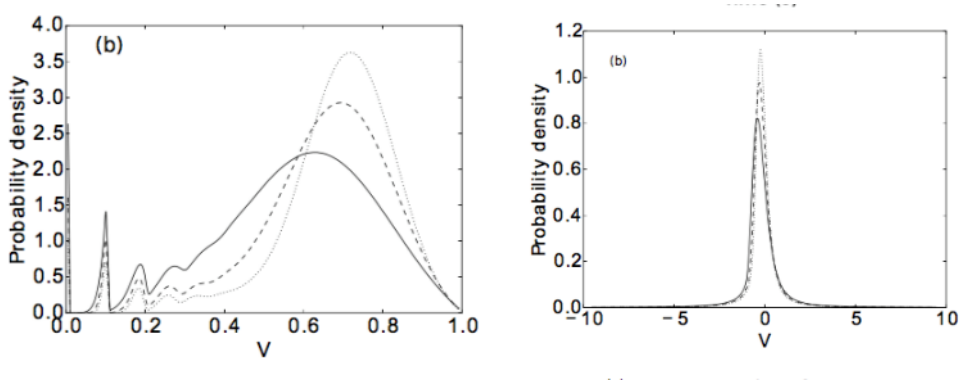

Figure 20 Density profile for LIF (left) and QIF (right) neurons for gamma distributed input spike trains for different shape factors

Implementation to platforms

Component 1030, "*Mean-field models of interacting populations of rate and spiking neurons*" (T4.1.3).

Implementation to platforms

The code was developed in Python. We will make a C++ implementation and integrate this in MIIND, which has been installed on the Simulator Platform.

Publications

Yi Ming Lai and Marc de Kamps Phys. Rev. E 95, 062125 – Published 20 June 2017

The actual or potential results for the different communities are discussed.

Achieved Impact

This is a very general method that allows the inclusion of non-Markov processes in population density techniques. It is relevant when spike statistics is not well explained by Poisson or white noise assumptions.

Component Dependencies

Summarized links to components this key result depends on.

Component ID	Component Name	HBP Internal	Comment

64 & 1034	*MIIND*	*Yes*	MIIND was used to help explain the difference in membrane potential distributions caused by different stochastic processes. The distributions between Markov (Poisson) and non-Markov (gamma distributed interstice intervals) lead to profound differences in the population response. To validate MIIND

2.1.12 Development of the MIIND simulator (T4.1.3)

ULEEDS : At the 8th of January 2018 we made the full 2D simulator available at http://miind.sf.net. We uploaded a number of meshes that we used in the preparation of bioarxiv paper These meshes are also available in the collab. On 16 February 2018 MIIND was installed on the Simulation Platform with the help of the Julch support team, so that an installed version is available to consortium. A tutorial is available at http://miind.sf.net/tutorial.pdf The Juelich team was abkle to surmount all installation issues using this document, without our interevention.

PhD student Hugh Osborne has integrated MIIND into the The Virtual Brain. We will briefly describe how this works, as this has ramifactions for the workflows that encompass MIIND.

The Virtual Brain and MIIND are both systems which facilitate the development of neural mass or mean field population models with explicit descriptions of how multiple populations are connected. In this way, the complex dynamics arising from interaction of these populations can be studied.

TVB provides a framework to describe a network of nodes (the connectivity) which, while it can be abstract, generally represents regions of the human or primate brain. Connections between nodes represent white matter tracts which transfer signals from one node to the next based on length and propagation speed. TVB also allows the description of “coupling” functions which modulate these signals as they pass from one node to another. Typically, the number of nodes is in the order of 100 or so. However, TVB also allows the definition of a “surface” which can be associated with 10s of thousands of nodes to simulate output from common medical recording techniques such as EEG and BOLD fMRI. TVB has impressive clinical relevance as well as supporting more theoretical neuroscience research. Users can build simulations using the graphical user interface or directly using the python source code.

While MIIND and TVB have many functional similarities, both have differing strengths with respect to the underlying simulation techniques and surrounding infrastructure. It was therefore clear that implementing the smaller system, MIIND, in the more developed infrastructure of TVB might yield benefits from both.

Although it is possible to model delayed connections and synaptic dynamics between populations in MIIND, TVB provides a quick and intuitive method of defining such structures and behaviours through the connectivity network and coupling functions. Some users of MIIND may find it useful and appropriate to house their simulations in a such structures. Furthermore, as there is some overlap of models used in both MIIND and TVB, there is opportunity to compare results using the same experimental conditions.

Currently, TVB allows only a single model definition for all nodes in the connectivity network. MIIND is not limited in this way so there is scope for developing more complex brain networks. Though not computationally as fast as integrating mean field models, MIIND’s one dimensional simulations run faster than integration techniques over neural circuits of comparable numbers of individual neurons and MIIND also supports MPI, a parallelisation method used in many high performance computing (HPC) systems. Implementing MIIND in TVB with an emphasis on speed will encourage use of MIIND simulations by TVB users and perhaps inform future development of parallelised TVB code.

Finally, MIIND’s population density technique provides a rigorous link between a population’s underlying neuron model and the dynamics of the population. Adding these techniques to TVB’s

repertoire would complement the existing mean field models and contribute to the goal of bridging scales.

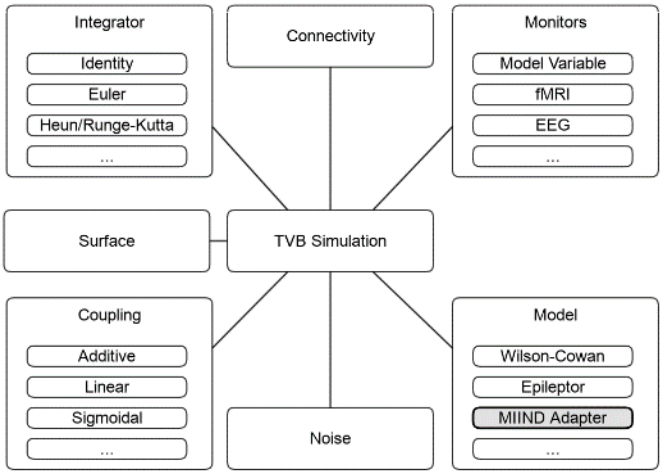

Figure 21 Components of a basic TVB Simulation with the addition of a new potential model object, MIIND Adapter

The figure above shows a subset of required components to run a simulation in TVB. Most existing models define a system of differential equations which are then integrated using, for example, Euler or Runge-Kutta methods. The Identity integrator performs no integration and simply returns the value given by the model. To implement MIIND in this system, an additional model has been added called MIIND Adapter. The MIIND Adapter makes calls to a MIIND generated shared library which initialises and manages its own simulation. The MIIND library simulates all nodes (as many as defined in the TVB connectivity matrix) such that the firing rate of each node in MIIND is output to the Identity integrator in TVB at the end of each iteration. This output can be picked up by the monitors and stored for analysis at the end of the simulation. TVB simulates propagation and transformation of the firing rate from source nodes via the connectivity and coupling components and passes the values back to MIIND to be input to each target node.

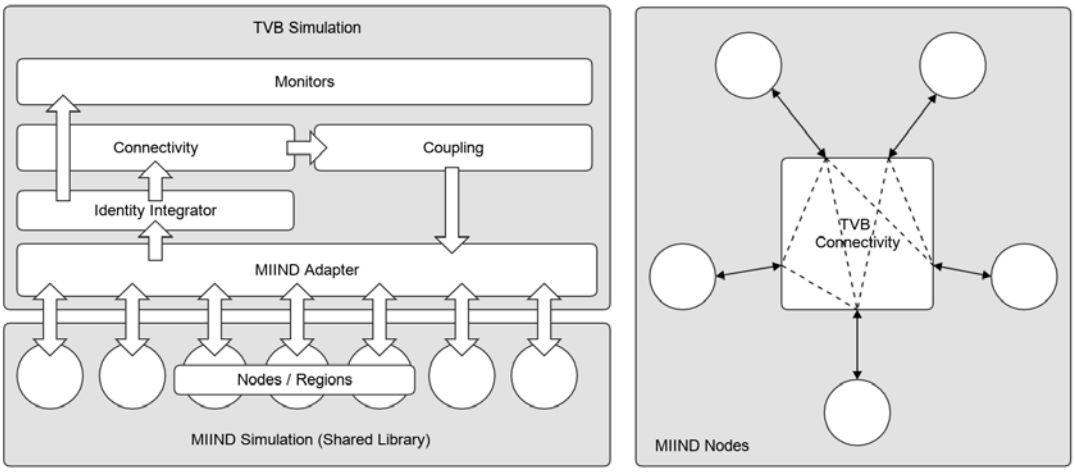

Figure 22

(left) Each node in the MIIND simulation passes its activity to the MIIND Adapter in TVB and receives incoming activity from the connectivity network. (right) In the simple case, nodes in MIIND are unconnected and are only concerned with a single input

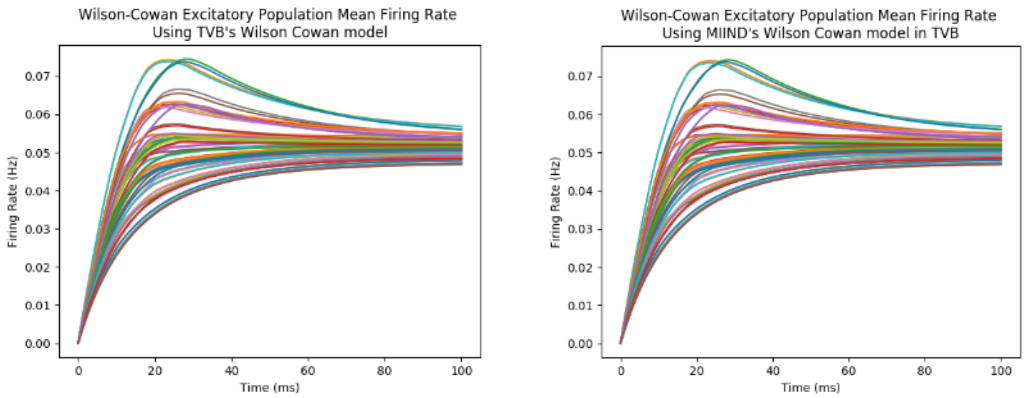

Figure 23

Running TVB with the default 76 node connectivity, white matter propagation speed and linear coupling with only the models and integrator definitions differing, in one case with TVB's standard Wilson-Cowan model and EulerDeterministic integrator, the other case using the MIIND Wilson-Cowan model with matching parameters and the Identity integrator; the output is almost identical but for some variation due to the different integration techniques.

Using the MIIND Adapter in TVB also allows for the possibility of generating more complex networks of populations within a single TVB node and for the networks and models to differ from node to node.

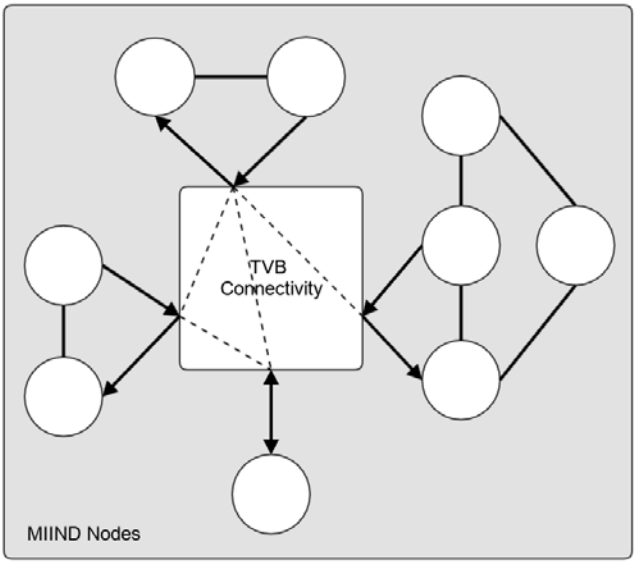

Figure 24 TVB is aware of four equal MIIND Adapter nodes in its network but the nodes themselves can differ in complexity and behaviour in MIIND

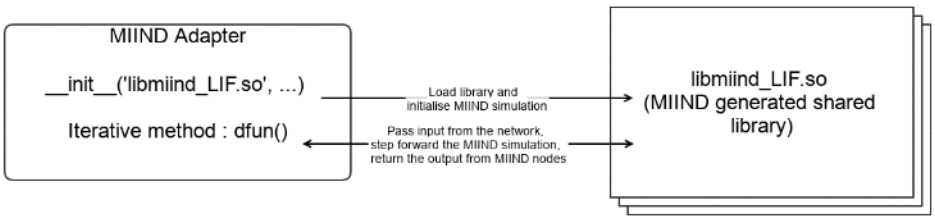

Figure 25

The MIIND Adapter expects a well defined interface for the shared library to allow it to initialise the MIIND simulation and send and receive activity from the nodes. However, as long as this interface is respected, any MIIND simulation with the correct number of input and output nodes can be generated and plugged into the adapter without the need for a code change in TVB. An example script is provided to demonstrate how a simple TVB simulation using the MIIND Adapter can be set up with populations of LIF neurons.

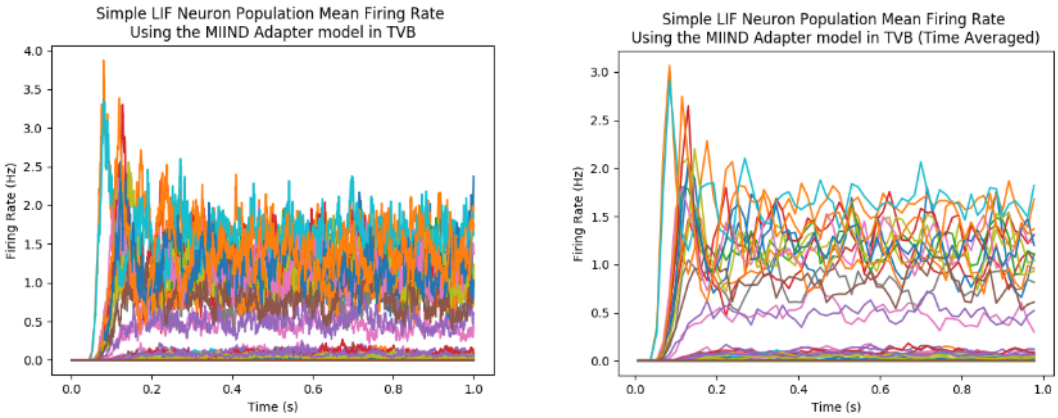

Figure 26 Two plots from another simple TVB simulation, this time using a MIIND generated shared library for populations of LIF neurons, the expected damped oscillatory behaviour is visible for many nodes.

Noise is apparent from the initial random node activity generated by default in TVB.

To generate a shared library file which can be used with TVB's MIIND Adapter, the C++ MIIND code is very similar to any normal "MIIND only" simulation

Implementation to platforms

Component 1030, "*Mean-field models of interacting populations of rate and spiking neurons*" (T4.1.3).

Implementation to platforms

MIIND was installed on the simulator platform on 16/02/2018 and is thereby available to the colloboration.

Publications

The MIIND tutorial: http://miind.sf.net/tutorial.pdf

Achieved Impact

With the release of the 2D code, MIIND makes two dimensional population density techniques publicly available. With these techniques any 2D system subject to shot noise can be simulated. 1D models such as LIF, QIF and EIF are available as well and run much more effciently. We are working on a Python workflow to allow simulations directly to be run from the collab. With integration in TVB its application scope has been extended considerably, and we hope also to have extended the possibilities for TVB.

MIIND has been taken up by Mikkel Lepperod from CINPLA, University of Oslo, and Martin-Preze-Guevara from NEUROSPIN, who based his thesis (http://www.theses.fr/s177132) on simulations performed with MIIND. Mikkel has pushed the AdExp simulations hard. The experiences of two independent users has led to substantial feedback on our workflow and has prompted us to put more effort into a Python interface.

Conclusion & Outlook (ULEEDS)

In the last year ULEEDS has implemented the 2D population density method and evaluated it applicability on a large number of models. The code is now very robust and has been released

publicly. A substantial drain of our time was to make the method work on Fitzhugh-Nagumo neurons, which have a complex state space presenting numerical problems. We learnt that it is acceptable to limit the grid in the presence of stationary points and nucllines and to infer motion of density. A substantial amount of our time was taken up by taking code that was working on our own machines and bringing it in a state where we comfortable for others to take this up. With the installation on the Simulation Platform, the prospects for further take up are much better. We will develop a Python workflow and will work with the Juelich HPC centre towards one that can be run directly from the collab. We also have created a Docker container, facilitating remote installation.

Modelling-wise, we will focus on networks of AdExp populations, as this model is studied intensively within the collaboration. Outside the collaboration we have demonstrated that the method also is useful in modelling central pattern generators as found in spinal cord. A good 2D model that captures this is Izhikevich neurons modelling persistent sodium channels. Preliminary simulations have indicated that the CPG behaviour is well captured by such models. Within the HBP this opens the possibilities for further collaboration.

Component Dependencies

Summarized links to components this key result depends on.

Component ID	Component Name	HBP Internal	Comment
64	MIIND	*Yes*	*Release of the model itself*

2.1.13 Mean-field Models of AdEx networks (T4.1.3)

Description of the model

The UNIC partner has worked on a mean-field model of neuronal population activity, for networks of Adaptive Exponential (AdEx) integrate and fire neurons. This model was described one year ago in deliverable D4.7.1, and was published (Zerlaut and Destexhe, 2017; Zerlaut et al., 2018). In the second year of SGA2, this model was extended towards modeling the VSD (see section 2.13 *Model for Voltage-Sensitive-Dye imaging (VSDi) (T4.1.3)*).

A second extension of the model is towards including recent measurements of cellular transfer functions. The transfer function is a central piece of the mean-field formalism, it maps the output of the neuron (expressed as a rate) as a function of its excitatory and inhibitory inputs. At first order, the time evolution of the mean-field model is given by:

$$T\frac{\partial \nu_\mu}{\partial t} = (\mathcal{F}_\mu - \nu_\mu)$$

where ν_μ is the mean activity of population μ, while $\mathcal{F}_\mu$ is its transfer function.

This formalism is based on a Master Equation (El Boustani and Destexhe, 2009) and can be applied to any population of neurons, provided its transfer function is known. This formalism was applied to networks of integrate-and-fire neurons, connected with conductance-based synapses, and was successful to predict the state space of such networks (El Boustani and Destexhe, 2009). It was more recently applied to more complex neuron types, such as the AdEx model. Here, the transfer function could be obtained from a semi-analytical procedure, where a mathematical template was fit to numerical simulations (Zerlaut and Destexhe, 2017). The resulting mean-field model could predict not only the level of spontaneous activity, but also the response of the network to external stimuli (Zerlaut and Destexhe, 2017).

The same approach could be done to more complex neurons, and it was applied to real neurons from mouse V1 (Zerlaut et al., 2016). In this approach, the same mathematical template was used and was constrained to recordings of neurons using conductance-based inputs injected using the dynamic-clamp technique. This technique allowed us to measure the transfer function from 30 neurons, electrophysiologically identified as RS neurons. However, the experiments revealed a very strong cell-to-cell diversity of transfer functions, which could only be accounted by diversity in the level of excitability of the neurons.

Components

Component 1554, "Mean-field models of AdEx networks, spontaneous activity and responsiveness" (T4.1.3).

Implementation to platforms

This model was integrated to the collaboratory and the Model Catalog in SP5.

References

El Boustani, S. and Destexhe, A. A master equation formalism for macroscopic modeling of asynchronous irregular activity states. Neural Computation 21: 46-100, 2009.

Publications

Zerlaut Y., Telenczuk, B., Deleuze, C., Bal, T., Ouanounou, G. and Destexhe, A. (2016) Heterogeneous firing rate response of mice layer V pyramidal neurons in the fluctuation-driven regime. Journal of Physiology 594: 3791-3808.

Zerlaut Y. and Destexhe A. (2017) A mean-field model for conductance-based networks of adaptive exponential integrate-and-fire models.

ArXiv preprint: https://arxiv.org/abs/1703.00698

Zerlaut Y., Chemla, S., Chavane F. and Destexhe A. (2018) Modeling mesoscopic cortical dynamics using a mean-field model of conductance-based networks of adaptive exponential integrate-and-fire models. *Journal of Computational Neuroscience* (in press).

bioRxiv preprint: https://www.biorxiv.org/content/early/2017/11/12/abs/168385

Achieved Impact

This model is now continued in different directions, include adaptation, model Up/Down states, and integrate in the Virtual Brain.

Conclusion & Outlook

This model aims at brigding two scales, from cellular (spiking neurons) to population-level aspects. It will certainly help bridging scales, one of the objectives of theoretical neuroscience in HBP. The model will be continued in the next period, in particular in the Virtual Brain, where it will be tested at larger scales. We will also investigate mean-field models based on the measurements of transfer functions in real neurons.

Component Dependencies

Summarized links to components this key result depends on.

Component ID	Component Name	HBP Internal	Comment
N/A	*Model of "dynamically realistic" network*	*yes*	*This component helps bridging scales*

2.1.14 Model for Voltage-Sensitive-Dye imaging (VSDi) (T4.1.3)

Description of the model

The UNIC partner has developed a model of the Voltage-Sensitive-Dye imaging signal, based on experimental data recorded in awake monkey in the laboratory of F. Chavane (CNRS Marseille). The experimentally recorded signal reflects the voltage change in primary visual cortex (V1) after the presentation of visual stimuli. According to the experimental system spatial resolution, every pixel in data represents the average voltage activity of around one to several thousand neurons. We thus modeled every spatial location as a population of excitatory and inhibitory Adaptive Exponential (AdEx) integrate and fire neurons. As we are interested in the average voltage of the population, we used a mean field model developed in T4.1.3 that describes the time evolution of the entire population and gives access to the population firing rate of excitatory and inhibitory neurons, ν_E and ν_I respectively. The average voltage of the population is then calculated according to the shot-noise theory (Destexhe, JCNS, 2009):

$$\mu_V = \frac{g_L E_L + \nu_E G_E E_E + \nu_I G_I E_I}{g_L + \nu_E G_E + \nu_I G_I}$$

where g_L,G_I,G_E and E_E, E_I, E_I are conductances and reversal potentials and μ_V the average population voltage. Each mean-field is then arranged over a ring and subpopulations interact with each other according to a Gaussian connectivity.

As a first step, the model has been tested on its capability to describe the response to a single viual stimuli. The response, in both model and experiment, is a propagating wave (see Figure 27). More than a qualitative accordance, the model reproduces quantitativey the velocity of propagation, which is around 0.3 m/s. The model is thus able to compare with VSDi data and to reproduce quantitatively and qualitatively the existence of propagating waves in the visual cortex.

Secondly, the model has been tested on its capability to predict the interaction of colliding propagating waves. In the experimental setup, two visual stimuli are presented at different times. The collision of the waves results in a suppressive response, i.e. the actual response is lower than the linear prediction based on the response to single stimuli separately presented. In the model, two different inputs are presented at different times, mimicking the experimental setup, and giving rise to colliding waves of response similar to the experimental protocol. The model predicts a sublinear response showing that, also in this case, the mean-field model is able to predict the suppression and its propagation (see Figure 28b).

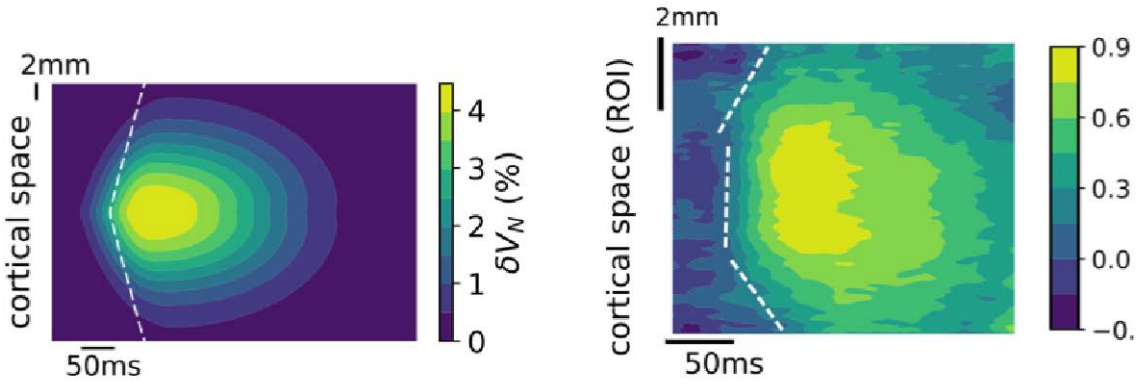

Figure 27 Spatio-temporal response to a stimuli: experiment and model.

On the left the experimental response to a presented visual stimuli. On the right the response simulated with the model. In both cases we observe a wave propagation. Lines show the front of each wave, calculated from its spatial derivative.

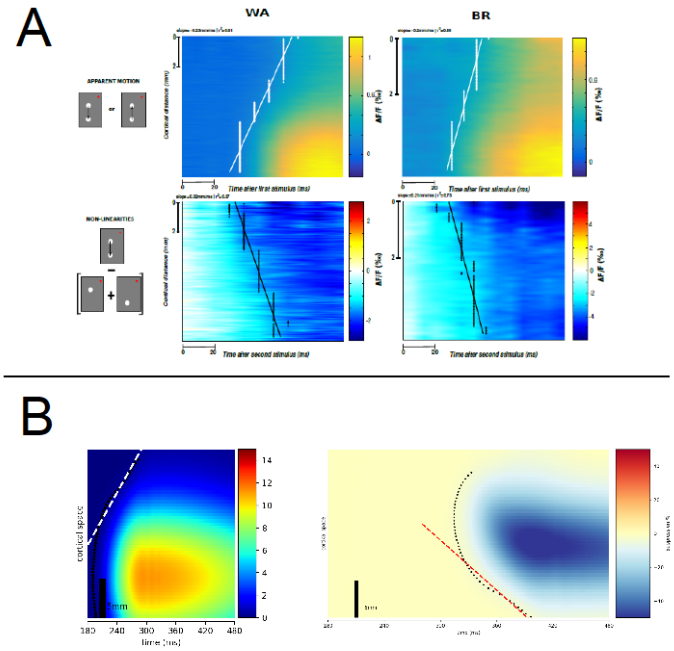

Figure 28 Suppressive interaction of colliding waves.

A. Experimental data. Top panels: space-time response to a single visual stimuli (two different monkeys). Lower panels: Difference between the linear prediction and the actual response to the presentation of two visual stimuli. B. Model. Left: response to a single stimulus. Right: suppression signal is calculated as in the experimental data.

Components

Component 1554, "Mean-field models of AdEx networks, spontaneous activity and responsiveness" (T4.1.3).

Implementation to platforms

This model was integrated to the collaboratory and the Model Catalog in SP5.

Publications

Zerlaut Y. and Destexhe A. (2017) A mean-field model for conductance-based networks of adaptive exponential integrate-and-fire models.

ArXiv preprint: https://arxiv.org/abs/1703.00698

Zerlaut Y., Chemla, S., Chavane F. and Destexhe A. (2018) Modeling mesoscopic cortical dynamics using a mean-field model of conductance-based networks of adaptive exponential integrate-and-fire models. *Journal of Computational Neuroscience* (in press).

bioRxiv preprint: https://www.biorxiv.org/content/early/2017/11/12/abs/168385

Achieved Impact

This model is now going to be updated according to the developments on the mean-field, e.g. including adaptation.

Conclusion & Outlook

This model aims at having a direct comparison between population models (mean-field) and suitable data measuring the average activity of large population of neurons (VSDi). The model is capable of reproducing experimental data and might be exploited to understand the mechanisms standing behind the observed activity. The model will be continued in SGA2, extending towards including adaptation and the diversity of experimental transfer functions. We also aim at including this model in the VirtualBrain environment.

Component Dependencies

Summarized links to components this key result depends on.

Component ID	Component Name	HBP Internal	Comment
1554	*Mean-field models of AdEx networks, spontaneous activity and responsiveness*	*Yes*	*This component helps bridging scales*

2.1.15 Simplified model of local field potentials (T4.1.4)

Description of the model

The UNIC partner has considered the LFP signal generated by a population of neurons firing correlated spikes from homogeneous Poisson distribution. The LFP signal was calculated as a linear sum of unitary contributions from each spike, which was modelled as a LFP kernel. For the purpose of this study, the same LFP kernel was used for all neurons.

To constrain the model, we analyzed data from rigid electrode arrays (Utah arrays), which allowed us to investigate both temporal and spatial aspects of the LFP signals. The properties of the LFP in space and time are determined to large degree by the correlations in the neural activity. We found that, in human Utah-array recordings, the correlation between unit activity and LFP is broad, but if one removes the correlations by denoising, the remaining relation has all the properties of unitary fields (Telenczuk et al., Nature Sci. Reports 2017). The unitary fields can be used as a "kernel" to calculate the LFP from population of neurons, solely from their spiking activity. This is the basis of our simplified model of LFPs.

We simulated the results of this analysis by generating correlated spike trains, and verified that the relationship between the population activity and unit activity was very similar to the data (Figure 29).

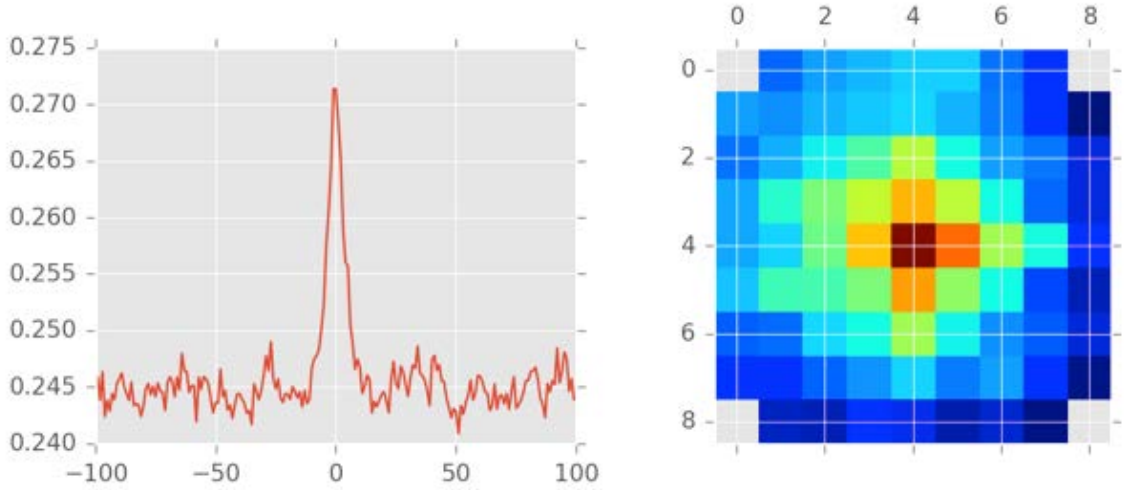

Figure 29 Correlations of simulated population activity (multi-unit activity) with the single-neuron response of a neuron in the center of the electrode array.

Left: Cross-correlogram averaged over neurons. Right: Spatial correlation map.

In a second step, we considered a "kernel" to calculate LFPs from unit recordings. The kernel includes both a temporal and a spatial component (Figure 30).

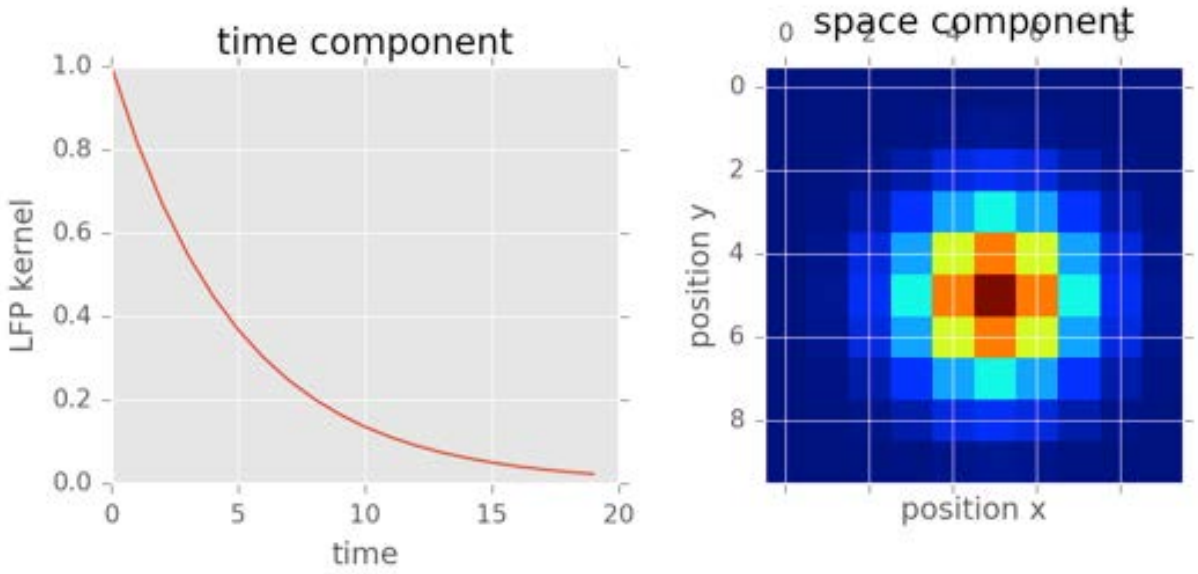

Figure 30 Temporal (left) and spatial (right) component of the simulated LFP kernel.

Note that the LFP kernel of each cell is centered at the position of the cell (here center of the electrode array)

To simulate the LFP, one applies a spatio-temporal convolution of the binned population spike counts with the LFP kernel, as shown in Figure 31.

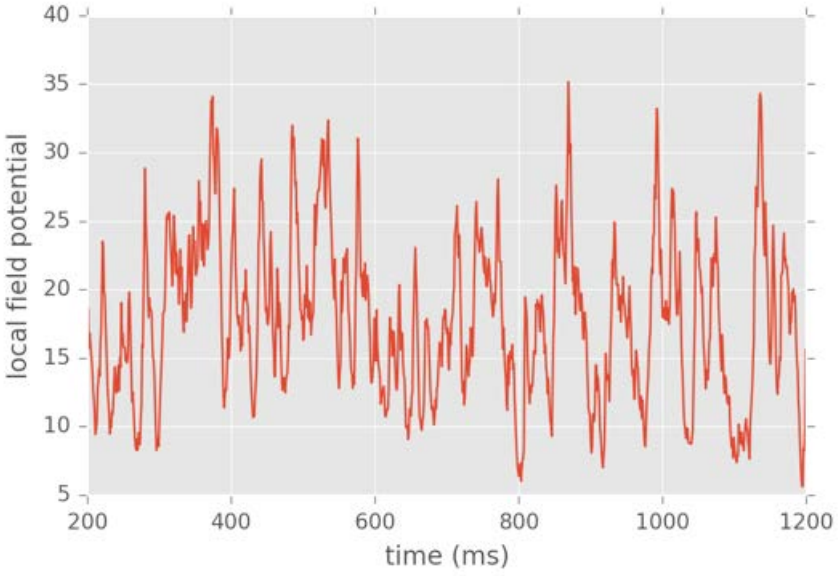

Figure 31 Example of simulated LFP

To verify that our model correctly accounts for the data, we calculated a LFP averaged on spikes of one of the simulated single neurons (spike-triggered LFP average, st-LFP; see Figure 32). As expected, the st-LFP is extended in space and time. This phenomenon could be responsible for broadening of the LFP signals recorded experimentally.

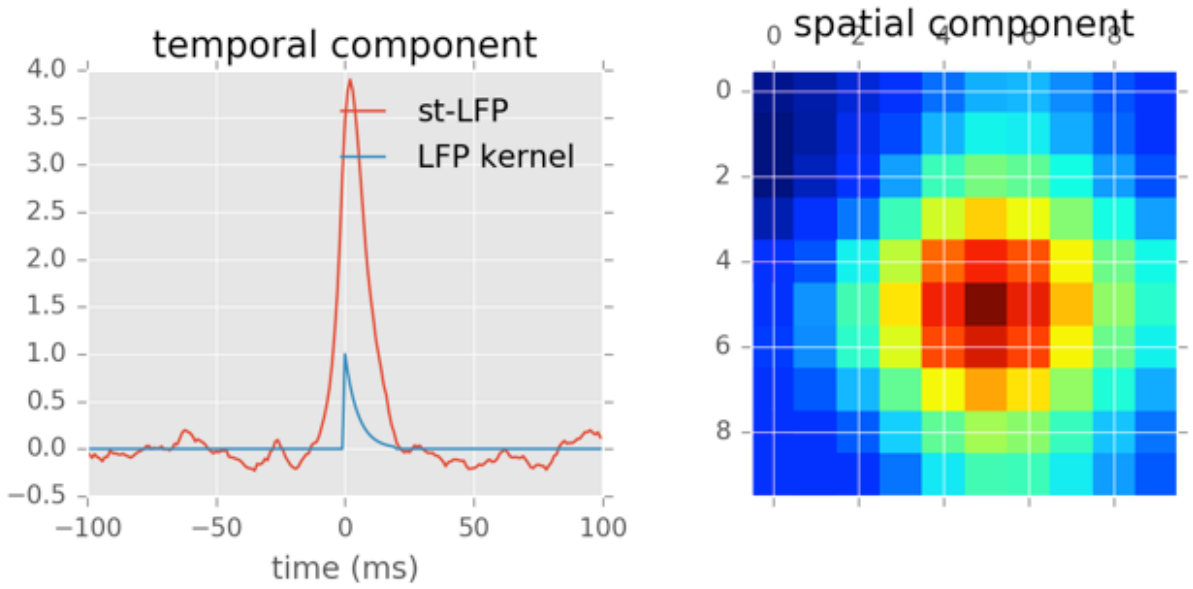

Figure 32 The spike-triggered LFP (st-LFP) calculated from simulated LFP.

Left: Comparison between spike-triggered LFP (red) and the used LFP kernel (blue). Note that the st-LFP is of higher amplitude and broader in time due to the effects of the correlations. Right : Spatial component of the st-LFP. The st-LFP is spatially broader than the LFP kernel (compare with Figure 30, right panel)

Implementation to platforms

This model was integrated to the collaboratory and the Model Catalog in SP5.

Publications

Telenczuk, B., Dehghani, N., Le Van Quyen, M., Cash, S., Halgren, E., Hatsopoulos, N.G. and Destexhe, A. Local field potentials primarily reflect inhibitory neuron activity in human and monkey cortex. Nature Scientific Reports 7: 40211, 2017.

Achieved Impact

This model is presently being written in a form usable by anyone in the HBP, to calculate LFPs from any spiking neuron simulation in HBP.

Conclusion & Outlook

This simplified model calculates the LFP from unit activity, based on the kernels calculated from human Utah-array recordings. It can be applied to any spiking neuron simulations. Three extensions are needed: (1) apply the model to a known case where LFP and unit activity are known, and compare the modeled LFP with the recorded LFP; (2) compare this model with the hybrid scheme for calculating LFPs; (3) release a python package so that any spiking network simulation can integrate the LFP signal.

Component Dependencies

Summarized links to components this key result depends on.

Component ID	Component Name	HBP Internal	Comment
N/A	*N/A*	*N/A*	*N/A*

2.1.16 Models of local magnetic fields (T4.1.4)

Description of the model

In the last couple years, the UNIC partner has worked on models of the local magnetic field (LMF). The LMF is measured in the neuronal tissue, and is therefore the magnetic correspondent to the LFP. However, in contrast to the LFP which is generated by membrane currents, the LMF is mostly generated by axial currents which are invisible to the LFP. We published a mixed experimental and modeling work of the LMF generated by muscle fibers (Barbieri et al., Nature Sci Reports, 2016) and we are now extending this approach to model the LMF generated by a population of hippocampal neurons.

The first part of this modeling work consisted of building a model of the LMF based on experimental measurements of LMF using a new device, the Magnetrode (Barbieri et al., 2016). This study recorded the LMF from muscle fibers, which can produce relatively strong magnetic fields. In addition, the propagation of the action potential (AP) in the muscle fiber is well understood and there exists computational models that can be used. Thus, we designed a computational model of AP propagation along the muscle fiber, which was modeled as a cylindrical cable composed of one thousand compartments of 10 µm length and 40 µm diameter. All compartments had a membrane capacitance of 1 µF/cm 2 and were endowed with sodium currents, TEA- and 4AP-sensitive potassium currents, Kir and leak currents. The central compartment of the cable was additionally provided with a mono-exponential excitatory synaptic current. In order to characterize the passive and active currents and the synaptic input, we started from the parameters obtained from voltage-clamp recordings on xenopus culture myocytes . We then adjusted those parameters in order to reproduce the AP shape recorded in the skeletal muscle cell. Figure 33 shows the comparison between the average AP across recordings and the simulated AP.

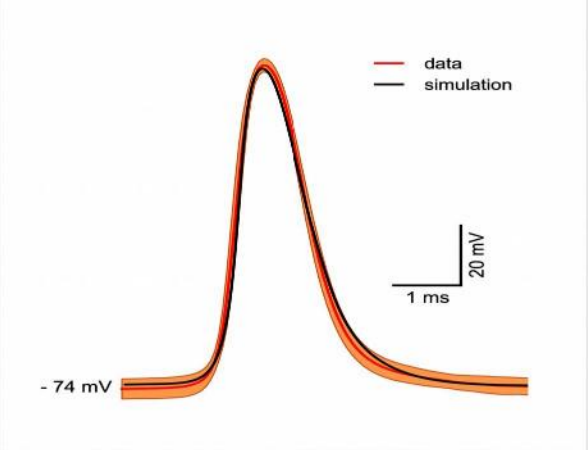

Figure 33 Comparison between action potential recorded in the mouse soleus muscle (red) and simulations.

All simulations were performed using the NEURON simulation environment (Hines and Carnevale 1997).

To calculate the LMF, we used the analytical approach developed by Roth and Wikswo (1985) for an axon in a nerve bundle, and we generalized it to the case of an arbitray arrangement of cylindric cables. The method of Roth and Wikswo (1985) consists in writing, in Fourier frequency space, the expression of the potential for each region of different conductivity, as an expansion in the eigenfunctions of Laplace's equation in cylindrical coordinates. The coefficients in these expansions were then determined from boundary conditions at the surfaces between regions. By differentiating the expressions of the potentials, it is then possible to calculate the current densities, through the relationship $J = -\sigma \nabla\varphi$, where J, σ and φ represent respectively the current density, the conductivity and the potential. From the expressions of the current densities, the azimuthal component of the MF was then calculated using Ampere's law. Because intra- and extra-cellular currents flow in opposite directions, each producing a LMF of opposite sign, we can expect that the LMF generated by the extra-cellular currents could screen, at least partially, the LMF generated by the intra-cellular currents. Using Ampere's law permits to evaluate the importance of these effects by calculating the contributions due to the different currents involved.

The MF generated by the entire muscle was calculated from the MF of each single fiber at different distances from the center, by using the superposition principle . The peak-to-peak amplitude of the magnetic signal calculated at a close distance from the muscle ranged between 3 and 12 nT, when varing the conductivities, σρ and σz , in a range of plausible values. Figure 34 shows that, taking into account the effect due to the dimension of the probe, the agreement between the theoretical and experimental magnetic signal was excellent, both in its amplitude and temporal pattern, for a set of biologically plausible values.

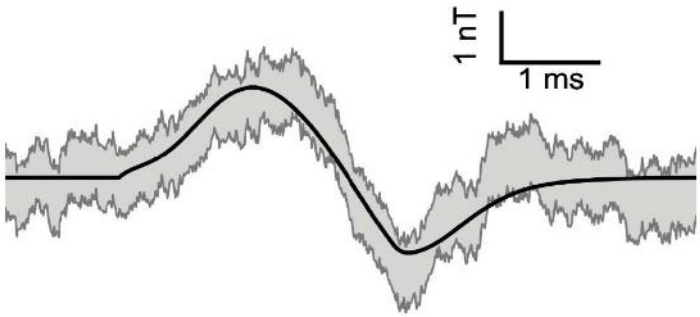

Figure 34 Magnetic field generated by the entire muscle. Comparison between experimental recordings using magnetrodes (gray; Barbieri et al., 2016), with simulations from a computational model comprising 900 fibers

To understand the magnetic fields generated by neurons, our first approach will be to use that model combined with the model of hippocampal slice that we are presently investigating (see Annexe : 2.2 *Models of hippocampal LFP and local magnetic fields (T4.1.4*)). This work will be done in SGA2.

References

Hines, M. L. and N. T. Carnevale (1997). The NEURON simulation environment. Neural computation 9 (6), 1179–209.

Roth, B. and J. Wikswo (1985). The electrical potential and the magnetic field of an axon in a nerve bundle. Mathematical biosciences 76 (1), 37–57.

Implementation to platforms

This model was integrated in the Model Catalog in SP5.

Publications

Barbieri, F., Trauchessec, V.. Caruso, L., Trejo Rosillo, J., Telenczuk, B., Paul, E., Bal, T., Destexhe, A., Fermon, C., Pannetier-Lecoeur, M. and Ouanounou, G. Local recording of biological magnetic fields using Giant Magneto Resistance-based micro-probes. Nature Scientific Reports 6: 39330, 2016.

Achieved Impact

This model is now used to calculate magnetic fields generated by larger-scale models of the hippocampus.

Conclusion & Outlook

This model provides a way to calculate the LMF based on detailed NEURON simulations. It can be potentially applied to any model using cellular morphologies, and dendrites. This model will be continued in SGA2, aiming to contribute to understanding magnetic signals at larger scales, such as in magneto-encephalography.

Component Dependencies

Summarized links to components this key result depends on.

Component ID	Component Name	HBP Internal	Comment
N/A	*N/A*	*N/A*	*N/A*

2.1.17 Models of hippocampal LFP and local magnetic fields (T4.1.4)

See HBP SGA1 M24 D472_ANNEX_restricted – 2.2 Models of hippocampal LFP and local magnetic fields (T4.1.4).

Achieved Impact

UNIC expect that this model will be extended towards calculating LFPs and magnetic fields generated by larger-scale models of the hippocampus.

Conclusion & Outlook

UNIC have shown that unitary inhibitory fields which are recorded in the hippocampus are originating from the synaptic distribution of basket cells placed on the somatas of pyramidal cells. Furthermore, we show that excitatory unitary may also be recordable from the hippocampus and that they contribute towards total appearance of the LFP in the hippocampus. This model not only tests a biophysical hypothesis concerning the strong contribution of inhibitory synaptic currents to LFPs. It can be applied to generate either simplified models, such as phenomenological models of the LFP, or more detailed models, such as large-scale models of neocortex or hippocampus.

We are presently integrating the calculation of the magnetic field by the hippocampal slice population. This work will be done in SGA2.

Component Dependencies

Summarized links to components this key result depends on.

Component ID	Component Name	HBP Internal	Comment
N/A	*N/A*	*N/A*	*N/A*

2.1.18 Improved LFP model with quasi-active conductances (T4.1.4)

Description of the model

NMBU: The local field potential (LFP), the low-frequency part of extracellular potentials recorded in neural tissue, is often used for probing neural circuit activity, however, interpreting the LFP signal in terms of neural activity is challenging, as in general thousands of neurons contribute to the recorded signal (Lindén et al., Neuron, 2011). While the cortical LFP is thought mainly to reflect synaptic inputs onto pyramidal neurons, little is known about the role of the various subthreshold active conductances in shaping the LFP (Einevoll et al., Nat Rev Neurosci, 2013).

By means of biophysical modelling, the NMBU partner has obtained a comprehensive qualitative understanding of how the LFP generated by single pyramidal neurons (Ness et al., J Physiol, 2016) and simple cortical populations (Ness et al., in review by J Neurosci) depends on active subthreshold currents, and we have identified the key role of the hyperpolarization activated I_h-current in shaping the LFP.

In particular it was found that the I_h-conductance could cause a strong peak in the LFP power spectrum (LFP-PSD) for synaptic input that selectively targeted the apical dendrite of either single-cells or cortical populations (Figure 35, top row, Ness et al., 2016). Such peaks are traditionally interpreted in terms of oscillatory neuronal spiking activity, but importantly, these

results demonstrate that peaks in the LFP-PSD can also be caused by the I_h-conductance in absence of any network oscillations.

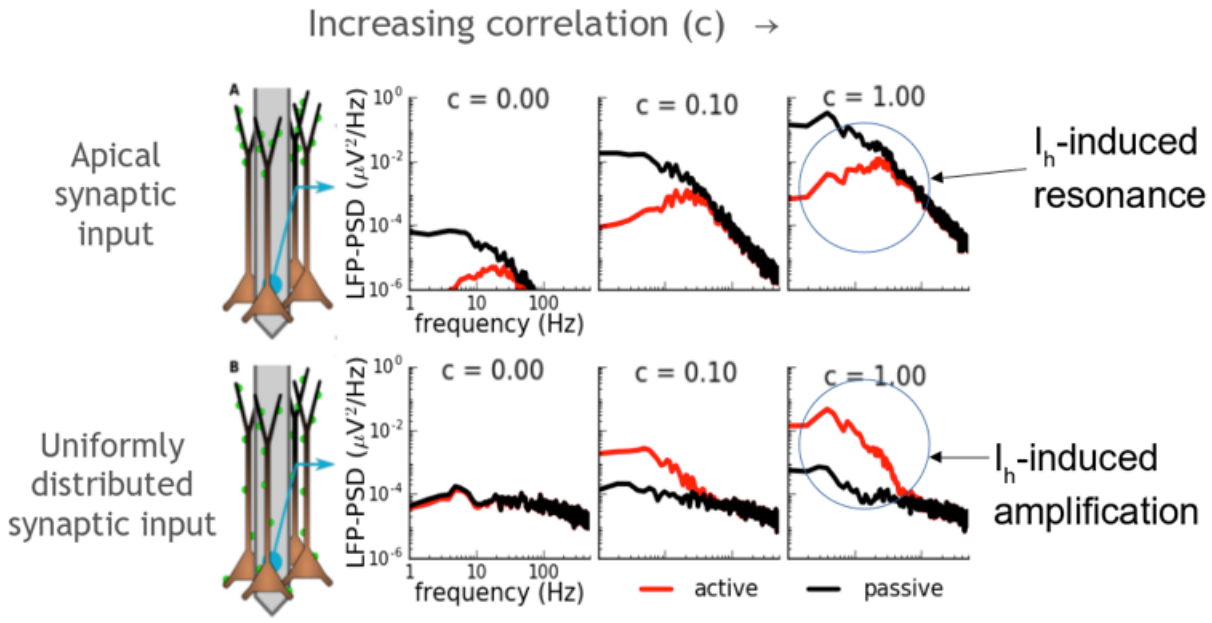

Figure 35 The LFP power spectrum (LFP-PSD) from cell populations with 4,000 L5 pyramidal cells receiving synaptic input with different levels of correlations (columns) to the apical dendrite (top row) or uniformly distributed (bottom row).

The cell models either contain all original active conductances (red), or all active conductances have been removed (black). It was confirmed that the difference between the two cases was caused almost exclusively by the I_h-conductance.

Furthermore, it was demonstrated that cortical populations which received uniformly distributed (Figure 35, bottom row) and correlated synaptic input, exhibited a very strong I_h-induced low-frequency amplification of the LFP-PSD, and the strength of this amplification could be more than two orders of magnitude (Ness et al., in review).

These two different effects of the same I_h-conductance based on the parameters of the synaptic input, i.e., a resonance peak in the LFP-PSD for distal apical synaptic input, and a low-frequency amplification for uniformly distributed correlated synaptic input, was reproduced for many different cell models, and under many different circumstances, demonstrating that it was a robust phenomenon. Using quasi-active conductances we were able to obtained a good qualitative understanding of the underlying mechanisms, and make experimentally testable predictions for when and how the I_h-conductance can shape the LFP.

We believe that this work is an important step in the direction of a better understanding of the cortical LFP signal, which is needed to take full advantage of this brain signal in the future.

Implementation to platforms

Component 896, "Improved LFP model with quasi-active conductances" (T4.1.4).

Implementation to platforms

Model Catalog entry name: Effect of active conductances on LFP from cortical population.

The model is also implemented in its own Collab: "Active conductances and LFPs from single cells", where the model can be used to reproduce the main findings from Ness et al. (2016):

https://collab.humanbrainproject.eu/#/collab/5170/nav/40008

Publications

Ness, Remme, Einevoll (2016) *Active subthreshold dendritic conductances shape the local field potential*. J Physiol 594:3809–3825.

Ness, Remme, Einevoll, *h-type membrane current shapes the local field potential (LFP) from populations of pyramidal neurons.* Under review by Journal of Neuroscience.

Achieved Impact

This model has proven very valuable in understanding the effect of subthreshold active conductances on the LFP, and the publication on the effect of active conductances on the LFP from single neurons was chosen for a Perspective article by Journal of Physiology (Nolan, 2016, *Local field potentials get funny*. J Physiol 594:3487–3488).

The developed model has also been adopted and used in at least one independent research project: Aspart et al., *Differential polarization of cortical pyramidal neuron dendrites through weak extracellular fields,* bioRxiv 216184.

We expect the model to be very useful for estimating the effect of active conductances on brain signals like the LFP, ECoG, EEG and MEG in future studies with larger neural networks.

Conclusion & Outlook

The main goal of "WP4.1 – Bridging scales" is to provide models linking different scales of investigation, and we have developed a model for investigating how the microscopic subthreshold active ion-channels can effect the mesoscopic LFP signal from single cells and small neural populations. This model will in the years to come be equally applicable to macroscopic large-scale neural network models and predictions of non-invasive brain signals like the EEG and MEG. In our work we identified the potential key importance of the I_h-conductance in shaping the LFP from cortical populations, and used our model to make experimentally testable predictions of how and when the I_h-conductance will affect the LFP.

Component Dependencies

Summarized links to components this key result depends on.

Component ID	Component Name	HBP Internal	Comment
101	*Nmc-portal (service)*	*Yes*	*We used cell models from the nmc-portal: https://bbp.epfl.ch/nmc-portal*
208	*NEURON (software)*	*No*	*The NEURON simulator was used for all neuron simulations*

2.1.19 Simplified EEG models (T4.1.4)

Description of the model

The NMBU partner has developed a simplified and memory efficient formalism for calculating electroencephalography (EEG) signals from neural simulations with detailed multi-compartment cell models. This will help relating large-scale brain simulations to experimentally measurable quantities like the EEG, and also greatly simplify analysis by simplifying the link between the EEG signal and the underlying neural sources.

Extracellular potentials arising from multi-compartment cell models are often calculated by a compartment-based approach (CB model), by summing the contributions to the extracellular potential from each cellular compartment (Figure 36A). We have developed and implemented an alternative dipole-based approach (DB model), where the extracellular potential following arbitrary neural activity is approximated by a single time-dependent dipole (Figure 36B). The extracellular potential from a single cell can have a complex shape close to the cell (Figure 36C),

and the dipole approximation is often not suited to represent the extracellular potential in this region (compare Figure 36C and Figure 36D). However, the extracellular potential will tend towards a more dipolar shape as the distance from the cell increases, making the the DB model suitable for approximating the contributions from cell models to signals such as the EEG and MEG, which are measured non-invasively outside the head (compare Figure 36E with Figure 36F). This approach can easily be added to existing large-scale network simulations, where each cell can be represented as a single current dipole, or the dipoles of all cells in different neural sub-populations can be summed to obtain population dipoles, greatly simplifying the connection between the EEG and the underlying signal generators.

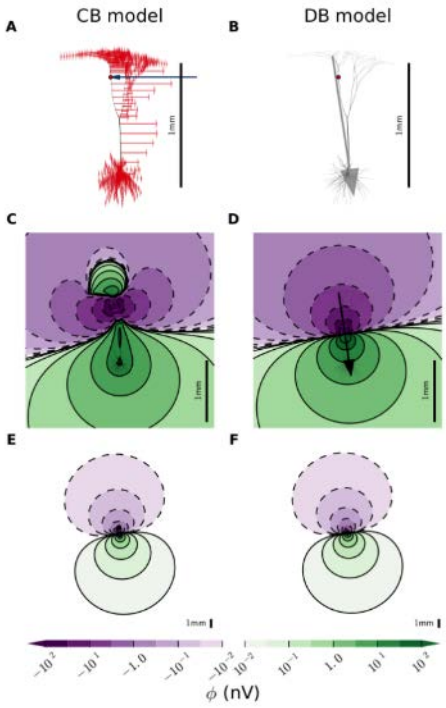

Figure 36 Extracellular potentials become increasingly dipolar with distance from the source.

A: A single synaptic input (red dot) to a pyramidal cell model gives rise to an extracellular potential. In the compartment-based model, the contribution to the extracellular potential from the current of each cell compartment (red arrows) is summed. B : In the dipole-based model, a single time-dependent dipole is instead used to approximate the contribution to the extracellular. C, D: Cross-section of the extracellular potential close to the cell for a chosen time-point. E,F: same as C,D but showing a larger region (zoomed out).

To calculate the EEG signals arising from neuronal current dipoles requires a head model. A good starting point for building intuition and benchmarking more complicated numerical methods is the analytic four-sphere model, which takes into account the different electrical conductivity of the brain, cerebrospinal fluid (CSF), skull and scalp (Figure 37A). We found serious typographical errors in formulas presented in literature (Nunez & Srinivasan, 2006, *Electric Fields of the Brain*), and presented in Næss et al. (2017) a corrected version of the four-sphere model, with accompanying open-source code, that had been numerically validated by the Finite Element Method (FEM; Figure 37B, Figure 37C). Note that the obtained current-dipoles can also be used in combination with arbitrarily complicated head models.

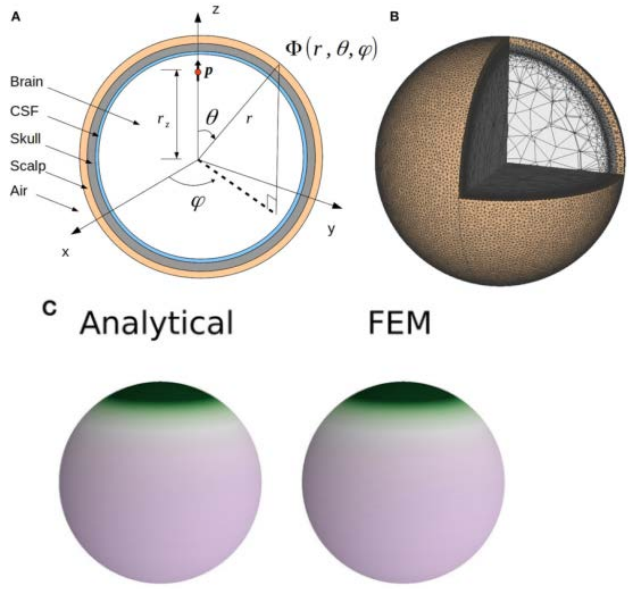

Figure 37

A: Four-sphere head model, with different conductivity for the brain, cerebrospinal fluid (CSF), skull and scalp. B: A finite element mesh of the four-sphere model for validation of the analytic four-sphere model. C: The analytic and the FEM version of the four-sphere models give indistinguishable EEG surface potentials for current dipoles in cortex (Næss et al. 2017)

Implementation to platforms

Component 902, "Simplified EEG models" (T4.1.4).

Implementation to platforms

The four-sphere model has been implemented in the model catalog: "Corrected Four-Sphere Head Model for EEG Signals"

Publications

Næss, Chintaluri, Ness, Dale, Einevoll, Wójcik, 2017, *Corrected Four-Sphere Head Model for EEG Signals*. Front Hum Neurosci 11:1–7.

Næss, Ness, Hagen, Halnes, Halgren, Dale, Einevoll. *Biophysical modeling of single-neuron and population contributions to ECoG, EEG and MEG signals.* In preparation.

Achieved Impact

This model is already in use in several different research projects, and we expect it to be very valuable for understanding the biophysical origin of the EEG signal.

Conclusion & Outlook

We have implemented and verified the calculation of current dipoles, based on arbitrary neural activity in multi-compartment neurons, and a natural next step is to add this calculation of current dipoles to existing large-scale network simulations. This will allow for predictions of EEG signals based on either the simple four-sphere head model, or more realistic head models. The relative contribution to the EEG signal from different neuronal sub-populations can then be quantified, and we can test the feasibility of obtaining direct mappings from sub-population firing rates and population current dipoles. If feasible, this would allow for predictions of EEG signals directly from point-neuron network simulations or mean-field models while still being firmly rooted in the underlying biophysics.

This four-sphere model will also be implemented in the open-source software LFPy2.0, which runs on top of the NEURON simulator, allowing for easy simulation of EEG and MEG signals within a well-established software tool.

Component Dependencies

Summarized links to components this key result depends on.

Component ID	Component Name	HBP Internal	Comment
84	*Simplified EEG models*	*Yes*	*Human cell models were used for estimating the EEG contribution of different cell-types*
209	*NEST – The Neural Simulation Tool (software)*	*No*	*NEST was used for network simulations*
660	*NEST Support for Modellers (service)*	Yes	We received support in developing our NEST simulations
208	*NEURON (software)*	No	The NEURON simulator was used for biophysically detailed neuron simulations
896	*Improved LFP model with quasi-active conductances*	*Yes*	*This framework will be used to investigate the impact of active conductances on the EEG signal*

2.2 Generic Models of Brain circuits (WP 4.2)

2.2.1 Simplified network models of different cortical areas (T4.2.1)

The JUELICH partner has developed a layer-resolved multi-area spiking model of all vision-related areas of the macaque cortex (Figure 38). The model builds on a 1 mm^2 cortical microcircuit model which was developed previously (Potjans and Diesmann, Cereb Cortex, 2014) and which we ported to different platforms in this Task. The models consist of excitatory and inhibitory leaky integrate-and-fire neurons connected with population-specific connection probabilities and all neurons receiving an independent, homogeneous Poisson drive. Each area in the multi-area model is represented by a 1 mm^2 microcircuit with the full density of neurons and synapses. During the past year, we have described the porting of this model to the Collaboratory (Senk et al., LNCS, 2017), SpiNNaker (van Albada et al., in revision), and Open Source Brain (Gleeson et al., BioRxiv, 2018).

As a first step toward the multi-area model, a population-resolved connectivity map was derived from axonal tracing data, cortical architecture and geometry, and statistical regularities (Schmidt et al., Brain Struct Func, 2017; Figure 38). Assuming a constant volume density of synapses, a hierarchical trend in neuron density yields larger numbers of synapses per neuron (indegrees) in higher areas. Statistical mapping of the laminar location of synapses to the location of the target cell bodies leads to the prediction that feedback also targets layer 4 neurons. The combined quantification of neuronal population sizes and connectivity enables translation between different connectivity measures, such as connection probabilities and indegrees, and yields the fundamental data needed to formulate dynamical models of the system at cellular resolution.

Based on this connectivity matrix and model definition, the JUELICH partner has performed large-scale simulations on the JUQUEEN supercomputer and validated the model by comparisons with experimental resting-state data (Schmidt et al., in revision) including V1 spiking data (Chu et al., CRCNS.org, 2014; Figure 39) and fMRI functional connectivity (Shen et al., J Neurosci, 2015; Fig. 1D). The model reproduces slow fluctuations not present in the isolated microcircuit model. The correspondence between predicted and measured spiking activity and functional connectivity is best for intermediate cortico-cortical connection strengths, where the network is in a metastable regime. This matches earlier work on multi-area models with simplified equations for the individual areas (Deco et al., PNAS, 2009; Cabral et al., NeuroImage, 2011, Deco et al., J Neurosci, 2012), and shows how the microscopic and macroscopic dynamics of cortex can be reconciled.

Activity in the model propagates predominantly in the feedback direction, akin to findings during visual imagery and sleep (Nir et al., Neuron, 2011; Dentico et al., NeuroImage, 2014; Sheroziya

and Timofeev, J Neurosci, 2014). Our recent work shows that this is due to the most unstable eigenvector of the network's effective connectivity having its largest entries in parietal cortex, where activity bursts originate in the model and propagate to temporal and occipital areas. This is a global network effect, as the stability of the areas in the model considered separately is not systematically related to the order of area activations.

Stronger cortico-cortical synapses onto inhibitory than onto excitatory neurons keep the model in a regime with plausible spike rates. Accordingly, a population-resolved Granger causality analysis shows more significant cortico-cortical interactions onto inhibitory than onto excitatory populations. Furthermore, the analysis shows that substantial effective communication can arise over a range of connection strengths due to the influence of the dynamical state of the populations, but that the weakest connections do not contribute significantly to communication.

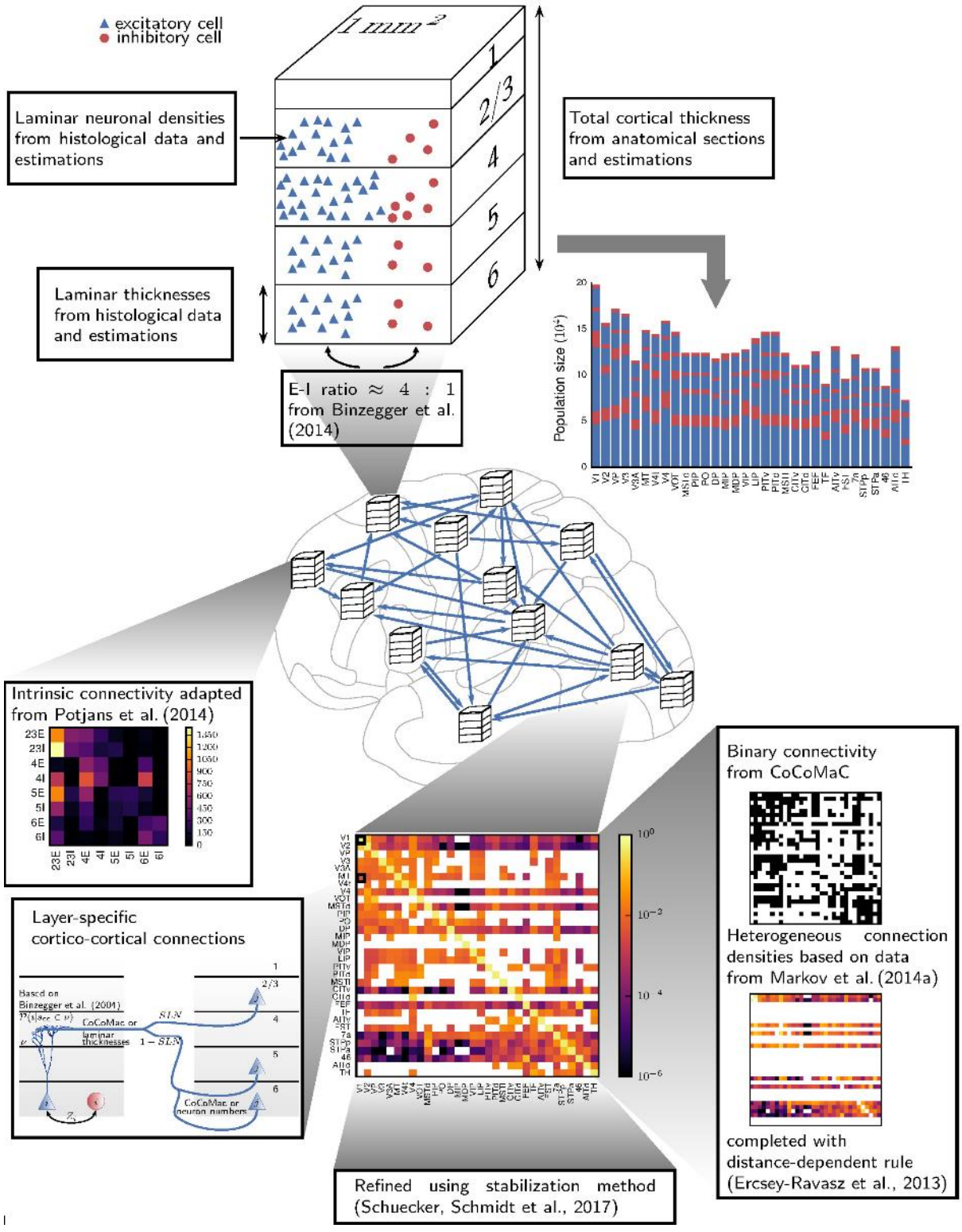

Figure 38 Construction principles of the model.

Top: Determination of the population sizes. Bottom: Construction of the model connectivity. Local connectivity within areas is based on the microcircuit model of Potjans and Diesmann (2014). Cortico-cortical connections are first determined on the area level from binary data from the CoCoMac database and quantitative tracing data from Markov et al. (2014), which is completed using the exponential fall-off of connection density with inter-areal distance (Ercsey-Ravasz et al., 2013). The resulting connectivity spans six orders of magnitude, as shown in the matrix plot of area-averaged indegrees (center bottom). Synapses between each pair of cortical areas are then distributed over source and target layers based on layer-specific tracing data from Markov et al. (2014) and CoCoMac. Synapses in the receiving area are subsequently assigned to cells according to layer- and cell-type-specific dendritic densities from Binzegger et al. (2004). These derivations result in disctinct laminar patterns between feedforward, feedback, and lateral connections. Based on a theoretical method using mean-field theory

(Schuecker et al., PLoS CB, 2017), the resulting connectivity matric is refined to improve the phase space of the network.

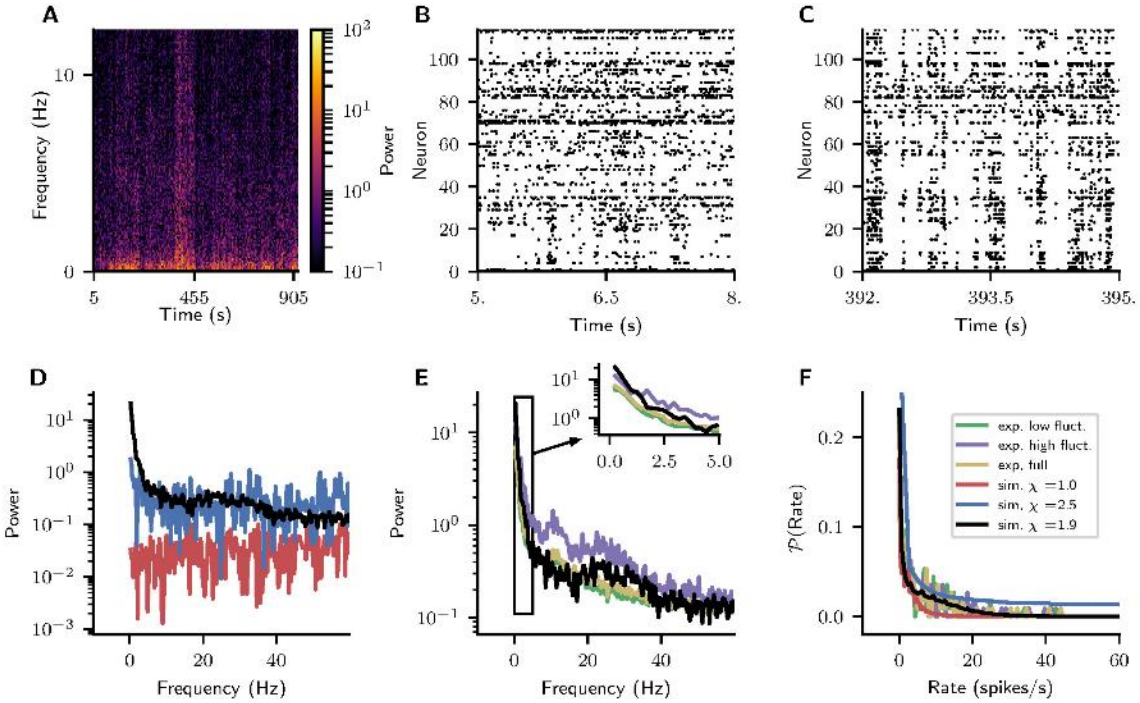

Figure 39 Comparison of the V1 spiking dynamics with spike recordings from 140 neurons across all layers in V1 of lightly anesthetized macaque (Chu et al., CRCNS.org, 2014).

(A) Spectrogram of the spike histogram across all neurons. (B) Raster plot of spiking activity for the initial recording phase. (C) Raster plot of spiking activity in the later recording phase, with higher synchrony presumably indicating drowsiness. Neurons are sorted according to depth of the recording electrodes with neurons closest to the surface of the brain at the top. (D) Power spectral density of spike histograms for the three different simulations with weak (χ=1), intermediate-strength (χ=1.9), and strong (χ=2.5) cortico-cortical synapses. (E) Comparison of simulated power spectral density with χ=1.9 (black) with experimental recording during low-fluctuation (green) and high-fluctuation (purple) phases and the full recording (yellow), and simulated activity of 140 neurons (grays) and all neurons (black) across all populations of area V1. Inset : enlargement for frequencies up to 5Hz. (F) Distribution of spike rates across single cells in experimental data (green, purple, yellow) and for simulated spike trains across all layers and populations of V1.

Implementation on platforms

The microcircuit model of Potjans and Diesmann was already implemented on the High-Performance Analytics & Computing platform, and in this Task has been additionally ported to the Collaboratory and to the Neuromorphic Computing Platform.

The multi-area model has been implemented on the High-Performance Analytics & Computing platform, has been made available within HBP via the collaboratory, and will be made available via GitHub. Both the microcircuit model and the multi-area model have been added to the model catalog.

Publications

Gleeson P, Cantarelli M, Marin B, … van Albada SJ, van Geit W, R Silver RA. Open Source Brain: a collaborative resource for visualizing, analyzing, simulating and developing standardized models of neurons and circuits (2018) bioRxiv:29484

Schmidt M, Bakker R, Hilgetag CC, Diesmann M, van Albada SJ. Multi-scale account of the network structure of macaque visual cortex (2017) Brain Struct Func.

Schmidt M, Bakker R, Shen K, Bezgin G, Diesmann M, van Albada SJ. A multi-scale layer-resolved spiking network model of resting-state dynamics in macaque cortex. In revision.

Schuecker J, Schmidt M, van Albada SJ, Diesmann M, Helias M. Fundamental activity constraints lead to specific interpretations of the connectome (2017) PLoS CB 13(2):e1005179.

Senk J, Yegenoglu A, Amblet O, Brukau Y, Davison A, Lester D, Lührs A, Quaglio P, Rostami V, Rowley A, Schuller B, Stokes A, van Albada SJ, Zielasko D, Diesmann M, Weyers B, Denker M, Grün S. A Collaborative Simulation-Analysis Workflow for Computational Neuroscience Using HPC (2017) In: Di Napoli E, Hermanns MA, Iliev H, Lintermann A, Peyser A (eds) High-Performance Scientific Computing. JHPCS 2016. Lecture Notes in Computer Science, vol 10164, pp. 243–256. Springer, Cham.

van Albada SJ, Rowley AG, Senk J, Hopkins M, Schmidt M, Stokes AB, Lester DR, Diesmann M, Furber SB. Performance comparison of the digital neuromorphic hardware SpiNNaker and the neural network simulation software NEST for a full-scale cortical microcircuit model. In revision.

Component Dependencies

Summarized links to components this key result depends on.

Component ID	Component Name	HBP Internal	Comment
777	4x4 mm2 motor cortex model (model)	Yes	Generation of cortical mesocircuit model
944	Full density model of cortical microcircuit	Yes	Model has been published as Potjans TC and Diesmann M (2014)
348	Component 115-3: Elephant (software)	Yes	Software used for analysis of neural activity data
1207	Large-scale model of visuo-motor integration	Yes	Model
885	Macaque connectivity database (CoCoMac)	No	CoCoMac connectivity database (axonal tract-tracing) in a standard nomenclature
660	NEST Support for Modellers	Yes	Component provides support to groups using NEST as simulation tool
209	NEST - The Neural Simulation Tool	Yes	Software for simulation of mesocircuit model
330	HPC systems at JSC	Yes	HPC infrastructure used for simulation
517	Rule-and data-based connectivity generation in NEST	Yes	Software
679	SP6-T6.3.6-SGA1-Tools for configuring stimulation and recording in NEST simulations	Yes	Software
682	SP6-T6.3.6-SGA1-Tool for LFP recording in NEST simulations	Yes	Software
419	Python	No	Software
1851	T3.2.3(1) Detailed dynamical laminar organization in different	Yes	Data

	cortical areas (under consideration)		
373	Collaboratory Storage Service	Yes	Data storage for experimental data used in reproducible analysis workflow
2678	Prototype implementation of unified connectivity generation scheme for very large networks	Yes	Software
1030	Mean-field models of interacting populations of rate and spiking neurons	Yes	Model
861	SP2- Selective attention in perception and learning in humans and monkeys	Yes	Model
862	SP2- Ultra-high field fMRI of sub-units in higher-level visual areas and face areas in human and monkey	Yes	Data
662	NEST Requirements Management	Yes	Service
237	VisNEST	No	Software
819	Mouse cortical regions for object recognition learning	Yes	Data
2907	Synapse turnover in long-range projections	Yes	Data
324	Federated data storage with flexible permission management and remote access	Yes	Data storage for experimental and simulated data to be used in validation workflow

2.2.2 Model for neuron-glia interactions and dimensionality reduction (T4.2.2)

Description of the new model

The TUT partner has worked on modeling neuron-astrocyte interactions in order to provide computational models that can facilitate better understanding of the role of glial cells, specifically the astrocytes, in synaptic and network level plasticity and learning (Havela et al. 2017). The developed model is complex, consisting of a large number of equations. In brief, the well-established biophysical and biochemical mechanisms are described for the neuronal compartments. The astrocyte compartment of the model is presented as follows. The differential equation for the astrocytic calcium concentration is given as

$$\frac{d[Ca^{2+}]_{astro}}{dt} = J_{IP3R} + J_{leakER} - J_{SERCA},$$

where the major calcium processes in the astrocyte process are described by IP_3R channel (J_{IP3R}), leak current into the cytoplasm from the ER (J_{leakER}), and sarco/ER calcium-ATPase (SERCA) pump (J_{SERCA}). The calcium and IP_3 concentrations, as well as the active fraction of IP_3Rs, are modelled according to several earlier studies further analysed by Manninen et al. 2017 and Manninen et al. (in press). The differential equation for the astrocytic IP_3 concentration is given as

$$\frac{d[IP_3]_{astro}}{dt} = \frac{IP_3^* - [IP_3]_{astro}}{\tau_{IP3}} + r_{IP3}[2AG],$$

where IP_3^* = 0.16 μM is the baseline of IP_3 in the cytoplasm in the resting state, τ_{IP3} = 7000 ms is the IP3 decay rate, r_{IP3} = 0.0005 ms-1 is the IP_3 production rate, and [2*AG*] is the concentration of endocannabinoid (2-AG) released from the postsynaptic neuron. A classical stimulation protocol of long-term plasticity was used to test the model functionality.

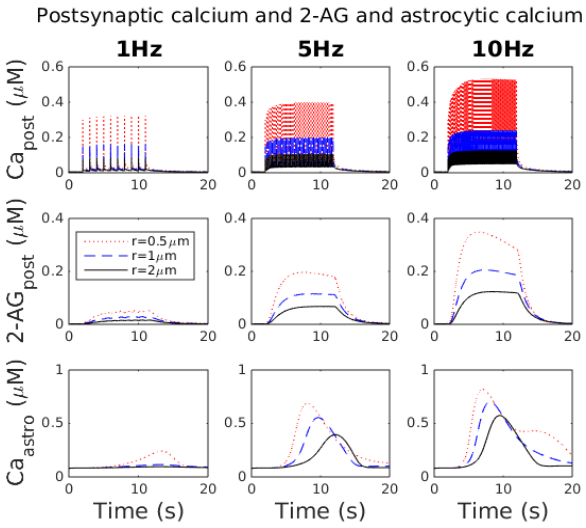

Figure 40 Simulation of the model by varying the frequency of the stimuli and the volume of the postsynaptic terminal (equivalent to spine).

Stimulation frequencies used were 1 Hz, 5 Hz, and 10 Hz. Top row) Postsynaptic calcium levels with spine radius 0.5, 1, and 2μm. Middle row) 2-AG production with spine radius 0.5, 1, and 2μm. Bottom row) Astrocytic calcium responses with spine radius 0.5, 1, and 2 μm. (Havela et al. 2017).

As an extension of the work, dimensionality reduction was applied to a nonlinear mathematical model of synaptic signal transduction pathway related to neuron-astrocyte interactions (Lehtimäki et al. 2017). A combination of Proper Orthogonal Decomposition (POD) and Discrete Empirical Interpolation Method (DEIM) was used to simulate the system dynamics in a lower dimension without losing the complexity of the model. This a fundamental step required to analyze the system dynamics for the mathematical abstraction of astroglial functions and, consequently, for novel plasticity algorithms.

In summary, we report here the first results of a model that has the potential to become a prototype synapse model involving neuron-glia interactions to modulate synapses in network models. The integrated model was validated against typical neuronal spiking and astrocyte calcium excitability data. The model was able to capture the dynamical responses of both neurons and

astrocytes during the simulation of the full model when varying the frequency of the stimuli and the volume of the postsynaptic neuron compartment (Figure 40). As an extension of the work, dimensionality reduction was shown to consume considerably less computational resources than the original model. Dimensionality reduction is an essential theoretical tool for improving the scale and quality of future computational models of the brain by connecting reduced small scale models via the inputs and outputs to form optimally performing large scale models as well as for abstracting the dynamics of complex biophysical models.

Implementation to platforms

Component ID 70: Astrocyte neuron interaction SYNAPSE model (ANI model) (T4.2.2.).

Implementation to platforms

This model was integrated to the collaboratory and the Model Catalog in SP5.

Publications

R. Havela, T. Manninen, A. Saudargiene, M.-L. Linne. Modeling neuron-astrocyte interactions: towards understanding synaptic plasticity and learning in the brain. Lecture Notes in Computer Science 10362 (eds. D.-S. Huang et al.), pp. 157-168, 2017.

https://link.springer.com/chapter/10.1007%2F978-3-319-63312-1_14

M. Lehtimäki, L. Paunonen, S. Pohjolainen, M.-L. Linne. Order reduction for a signaling pathway model of neuronal synaptic plasticity. Proceedings of the 20th IFAC World Congress, 50(1): 7687-7692, 2017.

https://www.sciencedirect.com/science/article/pii/S2405896317316385

Achieved Impact

T4.2.2. has ongoing discussion with SP6 (specifically T6.4.3.) to incorporate the neuron-astrocyte interaction model as part of the somatosensory and other simulation models. Dimensionality reduction was applied to the model to facilitate the analysis of synapse and network model dynamics and development of plasticity algorithms with SP4 collaborations. Novel results were obtained as mathematical model order reduction has not been applied in neuroscience without linearization of the mathematical model and never to the model type used here. In addition, the new models were presented to gliobiologists in several meetings in 2017, both at HBP and externally. The comments were encouraging and several scientists in the field contributed their knowledge to the development of T4.2.2. models.

Component Dependencies

Summarized links to components this key result depends on.

Component ID	Component Name	HBP Internal	Comment
N/A	*Astroglia model evaluation and analysis*	*Yes*	*Evaluation and analysis of simulated data for construction of new neuron-astrocyte interaction model*
358	*Collaboratory Jupyter Notebook*	*No*	*Software/Service*

2.2.3 Evaluation and reproducibility of synapse and network models (T4.2.2)

Description of the evaluation and reproducibility studies

The TUT partner has, in addition to development of the new model, done evaluation and reproducibility studies on existing glial models, both for synapses and networks (more than 100

models published by the end of 2017). Two publications (Manninen et al. 2017, Manninen et al. 2018) summarize the results of these extensive evaluations. We conclude that most of the models are generic in nature, not describing any specific brain region, and they were generated from a small set of previously published models without clear explanation what was built on top of the previous models and what new predictions the models were able to show. Furthermore, only a few of the models are available online which makes it difficult to reproduce the simulation results and further develop the models.

Implementation to platforms

Component ID 70: Astrocyte neuron interaction SYNAPSE model (ANI model) (T4.2.2.).

Component ID 973: Astrocyte-neuron interaction NETWORK model (ANN model) (T4.2.2.).

Implementation to platforms

The reports (the publications) were integrated to the collaboratory (HBP SP4 Collab: Storage repository 'TUT'), with links to reimplemented models in the model repositories. The four models reimplemented in Python and used in Manninen et al. 2017 can be found in ModelDB, Accession number 223648 (https://senselab.med.yale.edu/ModelDB/).

Publications

T. Manninen, R. Havela, M.-L. Linne. Reproducibility and comparability of computational models for astrocyte calcium excitability. Frontiers in Neuroinformatics 11:11, 2017.

https://www.frontiersin.org/articles/10.3389/fninf.2017.00011/full

T. Manninen, R. Havela, M.-L. Linne. Computational models for calcium-mediated astrocyte functions. Frontiers in Computational Neuroscience (in press; doi: 10.3389/fncom.2018.00014).

https://www.frontiersin.org/articles/10.3389/fncom.2018.00014/abstract

Achieved Impact

The evaluation and reproducibility work on glial models has been shared with several other SPs and tasks, including SP4, SP6, specifically T6.4.3., and SP9. T4.2.2 has been in contact with the developers of T6.4.3. and made visits to Geneva and Lausanne to discuss about the component. The work of T4.2.2. will influence the development of biophysically-detailed modeling of glial functions in different brain regions and model types. The work was also instrumental for the development of the new model (Havela et al. 2017, Lehtimäki et al. 2017).

Conclusion & Outlook (TUT)

The new model, and its background material, aims to help integrate the two important components of the brain, the conventionally modeled neuronal system with the less conventionally modeled glial system. This is an important step in SP4 while seeking to understand the neuromodulatory role of astrocytes in large-scale neuronal network dynamics, plasticity and learning. Although there are more than 100 models available we showed that none of the existing models have the capacity to properly represent the cortical astrocytes in plasticity and learning and therefore new validated models are required. The developed model will be utilized in the next period, in particular cortical network dynamics will be studied using a variety of influences from glial cells in synaptic and in extrasynaptic locations.

Component Dependencies

Summarized links to components this key result depends on.

Component ID	Component Name	HBP Internal	Comment
358	*Collaboratory Jupyter Notebook*	*No*	*Software/Service*

2.3 Learning and Memory (WP4.3)

2.3.1 STDP for structural Plasticity (WP4.3)

The EPFL Partner has worked on the problem of structural plasticity: Experimental results of many labs over the last 20 years have shown that synaptic contacts can appear or disappear, but that a pair of nearby cortical pyramidal neurons has either no contact at all or 4-8 contacts. The EPFL partner has developed a mathematical model that summarized synapse formation, growth, and deletion in a small number of phenomenological equations. These equations include Hebbian and anti-Hebbian terms that depend on spike timing as well as heterosynaptic terms that enable to control of firing rates.

Key findings have been

1) The synaptic plasticity model is intrinsically stable even if there are no hard bounds or soft bounds;
2) The synaptic plasticity model enables solutions such that some presynaptic neurons make multiple connections onto a given postsynaptic one whereas others make not contact at all;
3) The distribution of synaptic contact numbers is bimodal, similar to those observed in experiments;
4) The time scale of synapse elimination and synapse survival is consistent with experiments;
5) The synaptic plasticity model is suitable for large networks
6) Large-scale simulations of a simplified model of barrel cortex showed complex reorganization of cortical connectivity after a simulated lesion of whisker input.

The schematics of the model is shown in the next figure:

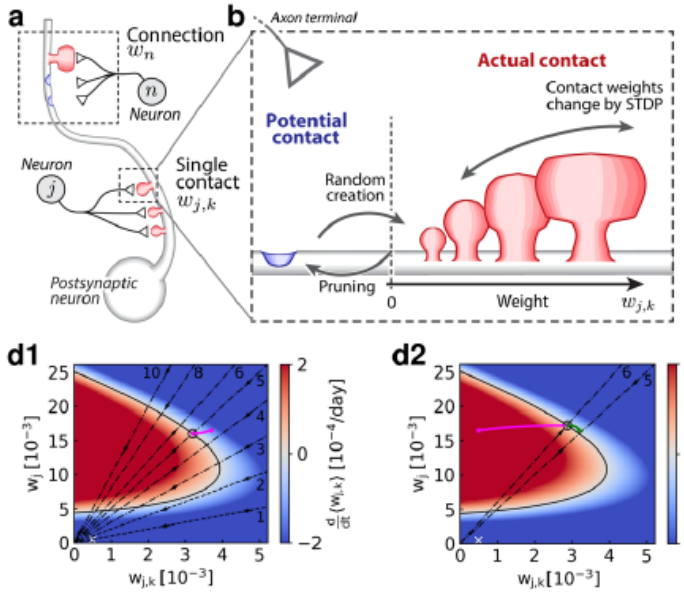

Figure 41

(a) Each presynaptic neuron can make multiple (up to 10) contacts onto the same postsynaptic neuron. (b) These contacts can grow, shrink, or disappear according to a local STDP learning rule that has Hebbian and anti-Hebbian terms. (c) The stable state of the learning rule is such that many presynaptic neurons make no connection at (number of contacts = 0). However, those that establish a connection, make about 4-8 contacts. Two contacts or 10 actual contacts are very rare. (d) The total connection weight w_j is the sum over all its weights $w_{j,k}$. Mathematical analysis of the learning rule shows that solutions with m contacts of equal weight exist if m>2. Solutions correspond to the intersection of the straight dashed lines (for different values of m) with the solid line. Contact weights grow in the red regime and decrease in the blue regime.

Achieved Impact

Short list, or narrative, outlining which impact has been achied to-data based on this result.

- The results have been published (print and free online) in the highly competitive journal Cerbral Cortex. M. Deger, A. Seeholzer and W. Gerstner (2018) Multi-contact synapses for stable networks: a spike-timing dependent model of dendritic spine plasticity and turnover.

Cerebral Cortex doi: 10.1093/cercor/bhx339

- The code is available online https://github.com/mdeger/nest-simulator/blob/stdp_structpl_synapse/models/stdp_structpl_connection_hom.h
- The code has been integrated into NEST as part of the HBP platform initiative

Component Dependencies

Summarized links to components this key result depends on.

Component ID	Component Name	HBP Internal	Comment
66	*Plasticity: STDP for structural Plasticity (STDPstructural)*	*No*	*This component has been crucial for our results published in the paper*
1066	*Plasticity models: SP4 (theory) T 4.3.1. synaptic plasticity and learning*	*No*	*This component provided the generic framework for the modelling efforts*
65	*Plasticity: STDP with heterosynaptic plasticity and homeostasis for memory formation*	No	This component provided the basis for component 66 (see above)
209	*NEST the neural simulation tool*	*No*	*This component provided the basis for the simulation done in this paper.* *In addition, the code of the model has now been integrated into NEST.*

2.3.2 Somato-dendritic prediction error learning under imperfect conditions (WP4.3)

The UBern partner has worked on the paradigm of somato-dendritic prediction error learning (Urbanczik & Senn, 2014). The main focus lay on exploring the functionality of the learning rule in more realistic settings which prohibit analytical analysis. The plasticity rule relies on comparing somatic firing to the firing rate based on a dendritic estimate, and on utilizing potentiation and depression to drive this difference to zero. Our work focused on the implications for learning that follow from various model components that were introduced to reproduce STDP plasticity experiments.

Key findings have been

- Multiple model components can lead to a systematic bias in the learning rule, precluding functional learning for even very simple tasks. Among these are spiking currents and the associated refractory periods, or probabilistic action potential backpropagation
- The dendritic estimate of the somatic firing rate can be used to restabilize learning at discrete fixed points, trading off stability and accuracy

- This already allows for useful learning in stereotyped learning tasks that focus on qualitative seperations in levels of activity, as already reported for unsupervised and reinforcement learning tasks
- For supervised learning, multiple dendrites can be combined in a way such that the convex combination of all their unreliable estimates leads to a close approximation of the learning signal (see figure for an illustration in a simplified setup)
- This coding scheme makes specific predictions about the kind of voltage-gated conductances we would expect to find in spines from different dendritic branches

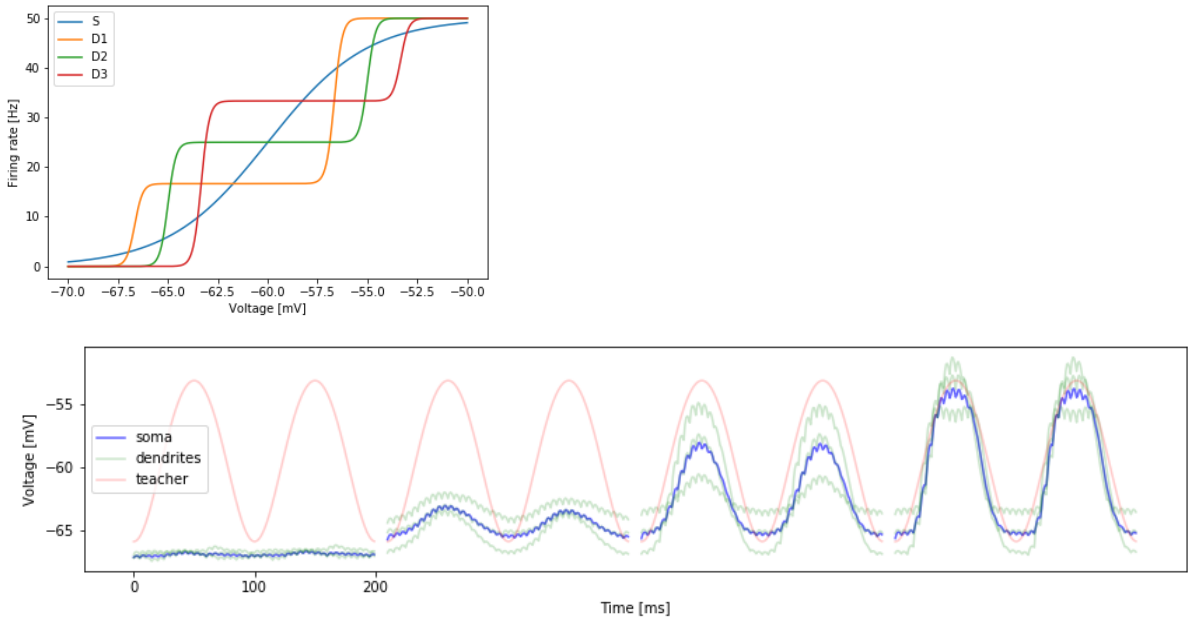

Figure 42

Left: The somatic firing rate in blue and the estimates thereof of three dendrites. Below: a periodic signal (red) is taught. Synaptic plasticity of synapses impinging onto the dendrites (green) convex-combine in the soma (blue) that progressively improves its tracking of the teacher through learning. For the periods shown, the teacher is turned off, i.e. the traces represent the current state of learning. For these simulations, spiking currents and the voltage backflow into the dendrite are set to zero.

Achieved Impact

The code is partly available on https://github.com/unibe-cns/STDP_Multicompartment. The paper is an extension of our previous model on dendritic error-backpropagation, Schiess, Urbanczik & Senn, PLoS Comp Biol 2016 (https://doi.org/10.1371/journal.pcbi.1004638), with code available at https://github.com/unibe-cns/dendriticBackprop

Component Dependencies

Summarized links to components this key result depends on.

Component ID	Component Name	HBP Internal	Comment
1032	*Plasticity: Dendritic predictive plasticity that reproduces STDP data (Algo STDP predictive)*	*Yes*	*This component built the basis for the model considered here*

2.3.3 Natural gradient learning for spiking neurons (WP4.3)

See Deliverable CDP5 1.1 Natural gradient learning for spiking neurons

Collaboration between SP4 (UBern) and SP9 (UHeidelberg) involving CDP5

Elena Kreutzer, Mihai Petrovici, Walter Senn (UBern)

2.3.4 Sequence learning by shaping hidden connectivity (WP4.3)

Please refer to Deliverable CDP5 - 1.2 Sequence learning by shaping hidden connectivity for details of the model.

Collaboration between SP4 (UBern) and SP9 (UHeidelberg) via CDP5
Kristin Völk, Mihai Petrovici, Walter Senn (UBern)

2.3.5 Error-backpropagation across cortical areas (WP4.3)

Please refer to Deliverable CDP5 - 1.3 Error backpropagation across cortical areas

for details of the model.

Collaboration between SP4 (UBern), SP9 (UHeidelberg) and external partner (UMontreal, YB)
João Sacramento, Rui Costa, Yoshua Bengio, Walter Senn (UBern)

2.3.6 Synaptic correlates of working memory and its capacity (WP4.3)

The Weizmann partner has worked on developing the synaptic theory of working memory and understanding within the framework of this theory of why working memory capacity is limited to 4 items for most people. This result is known from numerous behavioural experiments but its neuronal mechanism is unknown. The Weizmann partner constricted a recurrent neural network model with short-term synaptic plasticity (STP) and used analytical derivations and numerical simulations to relate the working memory capacity to parameters characterising short-term plasticity. The key insights from this project are:

(i) Recurrent networks with STP can maintain several items in working memory via periodic brief reactivations (population spikes, or PSs) of corresponding neuronal representations.
(ii) Working memory capacity scales with the time constants of synaptic depression and facilitation but decreases with the decay time constant of synaptic currents.
(iii) Working memory can be regulated by external excitatory input, which has to be above a critical value.
(iv) When the external input dips below the critical value, all items are removed from working memory.

The architecture of the network and example of working memory is shown below.

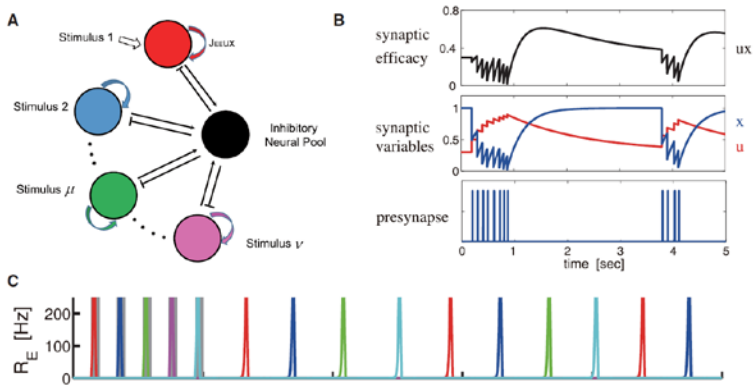

Figure 43

(A) Network architecture: a number of recurrent excitatory neural clusters, shown in different colors, reciprocally connected to an inhibitory neuron pool, shown in black. (B) Model of a synaptic connection with STP. In response to a presynaptic spike train (lowel panel), the neurotransmitter release probability u increases and the fraction of available neurotransmitter x decreases (middle panel), representing, correspondingly, synaptic facilitation and depression. The effective synaptic efficacy is proportional to ux (upper panel. (C) Network simulation with five loaded memory items. Upper panel : firing rates of different clusters. Five clusters are sequentially stimulated by brief external excitation (shaded colored rectangles). Different colors correspond to different clusters as in A. Following the stimulation, four clusters continue sequential activation in the form of PSs while the remaining item fades away.

Achieved Impact

Short list, or narrative, outlining which impact has been achied to-data based on this result.

The results of this project were published in the following publication in Neuron, one of the top three journals in the neurosciences:

Y. Mi, M. Katkov & M. Tsodyks. Synaptic correlates of working memory capacity. **Neuron,** 93: 323-330 (2017).

Component Dependencies

Summarized links to components this key result depends on.

Component ID	Component Name	HBP Internal	Comment
N/A	*N/A*	*N/A*	*N/A*

2.3.7 Phenomenological model of information recall from long-term memory (WP4.3)

The Weizmann partner has worked on mathematical modelling of information recall as probed by free recall of randomly assembled lists of words. The model is based on two basic principles of neuronal representation of information and associative retrieval. It is verified by comparing the performance of the recall in terms of the average number of words recalled from a list of increasing length. The main results that were achieved are the following:

(i) The average number of words recalled from the list of L randomly assembled words depends on the sparseness of neural representations of items in long-term memory.

(ii) In the limit of very sparse representations, the recall performance (number of words recalled on average from a list of L words) is given by the following simple formula:

$$Nrec = 2\sqrt{L}$$

(iii) Words that have larger neuronal representations and/or larger overlaps with other word representations have higher chance to be recalled

(iv) The model not only accounts for average recall performance observed experimentally but also predicts the correct distribution of the performance.

The graphical representation of the recall process and analytical solution to the model are illustrated in Figure 44 below:

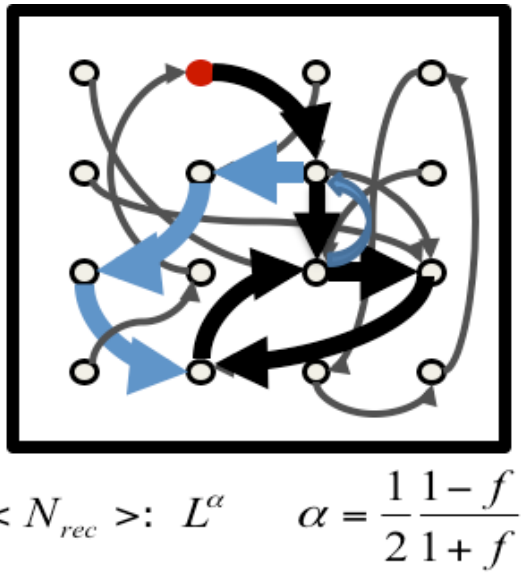

Figure 44

Graph representation of recall process. Each arrow points to a memory item that has largest overlap with the representation of the current item. Red circle is the initial item. After several items are retrieved, recall enters a loop after which no new items can be recalled. The formula below the figure gives the average number of words recalled as a function of the total number of words in the list, f is the sparseness parameter that represents the average fraction of neurons in the network that encode a single memory item.

Achieved Impact

(i) The results of this project are published in the paper in Neuron, one of the top three journals in the neurosciences.

M. Katkov, S. Romani & M. Tsodyks. Memory Retrieval from First Prinicples. Neuron, 94:1027-1032 (2017).

(ii). The code is available online at https://github.com/mkatkov/memoryRetrieval

Component Dependencies

Summarized links to components this key result depends on.

Component ID	Component Name	HBP Internal	Comment
N/A	*Penn Electrophysiology of encoding and retrieval study*	*No*	provides a comprehensive collection of raw data for 200 human subjects performing free recall experiments on multiple lists of words, that allowed to test the model predictions in a quantitatively precise manner.

2.3.8 Balancing new against old information: the role of puzzlement surprise in learning (WP4.3)

The EPFL partner has worked on a generalized model of synaptic plasticity under the influence of neuromodulation. It is well known that, in a reward-based learning paradigm, theories of reinforcement learning can be related to the action of the neuromodulator dopamine on synaptic plasticity. Here we asked the question whether, even in the absence of reward, surprise could play a role analogous to reward. To address this question, we developed a novel definition of

surprise that combines aspects of both the traditional Shannon-surprise and the well-known Baysian surprise measures, but also includes the level of commitment to an opinion. Our focus has been on the immediate surprise when confronted with an unexpected event, called puzzlement surprise in the following. Puzzlement surprise is different from enlightenment surprise that corresponds to the amount of 'gain in our understanding' after we have integrated the unexpected event into our world model. Examples of enlightenment surprise would be the Baysiane surprise measure or the compression progress measure proposed by J. Schmidhuber.

Puzzlement surprise *Scc* is a confidence-corrected (CC) surprise measure defined as the Kullback Leibler divergence

$$S_{cc}(X;\pi_n) = D_{KL}[\pi_n(\theta)||\hat{p}_X(\theta)] = \int_\theta \pi_n(\theta) \ln \frac{\pi_n(\theta)}{\hat{p}_X(\theta)}\, d\theta.$$

between the distribution

$\pi_n(\theta)$ that describes the momentary belief after having seen n examples

and

$\hat{p}_X(\theta)$ that describes the belief of a naïve observer for which the present example would be the first one.

Key findings with our novel puzzlement surprise measure are

(i) For the same level of confidence (commitment to an opinion), puzzlement surprise decreases with the likelihood of an event;
(ii) For the same level of low likelihood of an event, puzzlement surprise increases with the commitment to an opinion;
(iii) Puzzlement surprise in a one-dimensional task increases the learning rate at which new information is integrated (see Figure 45);
(iv) Puzzlement can also be used in high-dimensional and underspecified tasks where exact world models are difficult to formulate.

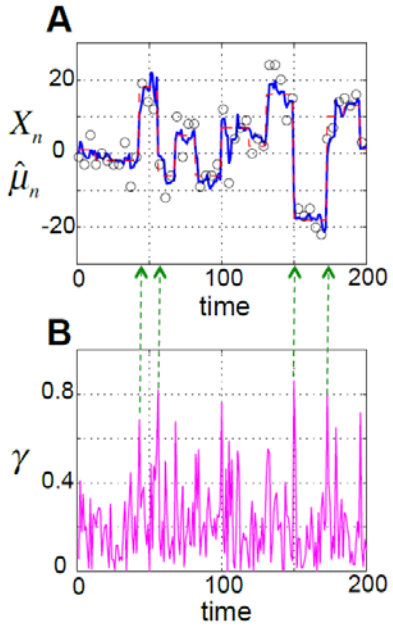

Figure 45 At each time step, a data sample Xn is independently drawn from a normal distribution whose underlying mean may change at unpredictable change points.

On average, the underlying mean remains unchanged for 15 time steps corresponding to a hazard rate H=0.066. The standard deviation of the distribution is fixed to 4 and is assumed to be known to the subject. A Using a surprise-modulated belief update the estimated mean (blue) quickly approaches the true mean (dashed red) ; observed samples shown in black circles. A few selected change points are indicated by green arrows. \textbf{B.} B. The weight factor gamma (magenta) with which new data is integrated increases at the change points, resulting in higher influence of newly acquired data samples on the new value of the mean

Achieved Impact

Our results have been published in Neural Computation, a highly respected theory journal.

M. Faraji, K. Preuschoff and W. Gerstner (2018)

Balancing New Against Old Information: The Role of Puzzlement Surprise in Learning Neural Computation 30: 34-83

Component Dependencies

Summarized links to components this key result depends on.

Component ID	Component Name	HBP Internal	Comment
1066	*Plasticity models: SP4 (theory) T 4.3.1. synaptic plasticity and learning*	*No*	*This component provided the generic framework for the modelling efforts for this key result.*

2.3.9 Stable local learning in a recurrent spiking network (WP4.3)

Please refer to Deliverable CDP5 - 1.5 Motor learning with spiking neurons through adaptive control for details of the model.

2.3.10 Learning rules that can be implemented on the neuromorphic platforms (WP4.3)

Please refer to Deliverable CDP5 – 3.5 Plasticity rules in neuromorphic hardware for details of the model.

2.3.11 Evolving the SpiNNaker neuromorphic platform to support Three-Factor learning rules (WP4.3)

Please refer to Deliverable CDP5 – 3.5 Plasticity rules in neuromorphic hardware for details of the model.

2.4 Models of Cognitive Processes (WP 4.4)

2.4.1 Topological similarity to estimate functional connectivity (T4.4.1)

Description of the model

UPF: The quest to understand how the structural network of interconnections shapes brain function lies at the heart of the field of brain connectivity. So far, we still lack a unitary model of the relationship between the shape of the brain's connectome and the emergent activity patterns. One of the main reasons is that interactions between different brain areas do not only depend on the structure of the connectome but also on the local and global dynamics characterizing a given brain state, such as rest, sleep, and anesthesia. The existence of different state dependent activity patterns sustained by the same underlying anatomy exposes how elusive is the relationship between the network structure and function.

The UPF partner has developed a model, named as *topological similarity*, to analytically estimate the contribution of the structural brain connectivity alone on the cross-correlations between brain areas at rest. The model is based on three axiomatic assumptions on the diffusion of influence or information over the network:

1. In a network, information travels along all possible paths (with equal probability). Very often, network approaches of information transmission consider only the shortest paths.
2. Information content (or signal power) decays with path distance. This assumption implies that despite information travels along all possible paths, shorter paths are still more influencial than longer paths.
3. Two brain regions are correlated if they receive inputs from the same sources.

The first two assumptions define how information travels along a network and determine how much the dynamics of one brain region affected the dynamics of any other brain region. Given that the structural connectivity is encoded by the weighted adjacency matrix **A**, where *A(i,j) > 0* if there is a link pointing from region *i* to region *j* and *A(i,j) = 0* if no such link exist, then the influence between any pair of nodes can be quantified by the communicability measure *C*. By definition, communicability is the matrix exponential of the adjacency matrix, *C = exp(g**A**)*, which is a weighted sum of the powers of the adjacency matrix, and *g* is a parameter for global coupling strength.

$$\mathcal{C} = e^{gA} = \mathbf{1} + gA + \frac{(gA)^2}{2!} + \frac{(gA)^3}{3!} + \dots \quad (1)$$

$$\mathcal{T} = \frac{\langle \mathbf{c}_i, \mathbf{c}_j \rangle}{||\mathbf{c}||\,||\mathbf{c}||} \quad (2)$$

Applying this model to structural human brain connectivity we were able to estimate the cross-correlations between brain regions which are expected in resting-state only due to the connectivity alone, Figure 46M for one hemisphere and Figure 46N for the whole brain. Comparing to empirically observed functional connectivities via fMRI during resting-state, Figure 46E and Figure 46F, we could quantify that the shape of the brain's connectome only accounts for up to 45% of the empirical functional connectivity.

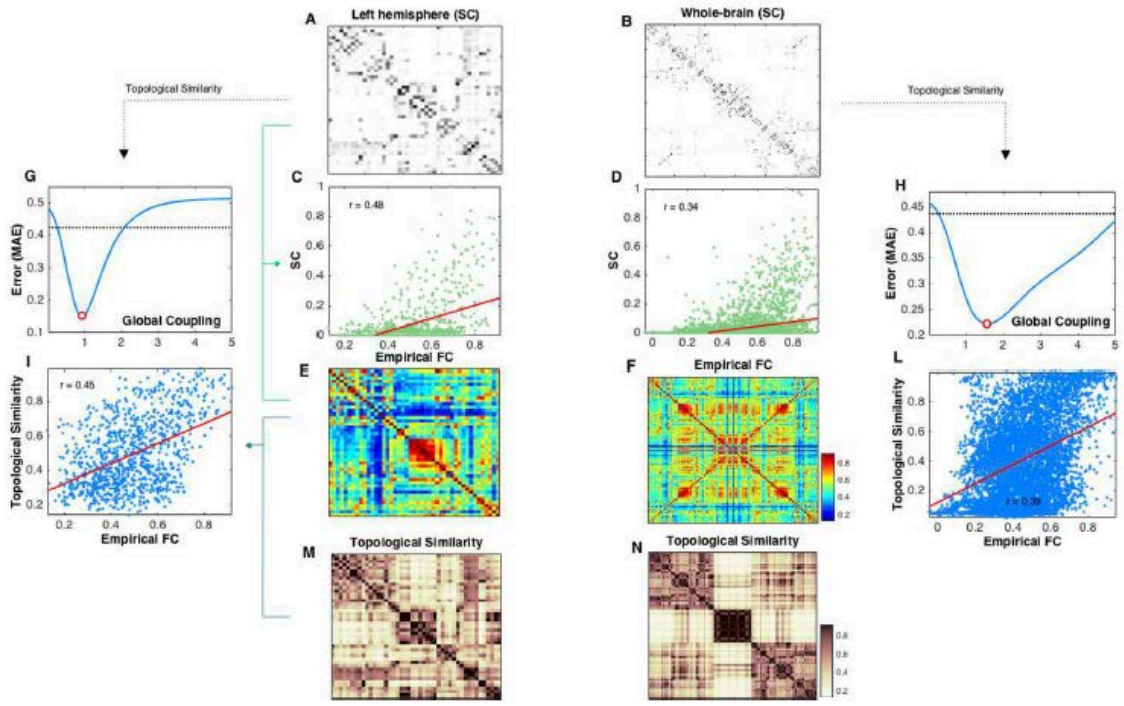

Figure 46 Contribution of whole-network common inputs to the brain's spontaneous correlation structure.

The figure shows results obtained separately for only one hemisphere (Left panels) and for the whole brain (Right panels). (a), (b) structural connectivity matrices (SC). (c), (d) Scatterplots depicting the relationship between SC and the empirical functional connectivity (FC). (e), (f) Empirical functional connectivity matrices (FC). (g), (h) Mean absolute error (MAE) between the empirical FC and the topological similarity T computed for different values of the global coupling parameter, g. The dotted lines correspond to the mean absolute error between the raw SC matrix and the empirical FC. (i), (l) Scatterplots of the empirical FC and the best-fitting topological similarity. (m), (n) Best-fitting Topological similarity matrices. We included also the Pearson's correlation values r corresponding to the best-fitting matrices obtained optimizing the mean absolute error.

Implementation to platforms

Component ID:1069, "Influence of topological heterogeneities on network activity" (T4.4.1).

Component ID:999, "Macroscopic model of spontaneous human brain activity" (T4.4.1).

Implementation to platforms

This model was integrated to the collaboratory and the Model Catalog in SP5.

Publications

R.G. Bettinardi, G. Deco, V.M. Karlaftis, T.J. Van Hartevelt, H. M. Fernandes, Z. Kourtzi, M.L. Kringelbach, and G. Zamora-López (2017) "*How structure sculpts function: Unveiling the contribution of anatomical connectivity to the brain's spontaneous correlation structure*" CHAOS 27, 047409.

http://aip.scitation.org/doi/10.1063/1.4980099

Achieved Impact

According to the records from the publisher's own records (The American Institute of Physics), the publication above is among the 10 most read articles of the journal CHAOS along 2017.

The model has served as the basis to define a generalised framework to describe the network-dynamic properties of weighted networks:

M. Gilson, G. Zamora-López, N.E. Kouvaris, and G. Deco (2017) "*Dynamic communicability and flow to describe complex network dynamics with linear feedback*" (in press)

arXiv preprint: https://arxiv.org/abs/1712.05693v1.

Conclusion & Outlook

This model has solved a long-standing question in the field of brain connectivity: *how the long-range brain connectome relates to resting-state functional connectivity*. Previous efforts to answer this question always relied in assuming simple local dynamics for the regions of the brain, e.g., Gaussian noise diffusion (Ornstein-Uhlenbeck process). Therefore, those approaches could not fully dissentangle the contribution of the structural connectome from that of local dynamics. Our approach is free of the local dynamics bias and is based uniquely on the simplest axiomatic assumptions possible, but yet realistic, on how information propagates on the network.

Therefore, the results arised from the model are crucial for understanding the capacity of more realistic network models of whole brain dynamics to resemble empirical observations. Any improvement achieved by adding more complexity to the models is only interpretable under the baseline the present model sets.

Component Dependencies

Summarized links to components this key result depends on.

Component ID	Component Name	HBP Internal	Comment
N/A	*N/A*	N/A	N/A

2.4.2 Macroscopic model of spontaneous human brain activity (T4.4.1)

Description of the model

In the human brain, spontaneous activity during rest consists of rapid transitions between functional network states over time but the underlying mechanisms are not understood. Several models have been proposed in the past to reproduce the whole-brain spontaneous activity. While those models could reasonably reproduce the time-averaged functional connectivity of the brain at rest, they have failed to capture its temporal fluctuations. The reason, we find, is the type of local dynamics those models used to characterise the local dynamics of brain regions. To explore identify the type of local dynamics giving rise to realistic fluctuations, the UPF partner has developed a whole brain network model where the local dynamics of the brain regions are characterised by the canonical form of the Hopf bifurcation.

The model considers the structural connectome for the human brain extracted via diffusion tensor imaging and tractography. The corresponding connectivity is encoded into the weighted adjacency matrix A where $A(i,j) > 0$ if there is a link pointing from region i to region j and $A(i,j) = 0$ if no such link exist. The local dynamics $z(i,t)$ of a brain region is characterised by the Hopf normal form, see Eq. (1), where $z(i,t)$ is a complex variable and $\eta(i,t)$ is an additive external Gaussian noise each region receives. The noise each region receives is independent. The local dynamics of each region i depends on two parameters:

- $a(i)$, the bifurcation parameter, and
- $\omega(i)$, the natural frequency of the region.

The bifurcation parameter sets the dynamical mode of the brain region. If $a < 0$ the local dynamics are characterised by the external noise $\eta(i,t)$ fluctuating around the fix point $z(t) = 0$. If $a > 0$ then $z(t)$ oscillate. In the vecinity of $a = 0$ the local dynamics are characterised by small noisy oscillations due to stochastic resonance. See Figure 47.

$$\dot{z} = (a + j\omega)\, z - z\,|z^2| + \beta\,\eta(t) \qquad (1)$$

$$\dot{z}_i = (a_i + j\omega_i)\, z_i - z_i\,|z_i^2| + g \sum_{k=1}^{N} A(z_k - z_i) + \beta_i\,\eta(t)_i \qquad (2)$$

Given the BOLD signals from resting-state fMRI, the natural frequencies *ω(i)* for each brain region are determined from the experimental data. While Eq. (1) represents the equation for each region, Eq. (2) represents the dynamics of the coupled system, where *g* is a global coupling parameter and the brain regions are diffusively coupled.

Using this model we could reveal the dynamical cortical core of the human brain, which is driving the activity of the rest of the whole brain.

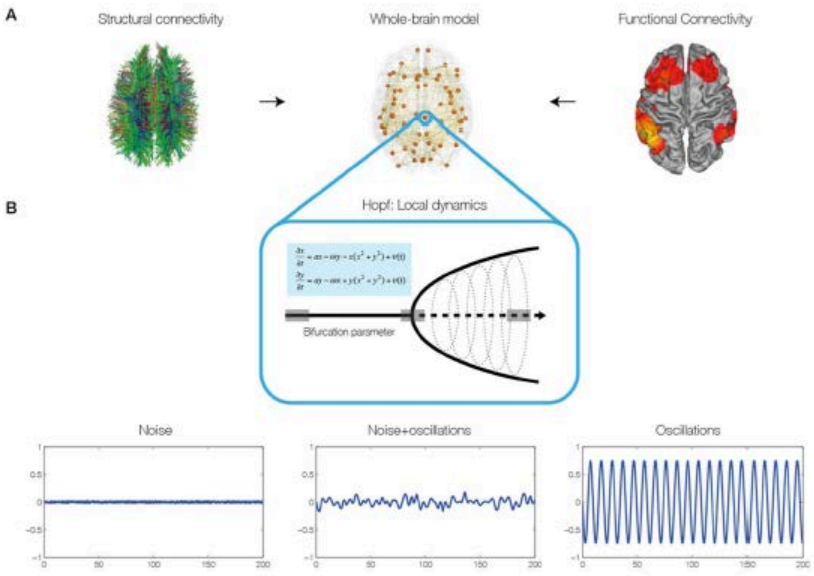

Figure 47 Construction of individual brain network models.

(A) The brain network model was based on individual structural connectivity (SC) matrices from 24 participants derived from tractography of DTI (left) between the 68 regions of the Desikan-Kahilly parcellation (middle). The control parameters of the models were tuned using the grand average FC and FCD derived from fMRI BOLD data (right). (B) For modelling local neural masses we used the normal form of a Hopf bifurcation, where depending on the bifurcation parameter, the local model generates a noisy signal (left), a mixed noisy and oscillatory signal (middle) or an oscillatory signal (right). It is at the border between noisy and oscillatory behaviour (middle), where the simulated signal looks like the empirical data, i.e. like noise with an oscillatory component around 0.05 Hz.

Implementation to platforms

Component ID:999, "Macroscopic model of spontaneous human brain activity" (T4.4.1).

Implementation to platforms

This model was integrated to the collaboratory and the Model Catalog in SP5.

Publications

G. Deco, M.L. Kringelbach, V.K. Jirsa, and P. Ritter (2017) "*The dynamics of resting fluctuations in the brain: metastability and its dynamical cortical core*" Sci. Reps. 7:3095.

https://www.nature.com/articles/s41598-017-03073-5

Achieved Impact

The model has served as the basis to investigate several questions of neuroscientific relevance such as Parkinson disease and the organization of state-dependent functional networks:

V.M. Saenger, J. Kahan, G. Deco, et al. (2017) "*Uncovering the underlying mechanisms and whole-brain dynamics of deep brain stimulation for Parkinson's disease*" Sci. Reps. 7:9882 (2017).

http://www.nature.com/articles/s41598-017-10003-y

M. Senden, N. Reuter, M.P. van den Heuvel, R. Goebel, G. Deco (2017) "*Cortical rich club regions can organize state-dependent functional network formation by engaging in oscillatory behavior*" NeuroImage 146, 561-574.

https://www.sciencedirect.com/science/article/pii/S1053811916306000?via=ihub

Conclusion & Outlook

This model was able to uncover the class of local dynamics of brain regions leading to fluctuations of the whole-brain dynamics observed in empirical measurements of resting-state fMRI in humans. Previous models of whole-brain dynamics could reproduce the time-average functional connectivity observed empirically, but were unable to reproduce the temporal fluctuations. Fine tuning of the dynamical regime was possible due to the simplicity of the normal form of the Hopf bifurcation, often also known as teh Stuart-Landau model in the physics literature. Future developments overlap with the study of biologically realistic mean-field models by other partners in the HBP. The generic local dynamics identified by the present model will be crucial to evaluate the mean-field model selection towards building more realistic whole-brain network models.

Component Dependencies

Summarized links to components this key result depends on.

Component ID	Component Name	HBP Internal	Comment
N/A	*Dataset from Charité (Berlin)*	No	Critical for validation

2.4.3 Model of "dynamically realistic" network states (T4.4.1)

Description of the model

The UNIC partner has designed a spiking network model containing two main types of neurons in cerebral cortex: the "regular-spiking" (RS) neurons, mostly excitatory and characterized by spike-frequency adaptation, and the "fast spiking" (FS) neurons, mostly inhibitory and who usually discharge at higher rates with negligible adaptation. RS and FS cells were modeled by the Adaptive Exponential (AdEx) integrate and fire neuron model. This model is similar model to a previous model described previously (Destexhe, 2009; see this paper for all details about the methods).

The model was constrained from data obtained using Utah-array recordings in human and monkey collected and analyzed in the last years (Peyrache et al., 2012; Dehghani et al., 2016; Le van Quyen et al., 2016). In particular, we aimed at reproducing the typical firing pattern seen in awake subjects, where neurons fire very irregularly and with low levels of synchrony, a state called "asynchronous-irregular" (AI). Figure 48 illustrates AI in awake human and monkey recordings.

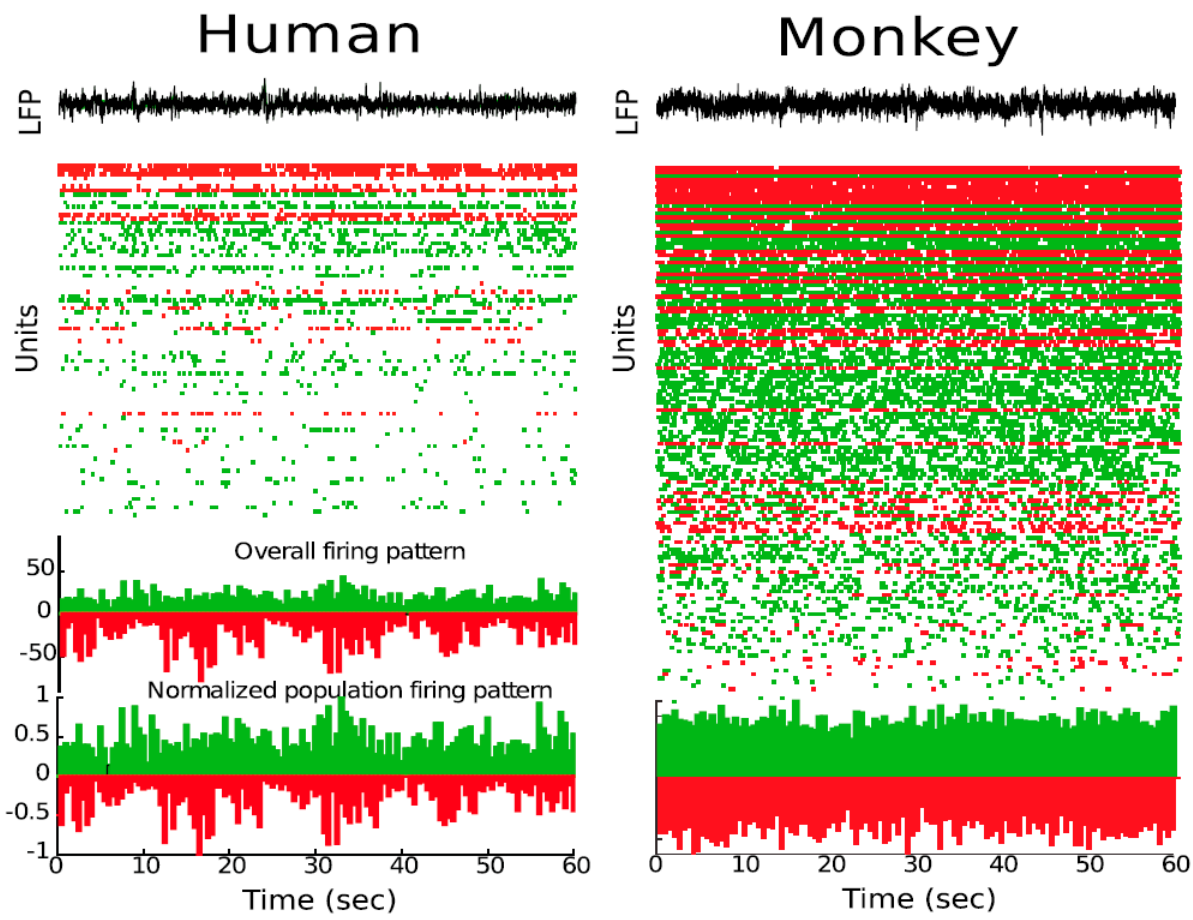

Figure 48 Asynchronous-irregular (AI) states in human and monkey cortical recordings using Utah arrays.

Excitatory (RS) cells are indicated in green, and inhibitory (FS) cells are shown in red. The bottom curves show the pooled activities of the two populations (figure modified from Zerlaut and Destexhe, 2017).

Figure 49 shows a network model of RS and FS cells displaying AI states. In this model, the firing pattern of RS and FS cells was consistent with experiments, with all cells displaying irregular activity with low levels of synchrony, and FS cells displaying higher rates than RS cells (Figure 49B). In addition, the model was constrained from conductance measurements in awake animals, which displayed stronger inhibitory conductances compared to excitatory conductances (Rudolph et al., 2007). This pattern could be obtained in the model (see total conductance in Figure 49C). The intracellular activity of excitatory neurons (Figure 49C, top curves) is also consistent with the typical intracellular activities measured in vivo.

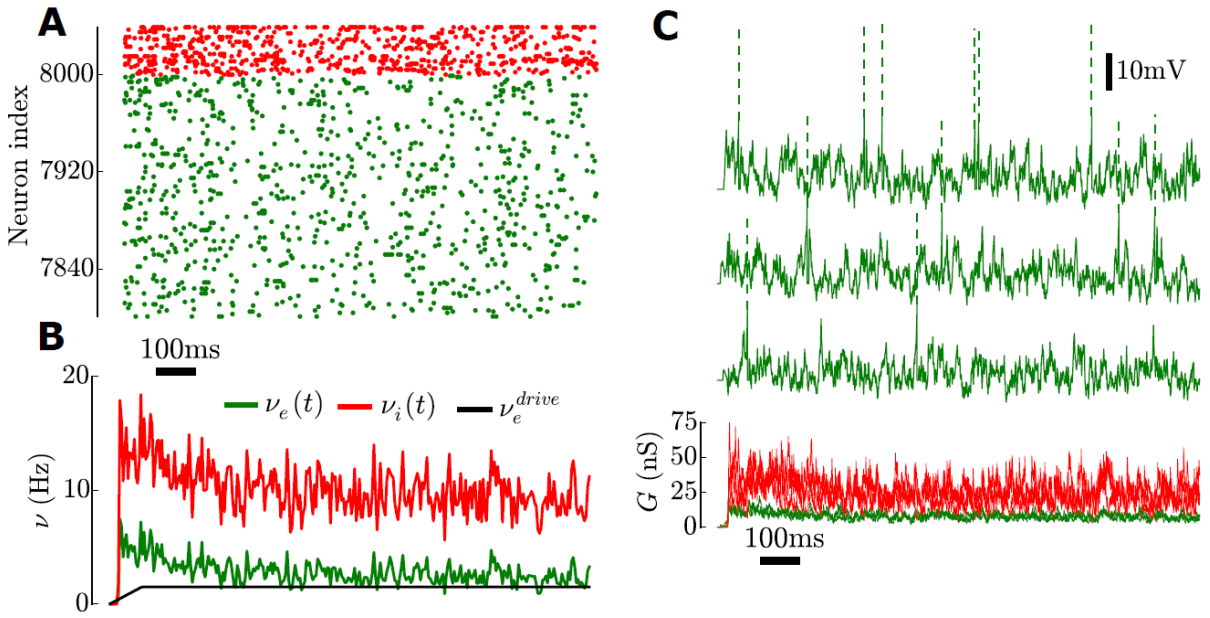

Figure 49 Network model of asynchronous-irregular activity states consistent with in vivo measurements.

A. Raster of the spiking activity of RS (green) and FS (red) cells during an AI state. The rate of each population is shown at the bottom. B. Activities of 3 example RS cells, together with the conductance pattern seen on single RS cells. The conductance values are consistent with in vivo measurements in awake cats. Modified from Zerlaut et al., 2018.

Thus, this RS-FS network model is the first, to our knowledge, to successfully reproduce the properties of AI states as constrained from all available in vivo recordings. At the extracellular level, the model reproduces the firing pattern of RS and FS cells, their low level of synchrony, and the difference of firing rate between RS and FS cells. At the intracellular level, the model correctly accounts for the membrane potential activity and the conductance patterns measured intracellularly in awake animals.

Components

Component "Model of "dynamically realistic" network states" (T4.4.1).

Implementation to platforms

This model was integrated to the collaboratory and the Model Catalog in SP5. It will also be ported to the neuromorphic platform.

References

Destexhe, A. Self-sustained asynchronous irregular states and Up/Down states in thalamic, cortical and thalamocortical networks of nonlinear integrate-and-fire neurons. *J. Computational Neurosci.* 27: 493-506, 2009.

Peyrache, A., Dehghani, N., Eskandar, E.N., Madsen, J.R., Anderson, W.S., Donoghue, J.S., Hochberg, L.R., Halgren, E., Cash, S.S., and Destexhe, A. Spatiotemporal dynamics of neocortical excitation and inhibition during human sleep. *Proc. Natl. Acad. Sci. USA* 109: 1731-1736, 2012.

Rudolph, M., Pospischil, M., Timofeev, I. and Destexhe, A. Inhibition determines membrane potential dynamics and controls action potential generation in awake and sleeping cat cortex. *J. Neurosci.* 27: 5280-5290, 2007.

Publications

Analysis of human and monkey data, done during the Ramp-up phase, but published during SGA1:

Dehghani, N., Peyrache, A., Telenczuk, B., Le Van Quyen, M., Halgren, E., Cash, S.S., Hatsopoulos, N.G. and Destexhe, A. Dynamic balance of excitation and inhibition in human and monkey neocortex. *Nature Sci. Reports* 6: 23176, 2016.

Le Van Quyen, M., Muller, L., Telenczuk, B., Cash, S.S., Halgren, E., Hatsopoulos, N.G., Dehghani, N. and Destexhe, A. High-frequency oscillations in human and monkey neocortex during the wake-sleep cycle. *Proc. Natl. Acad. Sci. USA* 113: 9363-9368, 2016.

Work done in SGA1:

Zerlaut, Y. and Destexhe, A. (2017) Enhanced responsiveness and low-level awareness in stochastic network states. *Neuron* 92: 1002-1009.

Zerlaut Y., Chemla, S., Chavane F. and Destexhe A. (2018) Modeling mesoscopic cortical dynamics using a mean-field model of conductance-based networks of adaptive exponential integrate-and-fire models. *Journal of Computational Neuroscience* (in press).

bioRxiv preprint: https://www.biorxiv.org/content/early/2017/11/12/abs/168385

Achieved Impact

This model had a strong impact, as different variants of this model are now continued in different directions, including Up/Down states or mean-field models.

Conclusion & Outlook

This model successfully reproduces the firing patterns and conductance levels found in vivo. It is presently extended to study the generation of Up/Down states. It is also used to investigate the responsiveness of networks to external inputs, and understand how information is propagated across successive layers. These aspects will be continued in SGA2.

Component Dependencies

Summarized links to components this key result depends on.

Component ID	Component Name	HBP Internal	Comment
1554	Mean-field models of AdEx networks, spontaneous activity and responsiveness	*Yes*	*This component helps bridging scales*

2.4.4 Model of spontaneous activity in awake mouse primary auditory cortex based on large scale Ca^{2+} imaging data (T4.4.1)

CNRS UNIC: The adult brain is characterized by a prominent ongoing activity underlying sensory responses and perception. This activity is not only determined by external stimuli but also by intrinsic patterns generated endogenously, such as up and down states. Despite the fact that the endogenous cortical states were mainly reported and characterized for the slow wave sleep and anesthesia, there are growing evidences that spontaneous fluctuations in population activity exist also during quiet wakefulness.

The project, carried out in a partnership between Prof. Alain Destexhe's and Dr. Brice Bathellier's labs (UNIC), aims at creating a computational model to disclose the mechanisms of intrinsic brain states generation in awake sensory cortices and eventually establishing their causal impact on perceptual behavior. To elucidate the network machinery that drives specifically primary auditory cortex endogenous dynamics, we use data obtained by chronic two-photon Ca^{2+} imaging of large populations of neurons (1x1 mm field of view) in superficial and deep layers (Figure 50 a, c) in awake head fixed mice.

Experimental measurements

We have collected experimental data to constrain the computational model. We characterized the spontaneous dynamics of primary auditory auditory cortex (A1) in the absence of auditory stimulation. We observed the occurrence of low frequency (0.05-0.1 Hz) large scale (spreading over the whole field of view, Figure 51 a, b) spontaneous synchronous events (duration up to 1s) (Figure 50 b, d). Their frequency was higher in deeper than in the superficial layers, as observed previously with multi-electrode recordings (Figure 50 b, d). Interestingly, the analysis of horizontal propagation of these synchronous events revealed that they rather correspond to large hotspots, instead of horizontally propagating waves with a clear front. (Figure 51 a for superficial and b for deep layers). The recordings were performed using *Gad2*$^{tm2(cre)}$ [1] mouse line, with labeled inhibitory neurons. The parallel tracking of eye pupil size and whiskers allows to reveal the correlation with arousal and exploring behavior (Figure 50 b, d).

Model

Based on these experimental data we are developing a computational model of 2D (25x25) neuronal networks of mouse superficial and deep layers (In PyNN simulator-independent language). The network is composed of two population of excitatory ("regular spiking" or RS) and inhibitory ("fast spiking" or FS) spiking neurons connected locally, in proportion according to experimental data derived from *Gad2tm2(cre)* mouse. The model aims at simulating the mechanisms underlying the generation of spontaneous activity, as we measured in awake A1 superficial and deep layers. 2-dimensional configuration of model networks allows simulation of horizontal propagation of these events. Once the model is able to reproduce spontaneous activity, we will introduce sensory inputs, to predict the mechanisms of how endogenous network states modulate evoked cortical response. This model will be simulated in NEURON [2] and will be reported in SGA2.

Components

Component Local-network model of spontaneous activity in cortex (T4.4.1).

Implementation to platforms

This model will be integrated in the Model Catalog in SP5.

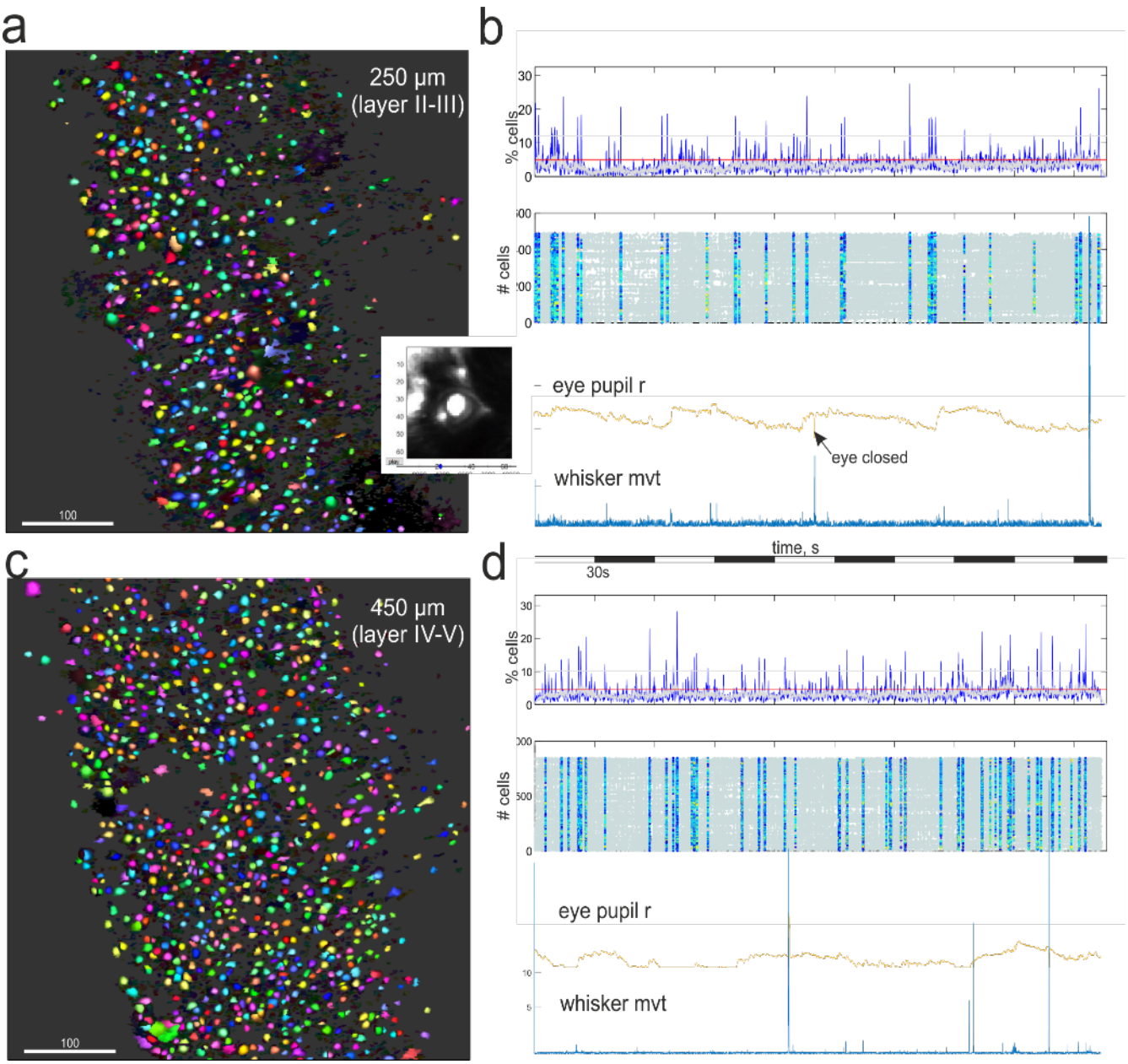

Figure 50 Population activity in awake

A1. Two-photon Ca^{2+} imaging of A1 neurons through cranial window in awake head fixed mouse, following the stereotaxic injection of an AAV-syn-GCAMP6s vector [3]. A. 560 neurons identified at the depth of 250 µm from the brain surface. Noisy Ca^{2+} signal was deconvoluted to identify Ca^{2+} spike using MLspike algorithm [4] . B. Firing rate and raster plot for the cells from A. Grey dashed line represents the threshold of stochastic coincidence above which the events are considered as synchronous not accidentally (color coded columns in the raster plot). 5 minutes soundless recordings of A1 (imaging rate 31.5 frames per second) were accompanied by simultaneous eye pupil (orange trace) and one whisker (blue trace) tracking. C. 890 neurons identified at the depth of 450 µm in the same mouse. D. Firing rate, raster plot, eye pupil radius and whisker movement during this deep layer recording. The sharp jumps in whisker and pupil traces correspond to the moments of eye closure.

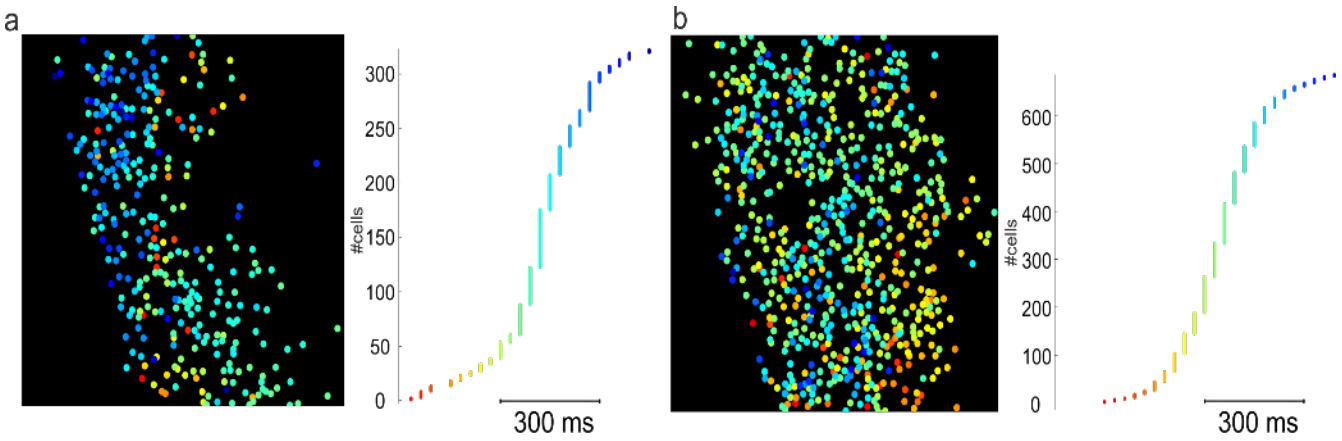

Figure 51 Horizontal propagation of "up-states" in awake A1.

a.The example of horizontal propagation of population synchronous event (up-state) in the upper layer (250 µm). Left panel: spatial pattern, where cells are color coded according to their temporal involvement (red ones are involved at the origin of the event; the dark blue ones engaged at the end). Right panel: temporal pattern of event evolution, reflecting the number of cells consequently involved every 30 ms (imaging rate). b. The example of horizontal propagation of population synchronous event (up-state) in the deep layer (450 µm).

Publications

(in preparation)

References

1. Taniguchi, H. et al. A resource of Cre driver lines for genetic targeting of GABAergic neurons in cerebral cortex. Neuron 71, 995-1013, doi:10.1016/j.neuron.2011.07.026 (2011).

2. Hines, M. L. & Carnevale, N. T. The NEURON simulation environment. Neural Comput 9, 1179-1209 (1997).

3. Chen, T. W. et al. Ultrasensitive fluorescent proteins for imaging neuronal activity. Nature 499, 295-300, doi:10.1038/nature12354 (2013).

4. Deneux, T. et al. Accurate spike estimation from noisy calcium signals for ultrafast three-dimensional imaging of large neuronal populations in vivo. Nat Commun 7, 12190, doi:10.1038/ncomms12190 (2016).

Achieved Impact

This model will be used predict how spontaneous activity interacts with evoked responses, and will be compared to other types of experimental data in mice and humans.

Conclusion & Outlook

The experimental data, obtained from large scale Ca^{2+} imaging in A1, provide a basis for construction of a novel realistic model of spontaneous activity generation and its impact on evoked sensory response in awake brain. We hope to extract general principles applicable to other sensory modalities in the mouse, and perhaps help explaining how human sensory responses depend on the ongoing-activity state.

Component Dependencies

Summarized links to components this key result depends on.

Component ID	Component Name	HBP Internal	Comment
N/A	Model of "dynamically realistic" network states	*Yes*	*Investigates key aspect of brain function*

2.4.5 Spiking model of slow waves during anesthesia (T4.4.1)

Please refer to Deliverable CDP1 - for details of the model.

Achieved Impact

This model has been proved to be a good tool to further investigate brain state transitions, such as the sleep-awake transitions in humans.

Conclusion & Outlook

The model has proven to be useful to understand the mechanisms underlying the cortical transitions between brain states, specifically, between the different levels of anesthesia. Moreover, it has been applied to the two-photon data provided by our collaborators from SP1 during SGA1, but will continue to be used with the wide-field data during SGA2.

Component Dependencies

Summarized links to components this key result depends on.

Component ID	Component Name	HBP Internal	Comment
N/A	Model of "dynamically realistic" network states	*Yes*	Investigates key aspect of brain function
656	*Analysis of meso-scale fluorescence functional data*	*Yes*	Data collection to constrain the model (in the framework of T1.3.1)

2.4.6 Model of retinal processing (T4.4.2)

Description of the model

UPMC:

The subunit model is a two-layer model that predicts the response of a ganglion cell to the moving bar. Each layer performs a linear combination of its inputs followed by a non-linear transformation. The first layer is a collection of identical and translated Linear-Non-Linear (LN) units. The second layer is a unique LN unit taking the output of the first layer as an input.

In the first layer, we tiled the space with 100 bipolar-like OFF subunits, and 100 ON subunits, on a one-dimensional lattice, with subunits equally spaced at 20 μm interval. Each unit had a receptive field with a Gaussian spatial profile of the right polarity and a biphasic temporal profile, modeled by a sinusoid. All units of a same polarity are identical up to a translation. The non-linearity was a rectified square function, h. The output of the ON subunit layer was therefore:

$$F(x,t) = h\Big(\int_{t-T_{\text{subunit}}}^{t} \int_{-\infty}^{\infty} \sin(2\pi\omega(t-t'))e^{-\frac{(x-x')^2}{2\sigma^2}} s(x',t')dx'dt'\Big)$$

where h is the rectified quadratic function (Deny et al, 2017).

For the OFF subunit, the equation was the same as ON subunit, except that was multiplied by -1. The values of all the constants in these equations and below are reported in (Deny et al, 2017).

The stimulus movie s(x,t) was one-dimensional in space because the stimulus was a long bar, whose length can be considered infinite. We used a temporal binning of 17ms, corresponding to the refresh rate (60Hz) of the screen used to project the movie on the retina.

The second layer consisted of a single Linear-Non-Linear Poisson unit. The unit pooled linearly its inputs from all the subunits of the first layer according to a kernel K, with an extension in time of 0.5 seconds. To obtain the firing rate r(t) of the cell, the weighted sum was passed through a non-linearity of the form f(x) = log(1+exp(x)). The spikes were then generated according to a Poisson process. The firing rate is therefore equal to:

$$r(t) \quad = \quad \alpha \log(1 + \exp(\beta G(t) + \theta))$$

where

$$G(t) = \int_0^{T_{\text{filter}}} \int_x K(x,t') F(x, t - t') dx dt'$$

This model was fitted to retinal recordings and allowed to predict the responses of ganglion cells (the retinal output) to dynamical stimuli in the center or the surround of their receptive field (Deny et al, 2017).

We also added gain control to the ganglion cell model (Deny et al, 2017) to predict how neurons balance the respective influence of stimuli in their centers and their surrounds (Deny et al, 2017). This gain control mechanism was of the form:

$$R_{\text{gain}}(t) \quad = \quad \frac{R(t)}{1 + H \int_{t-\tau}^{t} R(t') dt'}$$

where R(t° is the output of the previous model, ie the response of the ganglion cell. The parameters of the model were also fitted to the data and reported in (Deny et al, 2017).

Thanks to this model we could predict accurately how several types of ganglion cells, the retinal output, respond to complex stimuli in their centers and surrounds.

Implementation to platforms

This model was integrated to the collaboratory.

Publications

Deny S, Ferrari U, Mace E, Yger P, Caplette R, Picaud S, Tkacik G, Marre O (2017). Multiplexed computations in retinal ganglion cells of a single type. Nature Communications, 8: 1964.

Achieved Impact

This model is now continued in different directions to account for single cell variability and correlated variability (noise correlation) across cells.

Conclusion & Outlook

This model allow predicting the retinal activity in response to complex stimuli, and can be used to provide a realistic spiking input to cortical models. It shows that a simple filtering cannot account for the responses of retinal ganglion cells to complex stimuli.

Network models that include different sources of noise, including noise correlations, will be included in future work.

Component Dependencies

Summarized links to components this key result depends on.

Component ID	Component Name	HBP Internal	Comment
N/A	N/A	*N/A*	*N/A*

2.4.7 Model for high-level contributions to low level vision (T4.4.2)

Description of the model

WEIZMANN: In the model and algorithm, during feed-forward processing primary visual cortex extracts a large number of low-level features, including features coming from the object presented, together with clutter and noise. Using an object model stored in higher visual areas, top-down signals create what we call a 'full interpretation' of the object image: identifying all its parts, completing low-signal features, and eliminating clutter and noise (Ben-Yosef et al. 2017).

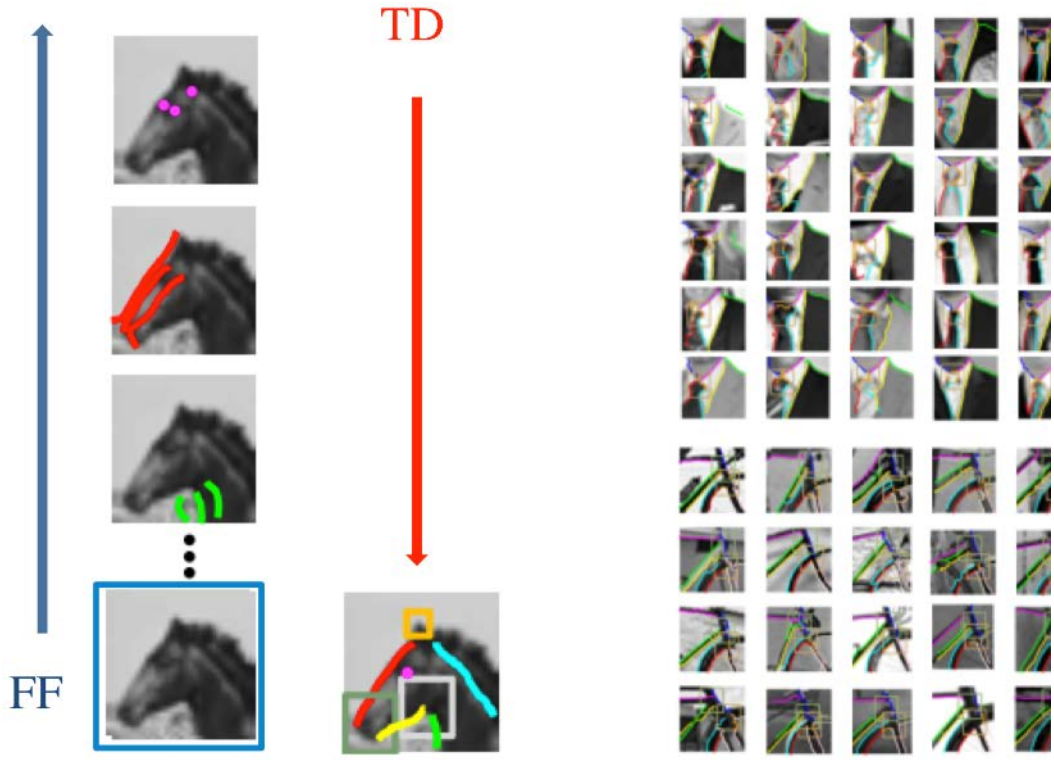

Figure 52 Algorithm for using information from higher-level visual areas back to primary visual cortex.

(a) Left: multiple features are detected by feed-forward (FF) processing in V1. For example, the V1 activation pattern includes multiple candidates for the horse's eye (top image), head contour (second from top), etc. (a) Right: Top-down (TD) processing identifies the correct image features. The process distinguishes between correct object features and spurious ones produced by noise and clutter, and it also enhances relevant object features with weak activation due to low SNR. (b) Results of the model applied to multiple images from two object categories (top: man's torso, bottom: bicycles part).

The model output correctly identifies the low-level features corresponding the object's internal structure. This is obtained by including pairwise relations stored in the higher-level object representation. Accuracy of identifying the correct object features was shown to be significantly higher than processing without the top-down contribution, and closer to humans' behavioral performance in identifying the corresponding image features. The model also explains the large drop in recognition observed in the recognition of minimal imates (Ullman et al. 2016, PNAS 113(10), 2744–2749).

Publications

Ben-Yosef G, Assif L, Ullman S. Full interpretation of minimal images *Cognition.* 2017, 171:65-84.

Ben-Yosef, G. Yachin, A. Ullman, S., A model for interpreting social interactions in local image regions. *Proc. AAAI Spring Symposium Series, Science of Intelligence, Palo Alto, CA,* 2017, 525-528

Conclusion & Outlook

The results of the model demonstrate the functional importance of high-level contributions to low-level visual areas such as primary visual cortex. Together with the retinal input model to primary visual cortex developed in task 4.4.2 (Olivier Marre), the models provide a more complete realistic characterization of the function of low-level visual areas. In the future, we plan to develop the model further during the next period in cooperation with work in SP2 on multi-scale processing in space, time and frequency, leading to a model of the integration of feed-forward and feed-back processing.

Component Dependencies

Summarized links to components this key result depends on.

Component ID	Component Name	HBP Internal	Comment
1066	Plasticity models : SP4 (theory) T 4.3.1 synaptic plasticity and learning	*No*	*Added value*

2.4.8 Basal Ganglia systems level model (T4.4.3)

KTH : A systems level model of the basal ganglia system consisting of 80000 point neurons, built earlier during SGA1 [1], is currently used for investigating several hypotheses on how basal ganglia process cortical inputs in health and disease. For instance, we formed hypotheses how oscillatory components, such as those seen during L-Dopa dyskinesias, can spread into the striatal networks from cortex. Here one prediction is that Fast Spiking interneurons are crucial [2]. Also, we are currently using the model in [1] to investigate what the role of the Arkypallidal neurons in the External Globus Pallidus nucleus (GPe) might be during stop tasks, signaled from cortex via the subthalamic nucleus (STN). An improved version of the systems level basal ganglia model is also underway (planned for SGA2). Furthermore, together with the Juelich collaborators, we have investigated how to estimate, in a more automatized manner, the unknown effective couplings strengths between basal ganglia nuclei [3].

The resulting insights received, together with the successively improved versions of the model will be valuable as such for the external community. For internal use, we will be able to use the already published model as a framework for building hybrid basal ganglia models, consisting of point neuron models modules linked with detailed microcircuit model modules (the latter ones built in SP6).

Publications:

[1] Lindahl M, Hellgren Kotaleski J (2017) eNeuro. Jan 12;3(6). pii: ENEURO.0156-16.2016. doi: 10.1523/ENEURO.0156-16.2016

[2] Belić JJ, Kumar A, Hellgren Kotaleski J (2017) Interplay between periodic stimulation and GABAergic inhibition in striatal network oscillations, PLoS One, Apr 6;12(4):e0175135. doi: 10.1371/journal.pone.0175135

[3] Bahuguna J, Tetzlaff T, Kumar A, Hellgren Kotaleski J, Morrison A. (2017) Homologous Basal Ganglia Network Models in Physiological and Parkinsonian Conditions, Front Comput Neurosci. Aug 22;11:79. doi: 10.3389/fncom.2017.00079.

Achieved Impact

The resulting insights received using the basal ganglia systems level model, together with the successively improved versions of the model will be valuable as such for the external community. For internal use, we will be able to use the already published model as a framework for building hybrid basal ganglia models, consisting of point neuron models modules linked with detailed microcircuit model modules (the latter ones built in SP6).

Component Dependencies

Summarized links to components this key result depends on.

Component ID	Component Name	HBP Internal	Comment
209	*NEST*	*yes*	Simulate the model
1836	*The integrated function of the basal ganglia and its control of downstream motor centres – structure and function of pallidal and subthalamic neurons*	*yes*	Improve the striatal component of the model

2.4.9 Modelling spatial navigation and memory (T4.4.4)

Model of striatal and hippocampal memory systems

We have implemented a simulation of hippocampal and striatal contributions to spatial navigation, following the identification of the relevant cognitive architecture (Chersi and Burgess, 2015; Figure 1). The model consists of a network of rate-coded neurons, with different learning rules governing the different brain areas. Specifically, the striatum learns ego-centric associations between sensory inputs and actions through a temporal difference algorithm relying on reward prediction errors. For example, it can learn the association between seeing a cue and turning right. The model hippocampus, by contrast, learns an allo-centric representation of the environment based on place cells. To test our model, we used it to solve an adaptation to the classic Morris Water Maze task (Pearce et al. 1998), where the goal is to find a hidden platform submerged under opaque water.

An example result of these simulations is shown in Figure 53. Both the striatal model and the hippocampal model can learn relatively short paths to the goal. However, because the striatal learning is dependent on reward prediction errors, it shows 'blocking': it does not learn to respond to a second cue when a preceding cue is already fully predictive of reward. This model provides a framework for application to a series of spatial and non-spatial cognitive tasks. All simulations were run using Python.

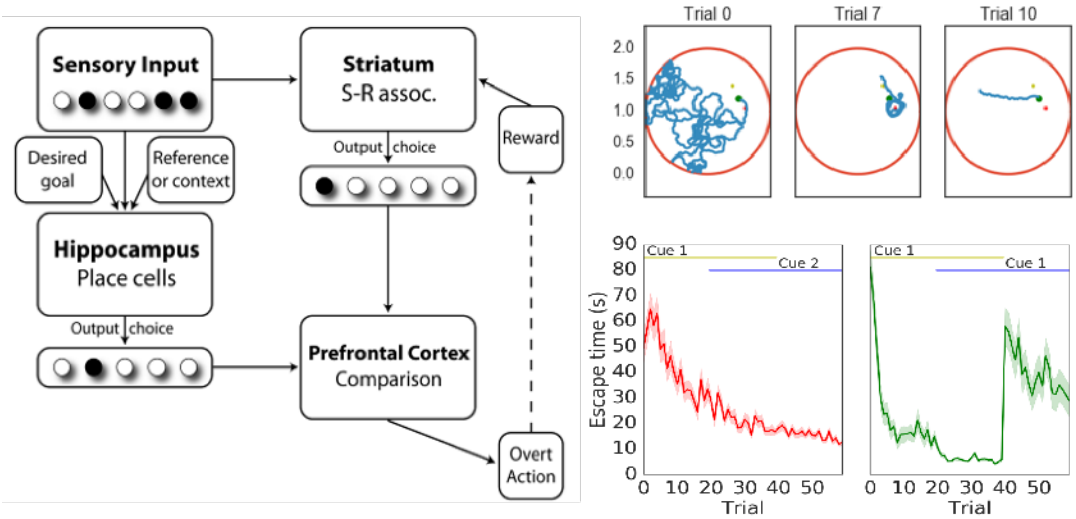

Figure 53 Model of hippocampal and striatal contributions to spatial navigation.

Left panel: model architecture. Separate navigational strategies are computed in the hippocampus and striatum, and the prefrontal cortex compares the respective outputs. Right upper panel: example trajectories showing learning in the Morris Water Maze over trials. Right lower panel: performance on the maze as measured by the

time needed to find the platform. Red and green horizontal lines indicate the presence of two spatial cues. Agents using a hippocampal learning strategy (red line) show learning of the platform location over trials, unaffected by changes in the landmark. Those using a striatal learning strategy (green line) exhibit 'blocking' of learning from a second cue, as evidenced by the drop in performance upon the disappearance of Cue 1.

Extending the model to episodic memory

Based on previous work on human episodic memory (Byrne et al. 2008) we have built a model of how neural representations of egocentric spatial experiences in the parietal lobe interface with viewpoint-independent representations in medial temporal lobe to enable key aspects of spatial cognition. The model shows how populations of know types of spatial cells (place cells, head-direction cells, boundary- and object-vector cells, grid cells, and parietal gain-field neurons) map onto higher cognitive function in a modular way. The interactions between these populations across multiple brain regions provide a mechanistic account of spatial memory, scene construction, novelty-detection, and mental navigation. In particular the model shows how so-called object vector cells (OVCs) may allow memory for items to be incorporated into a contextual representation based on extended environmental boundaries (as expressed in the firing of boundary vector cells; or BVCs). The same cells provide the neural correlated of objects in context during recall/visuospatial imagery (Figure 54). Simulations have been implemented in MatLab (using rate coded neurons) and a manuscript has been submitted to eLife (currently in revision).

Comparison to human episodic memory has been initiated in collaboration with SP3 Episense (Emrah Duzel): looking at human hippocampal involvement in pattern completion using 7T fMRI (Grande et al., 2017). Some aspects of the model are being shared with partners in SP3 Episense (Tony Prescott, Martin Pearson), who are developing a version of the spatial memory model for use on a robotic platform.

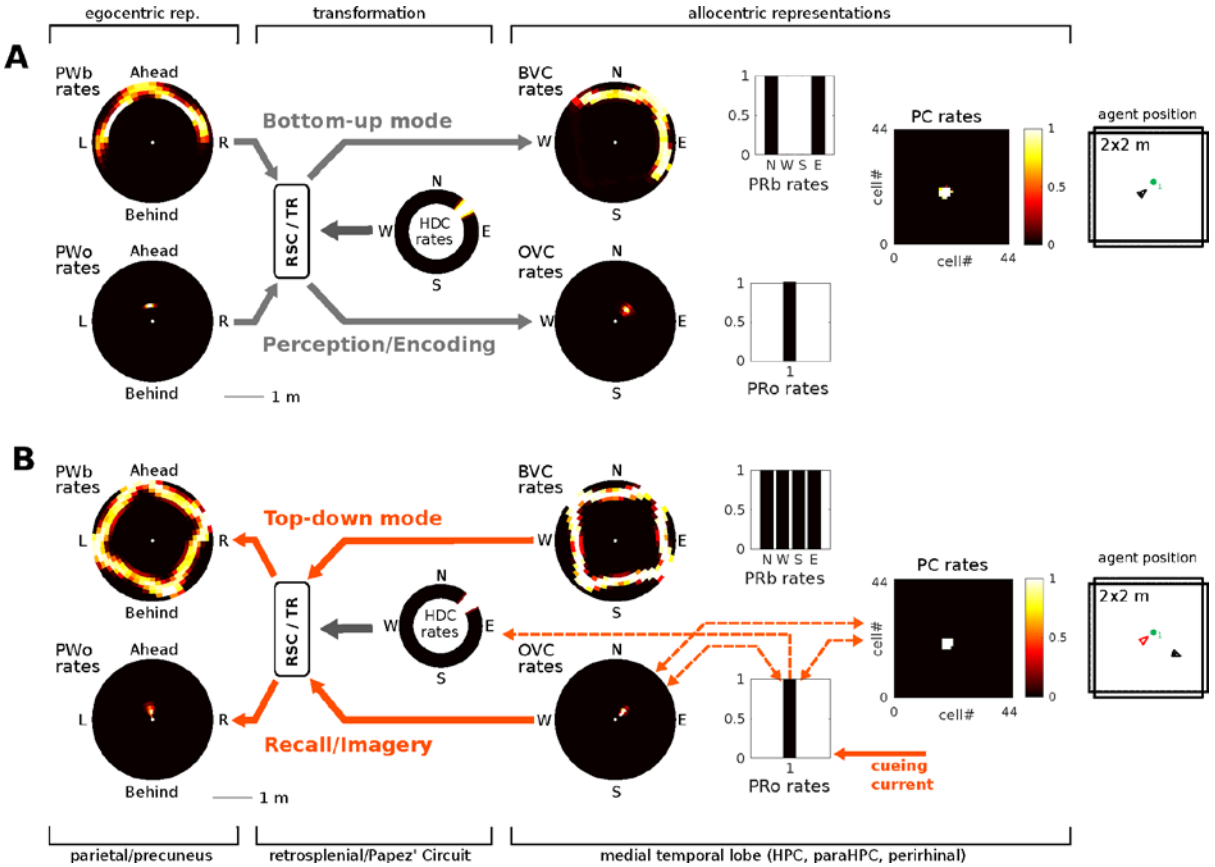

Figure 54 Extension to expisodic memory.

A) In the bottom-up mode of operation sensory inputs drive the model and items can be encoded into memory, when the agent encounters them in an environment (right panel, agent is a trinagle, the object a dot). Population snapshots of the model at the moment of encoding during an encounter with a single object in a familiar spatial context are shown. Left to right: PWb/o populations driven by sensory input form an egocentric representation of

the environment. These populations project to a head-direction-modulated transformation circuit (RSC/TR, hypothesised to be in retrosplenial cortex, details omitted for clarity); The transformation circuit projects to BVCs and OVCs which, together with perirhinal identity neurons constitute the main drive to place cell (PCs; coding for the agents location); perirhinal (PRb/o) neurons are driven externally, reflecting object recognition along the ventral visual stream. At the moment of encoding, reciprocal connections between PCs, OVCs, PRo neurons are learned. B) In the top-down mode of operation the model re-instates egocentric parietal representations (reflecting visuospatial imagery) reconstructed from memory. The agent has moved away from the object (current agent location: black triangle; right panel). Cueing the agent to remember the encounter with the object in (A), current is injected into the corresponding PRo neuron (right of panel). This drives firing of connected PCs (dashed orange connections, learned at encoding). PCs become the main drive to OVCs, BVCs and PRb neurons. BVC and OVC representations are transformed to their PW counterparts, thus reconstructing egocentric parietal representations (PWb/PWo) similar to those at the time of encoding (left of panel). Thus, the agent reconstructs the spatial scene of the encounter from the previous point of view (red triangle, in rightmost panel). Color code: heat maps show population firing rates frozen in time. Black: zero firing rate, white: maximal firing rate.

Modelling the integration of environmental and self-motion information in neural representations of location.

We have developed a model of grid cell firing in which grid cells combine path integration and environmentally anchored sensory information to generate an optimal estimation of the animal's current location within an environment. In this framework, the firing of the grid cell population represents a probability distribution of self-location across space. Path integration is performed by translating this distribution in response to the agent's self-motion, with associated noise. Environmental sensory information is provided by place cell inputs, whose weights are learned upon exposure to a novel environment. The localisation and learning features together constitute a neurally plausible system for simultaneous localization and mapping (SLAM; Durrant-White & Bailey, 2006). Weight stabilisation allows the model to account for place cell stabilisation in pre-weanling pups (Meussig et al., 2015). Non-uniform place cell densities can re-create grid cell firing pattern distortions (Figure I; Stensola et al., 2015), and grid patterns rescale in response to environmental manipulations (Figure 3H; Barry et al., 2007). The modelled grid cell firing patterns can be compared with experiments designed to measure the relative influence of self-motion and environmental sensory inputs (Chen et al. (submitted); SP3 Episence, Cacucci lab). Simulations have been implemented in Matlab.

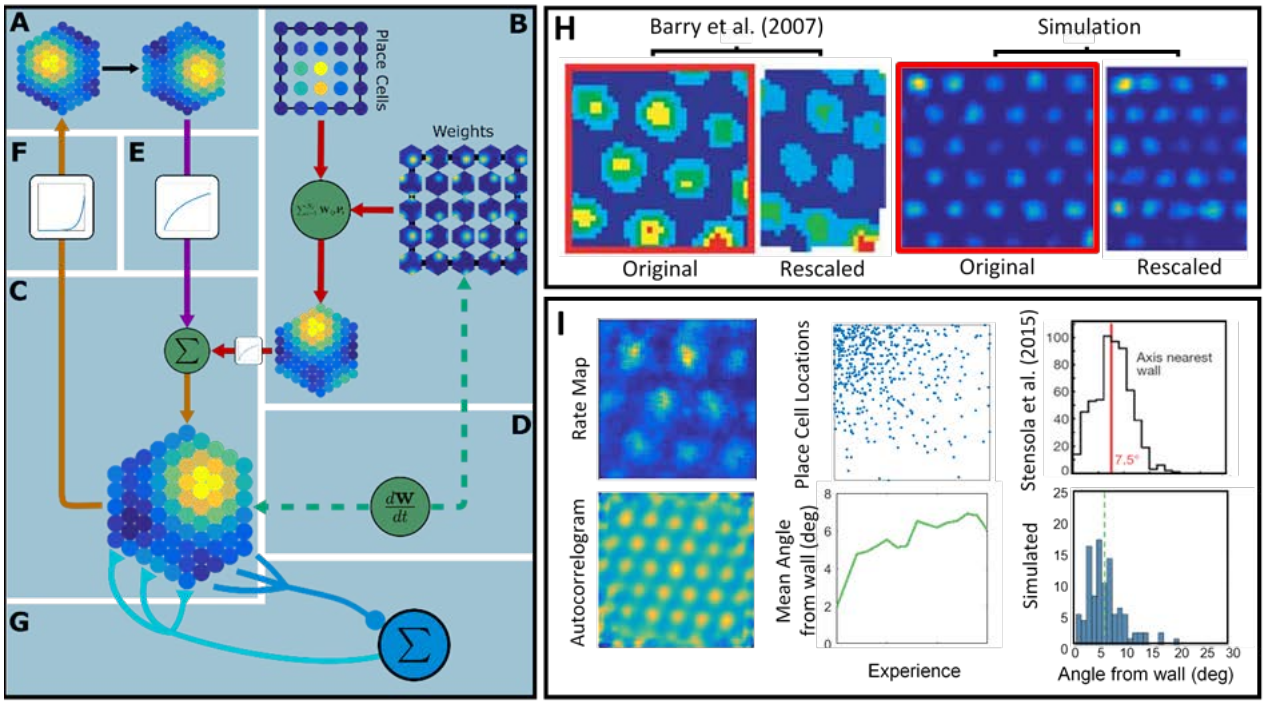

55 Integration of self motion and environmental information.

A) The grid population firing rates represent a probability distribution over location in periodic grid space. The distribution is translated, reflecting path integration (PI) according to the animal's movement. B) Weighted place cell firing rates generate an environmentally anchored sensory estimate of current location. C) The PI and sensory estimates are combined to produce a refined estimate of location. D) Learning between the place and grid cells

corrects errors between the PI and sensory estimates over time. E,F) Logarithmic and exponential transfer functions. G) Recurrent inhibition normalises the firing rates of the posterior distribution. H) The grid pattern rescales in response to environmental rescaling as observed experimentally. I) Nonuniform distributions of place cell firing fields (above, middle) causes a shearing of the grid pattern and an orientation offset from the wall of the environment which develops with increasing experience of the environment, as observed experimentally.

Extension to spiking neurons for use with the SpiNNaker platform

Modeling grid cell phase coding

One aspect of grid and place cell firing requires use of a spiking neural network model (rather than the firing rate models, above): namely 'theta phase precession' in which spiking occurs at progressively earlier phases of the 5-11Hz local field potential (LFP) theta oscillation as each firing field is traversed. This supports a phase code for location in rodents. But a puzzle is presented by human data, in which LFP oscillations are much more variable in frequency.

We have implemented a spiking neural network model that allows us to examine the putative function of rate and phase coding for multiplexing information about an animal's trajectory through space. We show that these properties can be accounted for if the intrinsic firing frequency of grid cells varies relative to some baseline frequency according to movement velocity. We then show that it is possible to simultaneously decode multiple types of information from the population: location from firing rates; movement direction from firing phase; running speed from mean firing rates; and an arbitrary fourth variable, such as anxiety, from the baseline oscillation frequency. Importantly, this is possible even if the baseline oscillation has a highly variable frequency – such as that observed in recordings from depth electrodes in human hippocampus (Bush et al., 2017). Finally, we describe analytical methods that can identify phase coding in the absence of a constant frequency oscillation, as in single unit recordings from the bat or human brain (Bush and Burgess, in prep). Simulations have been implemented in Matlab.

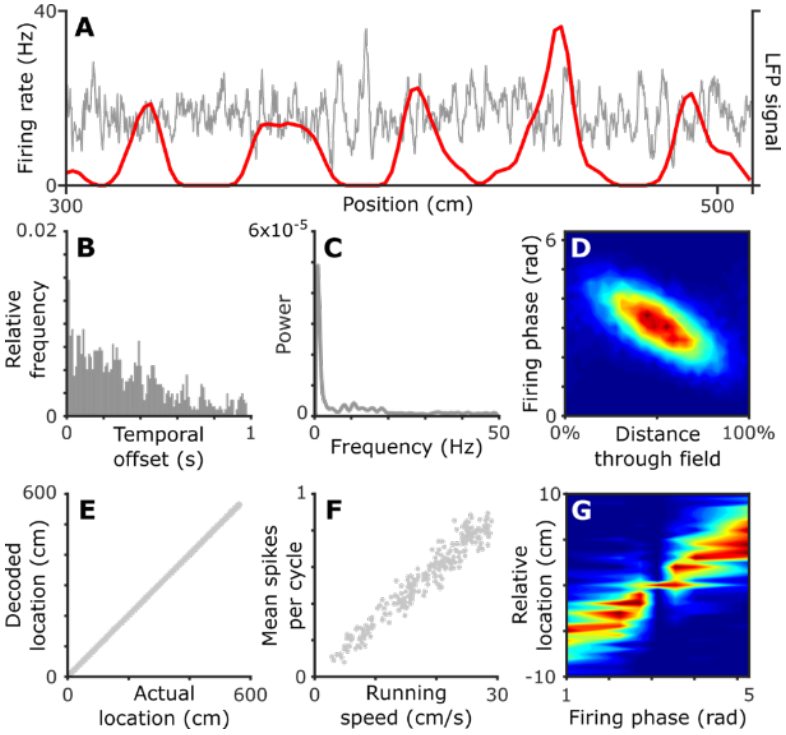

Figure 56 Grid cell firing patterns can encode multiplexed spatial information.

A) Grid cell firing rate along a 1D track (red line) generated using a baseline oscillation with highly variable frequency (grey line) recorded from depth electrodes in human hippocampus. B,C) Grid cell spike train auto-correlogram and power spectrum, which exhibit no clear rhythmicity. D) Grid cell firing phase relative to the baseline oscillation, which becomes progressively earlier as each firing field is traversed. E-G) Accurate decoding of multiplexed spatial information from grid cell population activity in each oscillatory cycle. Location on the track

can be recovered from population firing rates (E); running speed from the number of spikes in each cycle (F); and movement direction from population firing phase (G).

Current work is exploring the use of spiking neurons in a grid cell based navigation model (inspired by Bush et al. 2015), implemented in Python to run on the SpiNNaker platform.

Implementation to platforms

The above models have been added to the Collaboratory

References (# indicates HBP funded)

Barry C, Hayman R, Burgess N, Jeffery K (2007) Experience-dependent rescaling of entorhinal grids. Nature Neuroscience, 10:682 - 684.

Bicanski A, Burgess N (2018). A Model of Spatial Memory and Imagery - From

2 Single Neurons to Cognition (in revision at *eLife*)

Bush D, Burgess N, Phase coding without rhythmicity (in prep)

Bush D*, Bisby JA*, Bird CM*, Gollwitzer S, Rodionov R, Diehl B, McEvoy AW, Walker MC, Burgess N (2017) Human Hippocampal Theta Power Indicates Movement Onset and Distance Travelled. *PNAS* 114: 12297-12302

Bush D, Barry C, Manson D, Burgess N (2015) Using grid cells for navigation. Neuron. 87: 507-20.

Byrne P, Becker S, Burgess N (2007). Remembering the past and imagining the future: a neural model of spatial memory and imagery. Psychological Review 114 340-375.

Chen G, King JA, Lu Y, Cacucci F, Burgess N (2018) Spatial cell firing during virtual navigation of open arenas by head-restrained mice. bioRxiv https://www.biorxiv.org/content/early/2018/01/11/246744

Chen G, Lu Y, King JA, Cacucci F, Burgess N, Differential influences of environment and self-motion on place and grid cell firing patterns (in prep)

Chersi F, Burgess N (2015) The cognitive architecture of spatial navigation: Hippocampal and Striatal contributions. Neuron 88: 64-77.

Durrant-Whyte H, Bailey T (2006). "Simultaneous localization and mapping: part I." IEEE robotics & automation magazine 13: 99-110.

Evans ST, Burgess N, Integration of environmental sensory and self-motion information by grid cells (in prep)

Grande X, Bisby JA, Berron D, Horner AJ, Duzel E, Burgess N (2017) Hippocampal Subfield Contributions to the Recollection of Multi-Element Events: Functional Evidence at 7 Tesla. Society for Neuroscience Abstract 167.04 / SS19

Muessig L et al. (2015) A developmental switch in place cell accuracy coincides with grid cell maturation. Neuron 86: 1167-1173.

Stensola, T, et al. (2015) Shearing-induced asymmetry in entorhinal grid cells. Nature 518: 207.

Achieved Impact

Our consideration of how environmental and self-motion information combine to drive grid cell firing patterns (Evans & Burgess, in prep) is being tested in experiments that we have helped to design, in collaboration with SP3 Episense (Cacucci lab), see joint publications by Chen et al (bioRxiv & in prep).

Our consideration of episodic memory (Bicanski and Burgess, in prep) has helped to design an experiment on human hippocampal pattern completion, in collaboration with SP3 Episense (Duzel lab), see Grande et al (2017).

Our Code for the model for episodic memory has been shared with SP3 Episense (Pearson lab) for implementation on a mobile robot.

Conclusion & Outlook (UCL)

The above models aim to bridge scales between populations of rate coded neurons to the behaviour of the animal, within the context of spatial cognition and memory. Providing links to behaviour remain the main way for understanding whether a simulated brain is working in the same way as the real brain, i.e. in terms of its ultimate output, and using spatial cognition allows us make use of neuronal population encoding schemes known to be present in the brain. The simulations of striatal versus hippocampal memory systems allowed us to examine the behavioural effects of different learning rules and compare them to the (pre-existing) experimental data in the Morris Water Maze. It also allowed us to look at how two brain regions interact to control behaviour. The episodic memory model allows this understanding to be extended to aspects of human episodic memory, enabling simulation of recollection of the spatial scene in which an object was encountered, and comparison with (pre-existing) experimental data. We also examined how self-motion and environmental information are integrated in forming these neural representations of location, and have contributed the design of experiments to invesitgate this (collaboration with SP3 Episense). These models are being shared with investigators in SP3 (Pearson, Prescott) to aid their implementations of memory on robotic platforms. Spiking neuron models where used as didictated by the question which was investigated, e.g. when modeling phase coding, and will pave the way for implementation on SpiNNaker.

Component Dependencies

Summarized links to components this key result depends on.

Component ID	Component Name	HBP Internal	Comment
N/A	N/A	*N/A*	*N/A*

2.4.10 Large-scale model of visuo-motor integration (T4.4.5)

Please refer to Deliverable CDP4 – 2.4 Large-scale of visuo-motor integration (T4.4.5) for details of the model.

Component Dependencies

Summarized links to components this key result depends on.

Component ID	Component Name	HBP Internal	Comment
N/A	*N/A*	*N/A*	*N/A*

2.5 Linking Model Activity and Function to Experimental data (WP4.5)

2.5.1 Comparison of experimental and simulated neural activity data (T4.5.1)

The JUELICH partner continued to work on reproducible workflows [2] for the comparison between experimental and model data. The experimental data consist of recordings of neural spiking activity from macaque motor cortex [1, 6]. The spiking network simulations were performed by NEST [4] in collaboration with T4.2.1, T4.1.3 and T4.1.4. . Both, the experimental and the simulated data, are analysed with the same toolbox (Elephant, developed in T5.7.1) and the same analysis workflow [5]. The model validation is performed with software and frameworks collaboratively developed with T6.4.4 andT9.1.5.

The experimental data are massively parallel recordings during resting state (no task or stimulus) and during a reach to grasp task from macaque monkey motor cortex [1, 6]. The data consist of simultaneous single unit spiking activities and LFPs recorded with a 100 electrode Utah array covering 4x4mm² of cortex. For the resting state we also have a video of the monkey's behaviour available, while during the task the behavioural events were registered. Pre-processing involves the separation of the spiking activity into putative excitatory (E) and inhibitory (I) neurons, and the segmentation in behaviorally relevant epochs. We published a reproducible data analysis workflow where the spiking statistics (firing rate, coefficient of variation, correlation coefficient) during resting state have been analysed in the HBP Collaboratory (#2493). Ongoing work using principal component analysis of spike counts [3] show that inhibitory units modulate their firing rates more strongly than excitatory units with respect to behaviour.

The simulated data are generated using the extension of the cortical microcircuit model [4] to a size of 4x4mm² including lateral distance-dependent connectivity. It is composed of 8 neuronal populations (E&I point neurons in 4 layers), and a subsampling routine to record the same number of neurons as measured experimentally (about 140). For a preliminary version of the extended mesocircuit see component 777.

The workflow for comparison of electrophysiological and simulated data is developed together with T6.4.4 and T9.1.5. It is based on the NEST-Spinnaker workflow (provided in the Collaboratory #507) using the newly written Python module NetworkUnit and tools provided by task T5.7.1 (Elephant).

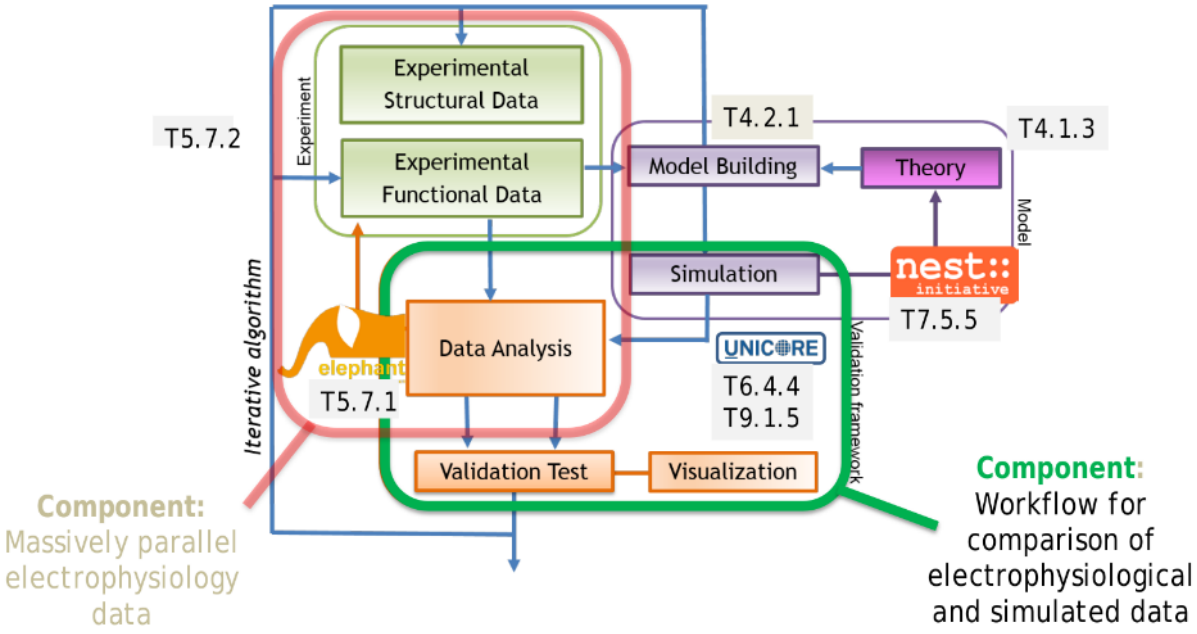

Figure 57 Schematic of the reproducible integrative loop workflow comprising the analysis steps for experimental and simulated data together.

Collaborating tasks are given at each step and contents of components are grouped in red and green rectangles.

Achieved Impact

Implementation to platforms

We published a reproducible workflow for the analysis of experimental data in the HBP Collaboratory (#2493). Simulation of the cortical microcircuit model is also available through the Collaboratory (#507).

Related Publications

[1] Brochier et al. (2018). Massively parallel recordings in macaque motor cortex during an instructed delayed reach-to-grasp task. Data publication, Scientific Data, Data available at *https://web.gin.g-node.org/INT/multielectrode_grasp*

[2] Denker & Grün (2016). Designing workflows for the reproducible analysis of electrophysiological data. in: Brain Inspired Computing, Amunts et al. (Eds.), Lecture notes in computer science, vol 10087. pp. 58–72. doi:10.1007/978-3-319-50862-7_5.

[3] Kass et al. (2018). Computational neuroscience: mathematical and statistical perspectives. Annual Review of Statistics and Its Application 5. doi:10.1146/annurev-statistics-041715-033733.

[4] Potjans & Diesmann (2014). The cell-type specific cortical microcircuit: relating structure and activity in a full scale spiking network model. Cereb Cortex, vol 24(3), 785-806. doi:10.1093/cercor/bhs358.

[5] Senk et al. (2016). A collaborative simulation-analysis workflow for computational neuroscience using HPC. in: Di Napoli et al. (Eds.), Lecture notes in computer science, vol 10164. doi:10.1007/978-3-319-53862-4_21.

[6] Torre et al. (2016). Synchronous Spike Patterns in Macaque Motor Cortex during an Instructed-Delay Reach-to-Grasp Task. J Neurosci, vol 36(32):8329-40. doi:10.1523/JNEUROSCI.4375-15.2016.

Conclusion & Outlook

The Juelich partner identified an appropriate use-case for the comparison between experimental and simulated data, namely to compare massively parallel recordings from monkey motor cortex during resting state with a mesocircuit model. We obtained the necessary experimental data and we delivered this data as component 418 (project-lifecycle.herokuapp.com/component/418), as described in MS 4.5.1.

We also published a Collaboratory (#2493) for the corresponding data analysis. The network model simulations (generic mesocircuit, component 777), as well as the subsequent validation framework for comparing different types of data (cf. Collaboratory #507) are ongoing projects. Both are strongly related to other HBP tasks and are therefore tackled together with other WPs and SPs (WP4.1, WP4.2, SP5, SP6, SP7, and SP9). Future work will include a detailed analysis of the experimental data and its implementation in the Neural Activity Resource (T5.7.2) together with metadata and preprocessing results. The generic mesocircuit model will be implemented in HBP platforms and model parameters will be adapted to reproduce the observations in the monkey motor cortex.

Component Dependencies

Summarized links to components this key result depends on.

Component ID	Component Name	HBP Internal	Comment
777	4x4 mm2 motor cortex model (model)	Yes	Generation of cortical mesocircuit model
418	Massively Parallel Electrophysiology data (data)	Yes	Analysis of experimental data

348	Component 115-3: Elephant (software)	Yes	Software used for analysis of neural activity data
358	Component 105-1c: Collaboratory Jupyter Notebook (service)	Yes	Notebooks used in the HBP Collaboratory
721	SP6-T6.4.4-SGA1-Model Validation Service (service)	Yes	Software for model validation
209	NEST - The Neural Simulation Tool	Yes	Software for simulation of mesocircuit model
330	HPC systems at JSC	Yes	HPC infrastructure used for simulation
373	Collaboratory Storage Service	Yes	Data storage for experimental data used in reproducible analysis workflow
324	SGA1 - Federated data storage with flexible permission management and remote access	Yes	Data storage for experimental and simulated data to be used in validation workflow

2.5.2 Models of mouse brain function from structure (T4.5.1 & T4.5.2)

Description of the model

The AMU partner has worked on a whole brain mouse models of spontaneous resting state activity, which were validated against mouse recordings. This work utilized the open source tracer dataset of the Allen Institute (Oh et al., 2014) that was implemented into The Virtual Brain (TVB) (Sanz et al. 2015), thus allowing detailed Structural Connectivity (SC) to be obtained (Melozzi et al 2017).

Within the framework of CDP1, the whole brain mouse network models were further validated against empirical data recorded in SP1 using calcium imaging. The top-down models systematically exploits the effects of the SC constraints upon network dynamics, and was compared with empirical cortical activation maps in SP1, in healthy, stroke and rehabilitation. The structural impact of the stroke and of the recovery was systematically analyzed, and the best fit was obtained for parameters which were in agreement with the experimental results for the structural damage during the stroke and the recovery.

Data analysis and modelling were performed for recordings of one hemisphere of one animal (SP1 data), and further recordings from both hemispheres are expected from 4 more animals.

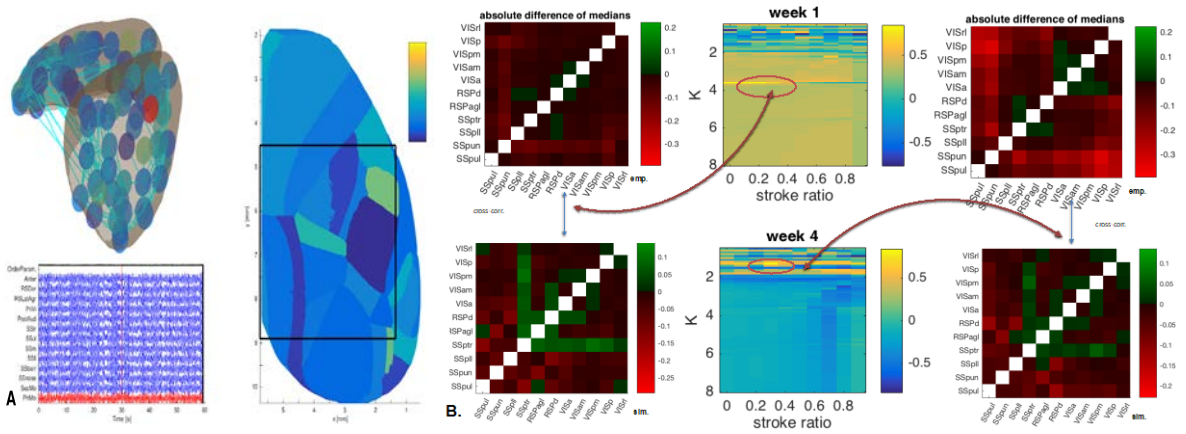

Figure 58

A. Brain network model of the cortical activity in mice during healthy state and stroke. The stroke occurs in M1 (primary motor cortex), and the dynamics of the areas visible in the calcium imaging experiment is modelled for different impacts of the stroke and the recovery B. Comparision for the functional connectivity between empirical data in first and in the fourth week after the stroke, and the model for one point in the parameters space. Generally better predictability is observed for higher damage and lower rebound at week1 than at week4, which is line with the experimental data for the structural damage and recovery.

Resting state stimulated and propagation patterns due to connectivity have been analyzed in line with the experimental data from voltage-sensitive dyes imaging. The propagation of activation patterns was systematically studied, thus helping to describe the excitability of different cortical areas of the mouse brain and to mathematically and computationally investigate the non-stationary properties and capacity of the models to propagate activations through the network.

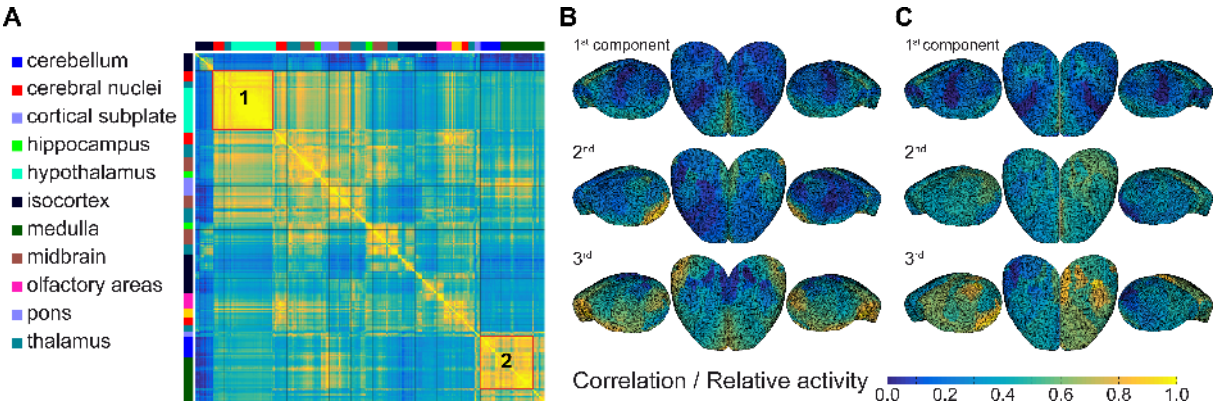

Figure 59 Specific focal stimulations activate similar networks.

Panel A is the similarity matrix of stimulation with the clusters 1 and 2. Panels B and C show the responsive networks (isocortex) of cluster 1 and of cluster 2.

Implementation to platforms

Component 998, “Allen Mouse Atlas (AMA) based brain network” (T4.5.2)

Component 1574, “Structural and functional connectivity at different scales” (T4.5.1)

Implementation to platforms

This model was integrated to the collaboratory.

Publications

Melozzi F, Bergmann E, Kahn I, Jirsa VK, Bernard C. Individual predictability and comparison between different structural connectivities (in preparation)

Petkoski S, Allegra L, Pavone F, Jirsa V. Brain network model for mouse stroke and recovery (in preparation)

Spiegler A, Mohajerani M, Jirsa V. Network dynamics after focal stimulation in a connectome-based network model of the mouse brain (in preparation)

Achieved impact

This model will be continued to include networks of spiking neurons and mean-field models.

Component Dependencies

Summarized links to components this key result depends on.

Component ID	Component Name	HBP Internal	Comment
998	*Allen Mouse Atlas (AMA) based brain network (T4.5.2)*	*Yes*	*Build the structure connectivity of the healthy, stroke and rehabilitation in mice*
1574	*Structural and functional connectivity at different scales (T4.5.1)*	*Yes*	*Explore the impact of structural lesions to the functions*
2303	*Sub-cortical recording and manipulation of neuronal activity in awake mice C1.3.4.2*	*Yes*	*Helped obtaining the level of the damage and the recovery (rewiring) due to stroke, which is used in the model*
552	*Fluorescence imaging of cortical activity after stroke*	*Yes*	*Validate the model with imaging data in stroke and recovery in mice.*

2.5.3 Comparison of models with mouse and human brains (T4.5.1)

Description of the model

AMU partner has reconstructed epileptic patients' brain networks, using their specific anatomical properties and used the Epileptor, a neural mass model capturing the temporal evolution of a seizure including on- and offset. Based on clinical hypothesis of EZ, we reproduced seizure propagation in silico as observed empirically with SEEG electrodes implanted in the patient. These propagation patterns cannot be captured by functional connectivity due to their inherent non-stationarity. We made the following steps: 1) Proix et al (2016) built the processing chain of all structural images (dMRI, MRI) required to build a virtual brain. 2) Jirsa et al (2017) demonstrated the methodology and proof of concept of how to create personalized models and fit them against empirical neuroimaging data. 3) Proix et al (2017) performed a pilot study (N=15), where we computed a score estimating the difference between the EZ identified by the brain model, and that identified by the clinicians during pre-surgical evaluation. This study demonstrated the favourable correlation between model prediction and surgery outcome. In other words: negative surgery outcome correlates with surgery not performed in line with model predictions.

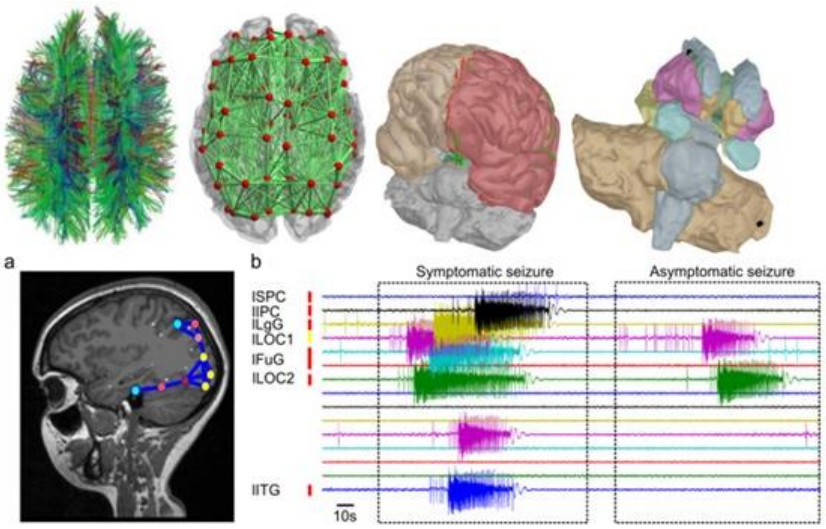

Figure 60 Components of personalized large-scale brain model network.

(Upper row from left to right) Connectivity derived from dMRI, large-scale network model, cortical and subcortical surfaces. (Bottom row, from left to right) Brain areas in model with increased epileptogenicity delineating the Epileptogenic Zone and Propagation Zone. (a), exemplary simulated time series of symptomatic/asymptomatic seizure (b).

AMU partner has also been involved in introducing a new neural field model that unifies and explains the previously observed diversity in spatiotemporal dynamics of seizure initiation, propagation and termination and their multiple time scales. The model demonstrated how the interplay between temporal and spatial scales leads to: (i) slow propagation of an ictal wavefront whose speed is hampered by fast oscillations, (ii) fast propagation of SWDs through coupled-oscillator dynamics, (iii) the formation of ictal clusters via stagewise recruitment with synchronous and asynchronous seizure termination. The model's predictions that SWD propagation and connection strength correlate with the type of spatial patterns of seizure recruitment and termination was confirmed in SEEG and tractography data recorded from patients with epilepsy.

Figure 61 The Epileptor field model reproduces multiscale features of spatiotemporal seizure dynamics.

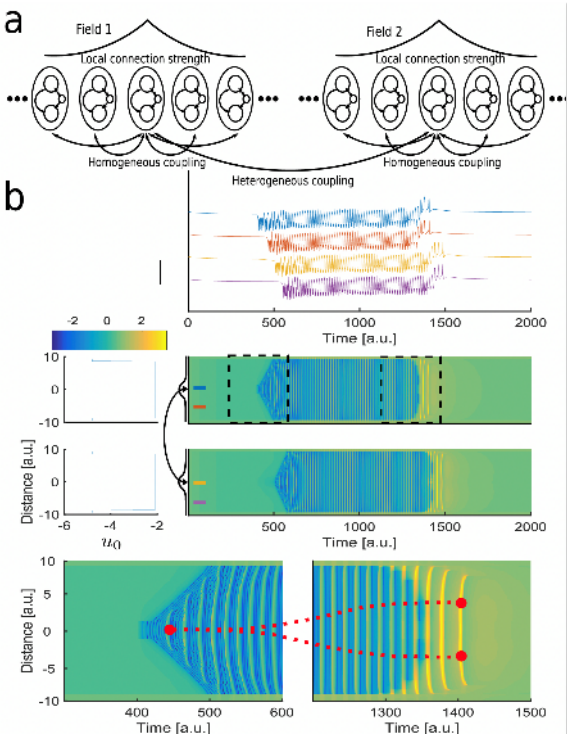

(a) Schematics for the Epileptor field model. At each spatial location of the neural field, an Epileptor site (oval) includes two neural populations and a slow permittivity variable (inner circles). Epileptors are connected to their neighbors via local homogeneous coupling, which decays exponentially with pairwise distances. Epileptors also connect to Epileptors in other fields through heterogeneous coupling. (b) Simulation of a model including two distant Epileptor fields (middle plot). The top field includes the seizure onset area, while the bottom field

represents a more distal brain area. Spatial values for excitability parameter (u0) and simulated spatiotemporal activity are shown on the left and right, respectively. The curved arrow indicates heterogeneous connections between the two fields. The connection kernels (black lines) were centered at the indicated locations. The seizure started in the top Epileptor field, slowly propagated throughout the field, then eventually recruited the bottom Epileptor field, where it slowly propagated as well. The horizontal colorbar indicates the activity level for the middle and lower plots. Time series at four spatial locations in the two fields (indicated by colored bars in the middle plot) are shown in the top plot. The two bottom plots show a zoomed in view of the spatiotemporal activity at seizure onset (left) and offset (right). Red dots mark the source location of the propagating SWDs at seizure onset and offset. As the seizure evolved, the source of SWDs changed along with the slow ictal wavefront across each field.

Achieved impact

This model will be continued in SGA2 to network models based on personalized DTI-derived connectome data for better identification of the epileptogenic zone and propagation patterns of epilepsy patients.

Implementation to platforms

Component 1574, "Structural and functional connectivity at different scales" (T4.5.1)

Implementation to platforms

This model was integrated to the collaboratory through TVB.

Publications

Proix T, Bartolomei F, Guye M, Jirsa V. Individual brain structure and modelling predict seizure propagation. Brain **140,** 641–654 (2017).

Proix T, Jirsa V, , Bartolomei F, Guye M, Trucollo W. Predicting the spatiotemporal diversity of seizure propagation and termination in human focal epilepsy. Nature Neuroscience (in press) (2018).

arXiv preprint: https://arxiv.org/pdf/1707.00772

Achieved Impact (AMU)

This model will continue in SGA2 with two tasks for identifying epileptogenic zones in epileptic patients and for studying the propagation zones.

Conclusion & Outlook (AMU)

AMU: The human epilepsy model alows validating empirical data of propagation of epileptic seizures with whole brain network models derived from human connectome data using neural mass models. The model will be continued in the next period in order to improve the identification of the epileptogenic zones and propagation patterns in the epileptic patients.

The mouse connectome model has demonstrated the constarins of the structure to the function, as observed in the mouse experimental data. The model will be continued in SGA2 and it will be validated against high-dimensional neuronal network models, enabling parameter space explorations to guide high performance computations (SP7).

Component Dependencies

Summarized links to components this key result depends on.

Component ID	Component Name	HBP Internal	Comment
1574	*Structural and functional connectivity at different scales (T4.5.1)*	*Yes*	Validate the model predictions on seizure propagation and patient-specific surgery outcome against empirical intracranial and clinical data from epileptic patients

263	*UNICORE (software)*	*Yes*	*Software to access HPC from within HBP Collaboratory*
361	*Component 115-3b: Neo (software)*	*Yes*	*Python packqage for data representation of experimental and simulated data*
360	*odML (software)*	*Yes*	*Meta data format for experimental and simulated data*
362	*Collaboratory Task Service (service)*	*Yes*	*Collaboratory task service for HPC tasks*
821	*Workflow for comparison of electrophysiological and simulated data (service)*	*Yes*	*Workflow to compare macaque motor cortex data with mesocircuit simulation (component owned by T4.5.1)*

2.6 The European Institute for Theoretical Neuroscience (WP4.6)

We report here all the models developed by the EITN postdocs, which describe collaborations between two HBP partners, within SP4, or between SP4 and another SP. EITN cosupervised post-docs activity details can be found in D4.6.2.

2.6.1 Comparison of Up and Down state oscillations in mouse and human

This work started in collaboration between UNIC (Alain Destexhe, Thierry Bal) and SP2 (Huib Mansvelder) to compare slow oscillations in brain slices, consisting of Up and Down states. The slow oscillations were obtained experimentally in mice, and we would like to apply the same experimental protocol to human slices.

The data will serve to constrain computational models of spiking network (AdEx neurons), and determine the connectivity requirements to account for differences between mouse and human oscillations.

This work just started and will be reported in SGA2.

2.6.2 Towards Third-Factor learning rules on SpiNNaker (T4.6.2)

Please refer to Deliverable CDP5 – 3.5 Plasticity rules in neuromorphic hardware for details of the model.

Anna Bulanova (EITN/SP4), Oliver Rhodes (UMAN/SP9), Steve Furber(UMAN/SP9), André Grüning (SURREY/SP4); collaboration between SP9 (U Manchester) and SP4 (U Surrey, EITN Paris)

Implementation to platforms

375 SP9: SpiNNaker software stack (software)

468 SP9: Principles for brain-like computation (model)

1066 SP4: Plasticity - Synaptic plasticity and learning (model)

1341 CDP5: Concept showcases in big-systems (model)

1342 CDP5: Guiding platform design on functional plasticity (model)

Implementation to platforms

The changes to SpiNNaker software are in *Fusi_plasticity* branch of the official SpiNNaker github repository. Eventually this branch will be merged into *master* branch, and installed on the HBP portal.

https://github.com/SpiNNakerManchester/sPyNNaker/tree/Fusi_plasticity

https://github.com/SpiNNakerManchester/sPyNNaker8/tree/Fusi_plasticity

Publications

Paper in preparation: working title: "Neuron-state dependent learning rules on Spinnaker"

Achieved Impact

During this project SpiNNaker software infrastructure was changed to facilitate usage of internal neuron variables in plasticity updates. This will make future implementation of all learning rules that require access to any neuron variables easier.

Conclusion & Outlook

As the first stepping stone of evolving SpiNNaker neuromorphic platform to support Third-Factor learning rules, we have implemented the Brader-Senn-Fusi rule (Brader et al., Neural Computation 2007). This rule expands the set of plasticity rules offered by SpiNNaker: in the past only spike timing dependent plasticity rules were available, and not those depending on internal states of the neuron like the Brader-Senn-Fusi rule. In addition to providing users with the learning rule we implemented, this will make future development of any rules that require access to the neuron state more straightforward.

Our short term plan is reproducing the classification experiments from the original paper (Brader et al., Neural Computation 2007). Long term, our work will be used as a stepping stone for SpiNNaker implementations of more complex learning rules that require multicompartmental neuron models.

Component Dependencies

Summarized links to components this key result depends on.

Component ID	Component Name	HBP Internal	Comment
375	*SpiNNaker software stack (SP9)*	*Yes*	*Use of spinnaker for simulations and co-development of SpiNNaker code*
468	*Principles for brain-like computation (model, SP9)*	*Yes*	*Basis for part of application of rules considered for SpiNNaker*
1066	*Plasticity.- synaptic plasticity and learning (model)*	*Yes*	*Basis for learning rules consider for SpiNNaker*
1341	*Concept showcases in big-systems (model, CDP5)*	*Yes*	*Contribute small scale test-bed systems*
1342	*Guiding platform design on functional plasticity (model)*	*Yes*	*Co-development and guidance of software development for SpiNNaker re plasticity*

2.6.3 Theoretical Mean-field Model for COBA networks of AdEx Neurons displaying alternation between Up and Downs (T4.6.2)

Description of the model

In collaboration with Maurizio Mattia (SP3) and Alain Destexhe (SP4), we apply a fully theoretical approach to work out a mean-field model of neuronal population activity, for conductance based (COBA) networks of Adaptive Exponential (AdEx) integrate and fire neurons. The network is based on two different cell types, excitatory (E), also known as "regular spiking" (RS), and inhibitory (I) or "fast spiking" (FS) neurons (Figure 62A). The mean-field model of RS-FS networks was based on a Master Equation Formalism proposed previously (El Boustani- Destexhe 2009), while the method to evaluate the transfer function is inspired from (Brunel 2000). The dynamics of the system can be described by the following equations

$$\begin{cases} \tau_E \frac{d\nu_E}{dt} = TF_E[\nu_E, \nu_I, W(t)] - \nu_E \\ \tau_I \frac{d\nu_I}{dt} = TF_I[\nu_E, \nu_I] - \nu_I \\ \frac{dW}{dt} = -\frac{W}{\tau_W} + b\nu_E - a(\mu_V^E - E_l) \end{cases}$$

where ¤E(t) and ¤I(t) are the excitatory and inhibitory population activities, and *W*(t) the level of adaptation, whose dynamics is defined by parameters *a* and *b*.

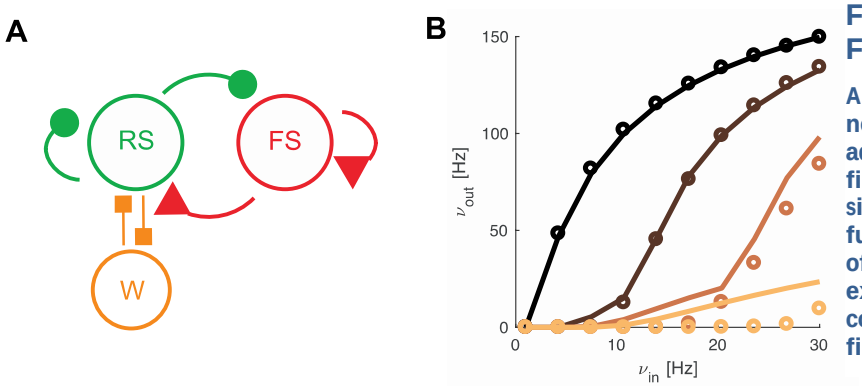

Figure 62 Theoretical Mean Field for RS-FS network:

A. Sketch of the structure of RS-FS network. RS is also affected by adaptation W. B. Comparison between firing rate evaluated through spiking simulations (circles) and transfer function prediction (lines) as a function of the input firing rates. On x axis excitatory firing rate, while different colors represent different inhibitory firing rates.

One of the major challenges of such model is to evaluate the transfer function for neurons provided of COBA integration of signals, that generates a complicated and bidirectional interaction between the statistics of the input and the statistics of the membrane potential. The mean-field model obtained was tested against numerical simulations of the network and, as shown in Figure 62B, the average firing rate of the population is well predicted by the theoretical transfer function. One possible application of the model is to explore a specific dynamical regime of the network that is the alternation between Up and Down states, also referred to as Slow Oscillations (SO). Here we report a preliminar result of the mean-field model, succesfully describing the oscillating activity of a RS-FS networks (Figure 63A), as observed in the spiking network. It is also possible to use standard metods for dynamical system to study the model as nullclines representation (Figure 63B). In Figure 63B is also showed how the average membrane potential changes across the dynamics (colorcoded in the background), that is a major point in COBA models.

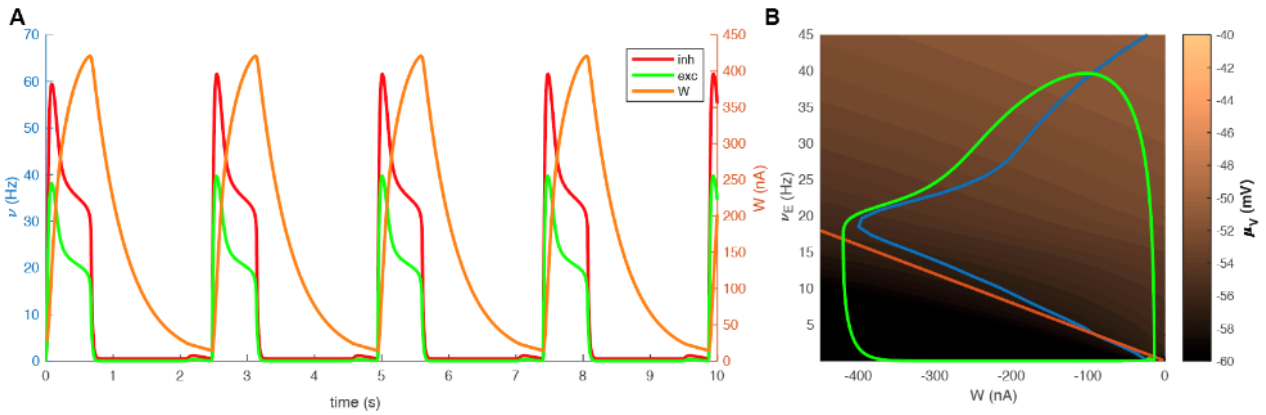

Figure 63 Mean-field model of slow Up-Down states oscillations.

A. Sample of RS-FS dynamics, respectively in green and red. In orange the adaptation dynamics is represented. B. Representation of nullclines (region where the derivative for the ODE are null) for RS population firing rate ¤E and adaptation variable W (respectively blue and red lines). The green lines represent the dynamics of the system in such plane. On the background, colorcoded, is represented the average of the membrane potential as a function of the position in this plane.

Implementation to platforms

This model will be integrated in the Collaboratory and in the Model Catalog in SP5.

Publications

Capone et al., Mean field for Slow Oscillation for COBA network of AdEx neuron. 2018. (in preparation).

References

[1] El Boustani S, Destexhe A (2009) A master equation formalism for macroscopic modeling of asynchronous irregular activity states. Neural computation 21: 46–100.

[2] Brunel, N. J Comput Neurosci (2000) 8: 183. https://doi.org/10.1023/A:1008925309027

[3] Capone C, Mattia M. (2017) Speed hysteresis and noise shaping of traveling fronts in neural fields: role of local circuitry and nonlocal connectivity. Sci Rep. 7:39611.

[4] C Capone, B Rebollo, A Muñoz, X Illa, P Del Giudice, MV Sanchez-Vives, M Mattia. (2017) Slow Waves in Cortical Slices: How Spontaneous Activity is Shaped by Laminar Structure, Cerebral Cortex, https://doi.org/10.1093/cercor/bhx326

Achieved Impact

This model can be soon extend to explore other dynamical regimes, and to describe more complicated systems as the thalamo-cortical loop, and the peculiar dynamics that it generates.

Concusion & Outlook

One of the main objective of the model is to provide a description of slow oscillatry dynamics experimentally observed in the cortex in specific conditions (such as deep sleep and anesthesia), to understand its mechanisms and wich is the effect of specific aspects on SO dynamics (e.g. COBA integration). This model is an extension of previous model developed by members of SP3 (Capone and Mattia, 2017) where the effect of COBA integrations was not considered. Also the model aims to brige microscopic scale (spiking neurons) to the macroscopic one (average population activity) that is one of the objectives of theoretical neuroscience in HBP. The model will be further developed to describe spatially extended regions of the brain and the thalamo-cortical system.

Component Dependencies

Summarized links to components this key result depends on.

Component ID	Component Name	HBP Internal	Comment
N/A	*Brunel 2000*	*No*	*Evaluate transfer function*
N/A	*El Boustani 2009*	*No*	*Master equation formalism*

2.6.4 Macroscopic model of brain function (T4.6.2)

Description of the model

This model, cosupervised by Destexhe, Jirsa, and Kherif groups, aims at obtaining a concise "top-down" description of brain activity, based on constraints from macroscopic recordings. In a second step, we will integrate a typical "bottom-up" approach, a mean-field model of cortical populations derived from spiking neurons. We will then attempt to bridge the two approaches in a common formalism to describe different brain states, normal and pathological.

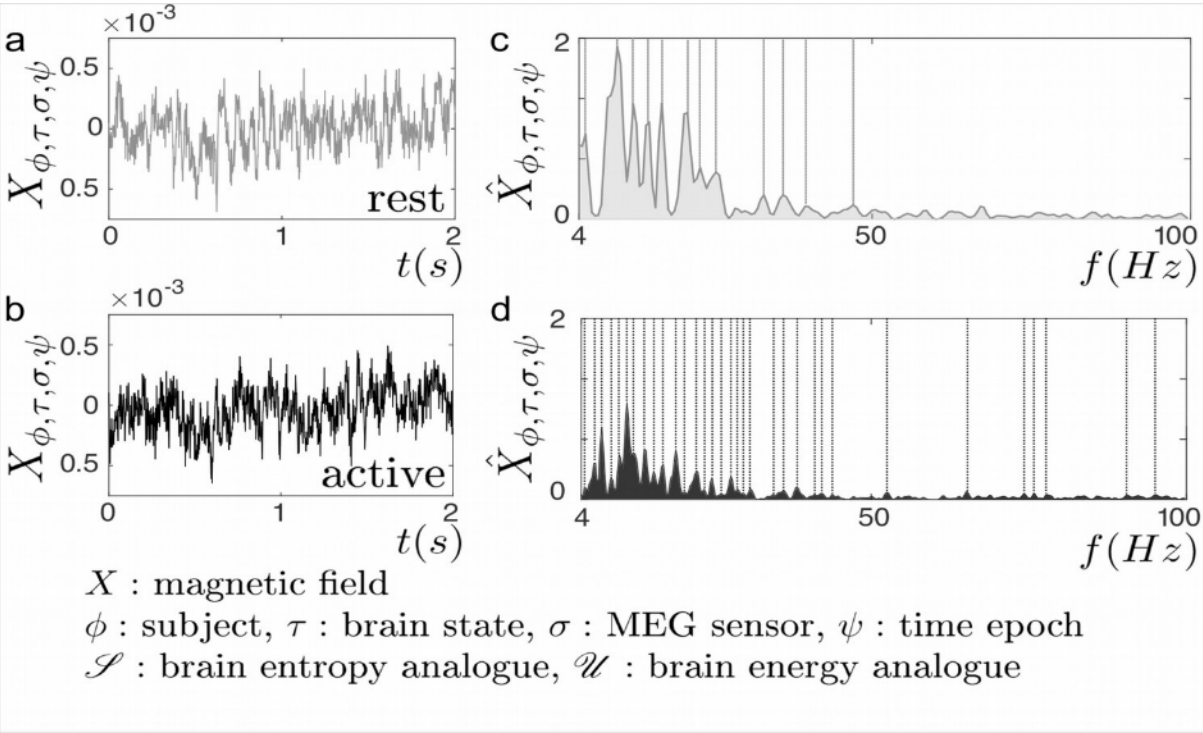

Figure 64 Different oscillatory modes of brain activity recorded from magnetoencephalography (MEG) can be used to define state variables, and particular relations between them.

Representative time courses of the magnetic field measured for each human subject, in each brain state, from each sensor, and epoch. (c-d) Corresponding power spectra of example signals shown in a-b. Dashed lines indicate local maxima at various frequencies (f) for which the corresponding energy (uf) is obtained.

Compared to resting or unconscious states, neural electromagnetic signals associated with high levels of cognitive vigilance is smaller in magnitude but higher in dimensionality. The first goal of this work was to investigate mechanisms underlying brain-state dependent changes in neural activity to achieve a formal description of macroscopic neural signals in health and disease. First, Magnetoencephalography (MEG) data from healthy human subjects in resting (Figure 64a) and active (Figure 64b) states were analysed using Welch windowing to generate power spectra (Figure 64c,d) in which resonances (local maxima) were identified.

To quantify the spectral organization of brain activity for each subject with respect to brain state, the following macroscopic variables were introduced:

$$\mathscr{U}_{\phi,\tau} \equiv \sum_{f\in\{\phi,\tau\}} u_f \quad (1)$$

$$\mathscr{S}_{\phi,\tau} \equiv -\sum_{f\in\{\phi,\tau\}} P(f)\ \ln\ P(f), \quad (2)$$

where u_f is the average power of resonances and P(*f*) is the probability of modes at each frequency generated from a vector of *f* values.

While the effective energy (eq.1) and effective entropy (eq.2) display considerable inter-subject variability (Figure 65; top right inset), examining the relationship between the macroscopic state variables, a robust linear relationship is apparent (Figure 65). To test the possibility that definitions posed in eq.1 and eq.2 could be tautological, the effective entropy was modified followed by a test of the energy and vice versa (Figure 65, bottom left inset). These experiments showed that the definitions of effective entropy and effective energy are not intrinsically related.

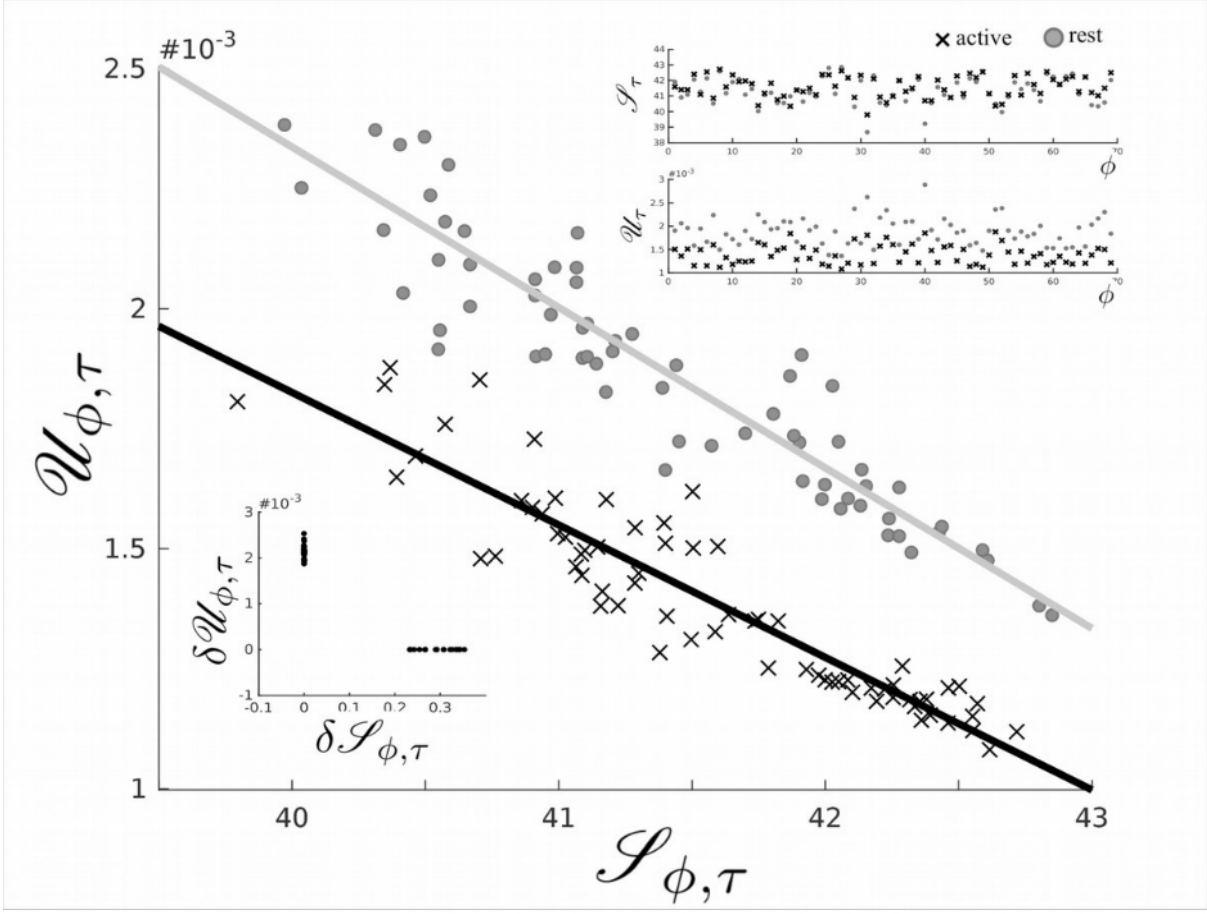

Figure 65 State variables in data from resting and active subjects.

Top right inset, considerable inter-subject variability in state variables when plotting the effective entropy and effective energy (upper and lower panels of top right inset). In the main regression, the effective entropy (x-axis) for each subject is strongly related to the effective energy (y-axis) for each subject in both resting state (grey) and active (black) recordings. A shift in both the intercept and slope of the line is observable between states. Pearson correlation, Rest; r2=0.94, p < 0.001. Active; r2=0.93, p < 0.001. The bottom left inset shows effective entropy of resonances in human data artificially modified with no resulting change in effective energy and the energy changed with no effect on entropy.

Next steps for this model are to first implement the mean field approximation describing interconnected populations of excitatory and inhibitory networks (El Boustani and Destexhe, 2009; Zerlaut et al., 2018) as nodes in The Virtual Brain (Sanz Leon et al., 2013) to generate a whole-brain simulation. This simulation will be compared to others generated by Wilson and Cowan and

Wang-Wong based mean field models for their ability to recapitulate the dynamics associated with epilepsy in collaboration with SP8. Because neural signals in epilepsy show a markedly reduced dimensionality (Babloyantz and Destexhe, 1986), the definitions proposed in the current model could account for the changes in magnitude and complexity of signals observed in epileptic patients recorded by Viktor Jirsa and colleagues. The current work will next investigate these aspects (in SGA2).

Implementation to platforms

This model will be integrated to the collaboratory and the Model Catalog in SP5.

Publications

Lina J.M., di Volo M., Capone C., Nguyn T.A., Evans A.C., Destexhe A., and Goldman J.S. Analogues of energy and entropy in the spectral structure of human brain activity. In preparation.

Goldman J.S., Evans A.C., Destexhe A.C., Lina J.M. State-dependent spectral organization of human brain resonances. In preparation.

Achieved Impact

This model has been generated based on non-invasive MEG recordings of human brain and is now continued in the analysis of data at various scales spanning single neuronal spikes to local field potentials (LFP) and electroencephalogram (EEG) from epileptic patients in collaboration with the lab of Viktor Jirsa (SP4) and Ferath Kherif (SP8).

Conclusion & Outlook

Simulations produced with The Virtual Brain will be examined using the model here described for mechanistic insight regarding the findings of this model. Mean field-models of neuronal networks incorporated in The Virtual Brain will generate scale integrated insight into the transitions from healthy brain states to epilepsy. Successful simulations will allow the prediction of patterns of activity capable of preventing or arresting seizures, to pursue therapeutic interventions based on these findings.

This study will also combine “top-down” and “bottom-up” approaches, therefore contributing to bridge these different aspects of modelling brain function present in HBP.

Component Dependencies

Summarized links to components this key result depends on.

Component ID	Component Name	HBP Internal	Comment
N/A	*The Virtual Brain (TVB)*	*Yes*	*Key aspect of brain function*

Addendum

1. Introduction

In this addendum, we detail the different outcomes of the SP4 models (see the main deliverable D4.7.2 for details about each model). We also list the implementation towards other SPs, in particular the HBP platforms.

This must be viewed as a summary of outputs from SP4 that are implementable in the IT sub-projects. The main deliverable should be consulted for more details about the models summarised here.

2. WP 4.1 Bridging Scales

2.1 T4.1.1 Simplified dendritic model

Simplified models of neurons

Possible outcomes and implementation towards other SPs

Detailed models of cortical neurons, both of rodents and presently of human pyramidal cells that we developed are key ingredient for large-scale realistic brain simulations. The models that we have built for a variety of cortical neuron types, and the methods underlying it (multiple objective optimization, morpho-electrical cell-type classification etc.) are now widely used in SP6 for developing models for other types of neurons in different brain regions (e.g. hippocampus). Our models also serve as reference for VLSI-based models under SP9. In coming months, we plan to release our new (Neron_reduce) method to analytically reduce the detailed cell models into simplified multi-polar cabe models. These models capture faithfully both passive and active (including dendritic nonlinearity) of the full models and run 200-times faster than the respective full models. They will be used in SP6, SP9 and SP3 (memory/cognitive processes) and most likely also in SP10 (neuro-robotics), as well as within SP4 (e.g., Deco, Diesmann) for investigating brain dynamics at different brain states. In particular, we envision that in SG3 phase our models of human neurons (both detailed and reduced) will serve for constructing, for the first time ever, realistic models of human cortex.

Simplified model of dendritic integration under in vivo conditions

Possible outcomes and implementation towards other SPs

The simplified models with excitable dendrites were conceived using the AdEx formalism, which is precisely the formalism implemented in the new generation of BrainScales hardware. They will therefore serve as a “first user” of this new prototype hardware. In SGA1, we have conceived the model, and studied this model numerically. In SGA2, the model will be implemented in neuromorphic hardware in SP9. We will test the computational properties of networks endowed with excitable dendrites.

Discrete model of dendritic spike propagation in dendrites

Possible outcomes and implementation towards other SPs

The two models developed in 2.1.3 and 2.1.6 are a prelude to mean-fields model of network of neurons with 2d generalised integrate and fire neurons with dendritic compartments which will be achieved in SGA2. This will help understanding how the microscopic neuron dynamics (bursting…) affect the network (global) dynamics. The discrete model of dendrite will be the basis of a new model of *ball and stick* neuron which will be embedded in a network and a mean field analysis will be performed. We plan to compare our prediction to the detailed models of SP6

when this one is released. We also plan to collaborate with SP9 to implement our model in a neuromorphic platform.

2.2 T4.1.2 Input-output transfer functions of morphologically detailed neuronal models

Information encoding in Reconstructed Human Neurons

Possible outcomes and implementation towards other SPs

A major outcome of combining SP1 and SP4, by integrating the results obtained in T4.1.2 with those of T1.2.2, 2.2.2 and 2.2.6, is the collaboration between M. Giugliano (SP4) and H. Mansvelder (SP1) and their manuscript currently submitted for publication. Active bidirectional flow of information occurred between partners: SP1's digital reconstructions of cortical human neurons were provided to Giugliano (SP4), who in return offered Mansvelder (SP1) with spiking neuronal models based on those morphologies, together with *in silico* predictions of in vitro experimental properties of those neurons.

Another outcome, demonstrating the integration of the results of other SPs, is the collaboration between M. Giugliano (SP4) and M. Migliore (SP6) and their Brain Simulation Platform, represented by a contributed online "Collab". Active bidirectional flow of information occurred between partners: SP6's Jupyter-based platform implementation details were provided to Giugliano (SP4), who in return offered an actual implementation of integrate-and-fire as well as conductance-based modelling, demonstrating interactive simulation.

2.3 T4.1.3 Mean-field and population models

Mean-field Models of GIM networks

Possible outcomes and implementation towards other SPs

We have derived mean-field and population models from point neuron models and studied the influence of network connectivity and of correlations in the noise and the network heterogeneity. The planned comparison of mean-field and spiking models was done, where the mean-field model was shown to reproduce both the level of spontaneous activity and the response of the network. The comparison of such models to the detailed models of SP6 will be done in SGA2, once the mouse cortical column model will be released (end of SGA1). In order to explore possible hardware acceleration of multi-dimensional population density techniques we have started experimenting with GPUs.

Long range dependence in Integrate and Fire models

Possible outcomes and implementation towards other SPs

This model aims at understanding deeply the nature of noise in individual neurons and the effect on the associated mean-field network. We also plan to compare the data acquired from SP3 to our statistical tests. Indeed, it will help to understand if the long-time correlation is mostly due to memory of the neuronal noise or to the time evolution of the network, that is plasticity. In addition, after validation with the data, the new non Markovian models ($\alpha \neq 0.5$) will be added in SP6. Understanding the best noise model at each scale of brain area is a big challenge.

Development of the MIIND simulator

Possible outcomes and implementation towards other SPs

ULEEDS has developed novel methods for simulating neural populations, implemented them and made the implementations available, first as Open Source, and now through installation on the HPC platform, the JURON machines. Within SP4, it has created an interface for The Virtual Brain (TVB), so that TVB now effective can run MIIND simulations on whatever platform that supports it –currently UNIX/LINUX clusters and GPGPUs- thereby opening up the possibility to instantiate simulations that combine cortical connectivity parameters with an increasingly realistic modelling of neural dynamics, which is something we will explore in SGA2. The Pallier lab has adopted the MIIND simulator, which already led to a model, which has been published as a PhD thesis (Martin Perez-Guevara, Paris Descartes) and is currently drafted as a publication. Pallier lab was part of SP3 during the ramp up phase. It is unfortunate that they are no longer with the project, but it goes to show that the time between the first contacts, where experimentalists and modellers have to learn to communicate in a common language, and the write up, can be three years. It is unfortunate that after having worked hard to establish these contacts within HBP (SP4/SP3), they now have to be continued outside. It has taken SGA to produce robust software and documentation that can be handed to novel users. We will push its use in SGA2 and SGA3.

Mean-field Models of AdEx networks

Possible outcomes and implementation towards other SPs

In SGA1, we generated a mean-field model of conductance-based spiking networks, and which is applicable to conductance-based synaptic interactions, and to networks were there are different intrinsic firing properties, modelled by the AdEx model. This mean-field model is among the most "realistic" mean-field models ever done, and is able to predict the activity of networks of spiking neurons. In SGA2, it will be integrated in the Virtual Brain, and used to study the dynamics of very large networks, up to the whole brain.

2.4 T4.1.4 Models of brain signals

Models of Voltage-Sensitive-Dye imaging (VSDi), Simplified model of local field potential (LFP) and models of local magnetic fields

Possible outcomes and implementation towards other SPs

The models of LFP and LMF developed in SGA1 will be implemented in the brain simulation platform in SP6. We will first consider models of LFPs (unitary fields and full LFP) in the hippocampus using the detailed hippocampal model developed in SP6. We will compare the simulations with data from, hippocampal slices. We will next simulate LFPs in the mouse cortical column developed in SP6. Here, the results will be compared to multi-electrode array recordings where we could relate LFP with single unit activity (Telenczuk *et al.*, Sci Reports 2017). This work will be done in SGA2.

Similarly, we will use the models of local magnetic fields (LMF) developed in SGA1 (Barbieri *et al.*, Sci Reports 2016). We will calculate the LMF of hippocampal slices, using the SP6 model. This model will guide further experiments on measuring magnetic fields from hippocampal slices. Magnetic fields will also be calculated from the cortical column of SP6. Such simulations will serve as the basis of a detailed model of cortical magnetic signals. This work will be done in SGA2.

Finally, a model of VSD signals was developed in SGA1 and was compared to VSD recordings in monkey V1 (Zerlaut *et al.*, J Computational Neurosci. 2018). In SGA2, this model will be compared to the detailed VSD model developed in SP6. In particular, we will consider the case of propagating waves of activity as recorded in V1 of the awake monkey.

Improved LFP model with quasi-active conductances

Possible outcomes and implementation towards other SPs

Our work in this component concerned the effect of active conductances on the Local Field Potential (LFP). The work resulted in two publications, and for both of these projects we have implemented interactive examples in Jupyter Notebook on the Collaboratory that allows HBP members to use our models to recreate our main results. This allows for easy adoption of our models by HBP members, since these examples demonstrate how to implement and use our models on the Collaboratory.

The results and models from this component are highly relevant for the HBP, and especially for SP6 which are performing large-scale brain simulations with calculation of LFPs. For example, based on the cortical microcircuit model that was developed by the Blue Brain Project, and is currently further developed by the HBP, the role of active conductances on the LFP was estimated (Reimann *et al.*, 2013, Neuron 79). We expect that our results and models will help guide future extensions of this work. Our results also indicate that active conductances might have important effects on electroencephalography (EEG) and magnetoencephalography (MEG) signals recorded non-invasively from humans. To look for the signature of active conductances here, our framework could be used in combination with the large brain simulations from SP6, with concurrent calculation of LFP, EEG and MEG signals.

Collabs which demonstrate our models and results:

https://collab.humanbrainproject.eu/#/collab/5170/nav/40008

https://collab.humanbrainproject.eu/#/collab/8555/nav/64785

Simplified EEG models

To connect large-scale brain simulations to experimental data is vitally important for the HBP, and in this component we have developed a framework which greatly simplifies the process of calculating electroencephalography (EEG) signals from simulated neural activity. This component is relevant for the HBP since it can help tie large-scale brain simulations from SP6 to experiments. For biophysically detailed simulations implemented in the NEURON simulator, the implementation of our framework for EEG calculation should be straightforward.

Our framework also offers the possibility of obtaining EEG proxies from point-neuron simulations, analog to what has been done for LFP signals in the component “SGA1-T6.3.6 - Tool for LFP recording in NEST simulations”, where we contributed. An example of this can be seen in the "NEST Instrumentation App" (SGA1-T6.3.6) at the Collaboratory, where LFP predictions can be made directly from the large-scale Potjans-Diesmann model implemented in NEST.

3. WP 4.2 Generic models of brain circuits

3.1 T4.2.1 Simplified network models of different cortical areas

Simplified network models of different cortical areas

Possible outcomes and implementation towards other SPs

In this task, the JUELICH partner is developing two models of cortical circuits using leaky integrate-and-fire (LIF) neurons: a model of a 1 mm2 cortical microcircuit with the full density of neurons and synapses (Potjans and Diesmann, 2014), and a model of all vision-related areas of one hemisphere of macaque cortex where each of 32 areas is represented by 1 mm2 (Schmidt *et al.*,

2018; Schmidt *et al.*, accepted). The former model has about 80,000 neurons connected via 300 million synapses; the latter has about 4 million neurons connected via 24 billion synapses. In SGA1, we have finished and described the porting of the microcircuit model to the Collaboratory (Senk *et al.*, 2017), SpiNNaker (van Albada *et al.*, 2018), and Open Source Brain (Gleeson *et al.*, 2018). The porting to SpiNNaker was done in collaboration with SP7 and SP9. The microcircuit model has further served as a test case for the tools and workflows available via the Collaboratory, thus establishing a link to SP5. The implementation of the model in a Collab and the workflow including the use of high-performance computing resources, statistical analysis with Elephant (SP5) and visualization were described by Senk *et al.* (2017). The multi-area model of macaque cortex is currently the only neuroscientific model in NEST requiring supercomputing resources, and is thereby essential as a use case for SP7. The complete code for the model and its analysis and visualization has now been published at https://github.com/INM-6/multi-area-model. This model can serve as a new test case for SpiNNaker in SP9.

3.2 T4.2.2 Network models including neuron-glia interactions

Model for neuron-glia interactions and dimensionality reduction

Possible outcomes and implementation towards other SPs

T4.2.2. will develop new collaboration with SP1 (Javier DeFelipe) on astrocyte morphology and connectivity in the cerebral cortex. The existing data on neuron and astrocyte morphologies will be analysed in terms of the number of astrocytes reaching closeby synapses and, on the other hand, the number of synapses covered by astrocytes. This data will be used to develop the network model with glial influences in the SGA2. Another collaboration is set up jointly with SP4/Markus Diesmann and SP9/Steve Furber to make an extension of Potjans-Diesmann model with glia influence. The model will be implemented first using the Nest simulator and several hypotheses on glial contributions, including the hypothesis on network synchronization, will be tested. Implementation on Nest promotes further implementation on neuromorphic hardware, specifically on the SpiNNaker.

4. WP 4.3 Learning and memory

4.1 T4.3.1 Plasticity algorithms

STDP for structural Plasticity (WP4.3)

Possible outcomes and implementation towards other SPs

The model has been implemented in NEST and has already been transferred to the simulation SP (NEST - the neural simulation tool, component 209, linked to SP6). The model is also formulated in a way that would make an implementation in neuromorphic hardware possible. A possible transfer has been discussed at a CDP5 meeting.

4.2 T4.3.2 Learning in networks of neurons

Somato-dendritic prediction error learning under imperfect conditions

Component Dependencies

Summarized links to components this Key Result depends on.

Component ID	Component Name	HBP Internal	Comment
1032	Plasticity: Dendritic predictive plasticity that reproduces STDP data (Algo STDP predictive)	Yes	This component built the basis for the model considered here
2419	Plasticity - Algorithms for multicompartment models	Yes	This component delivered input for the stabilisation of dendritic learning under imperfect conditions
468	Principles for brain-like computation (model)	Yes	This component can profit from the described research (via CDP5)
2551	Methods for deep learning that can be implemented in neuromorphic hardware	Yes	This component will also integrate the current findings.

Natural gradient learning for spiking neurons, sequence leaning by shaping hidden activity and Error-backpropagation across cortical areas

Possible outcomes and implementation towards other SPs

To ensure the transfer of the research in WP4.3 (Learning and plasticity) to the simulation Platforms (mainly SP9 - Neuromorphic Computing, but also SP10 - Neurorobotics), most of the UBern HBP research funded via SP4 takes place in the collaborative framework of CDP5. In fact, Mihai Petrovici, theory group leader at UHeidelberg, principal investigator in SP9 for SGA2 and CDP5 leader from SGA2 onwards, joined the research team at UBern in the course of SGA1. Based on this collaboration, many research questions at UBern on have been adopted to be integrated in the Neuromorphic Computing Platform of SP9. Sections 2.3.3/4/5 of the D4.7.2 highlight some of this collaborative research that is described in the CDP M24 Deliverables. Publications are in preparation. A recent collaborative work, initiated by UHeidelberg, is "Spiking neurons with short-term synaptic plasticity form superior generative networks" by luziwei leng, Roman Martel, Oliver Breitwieser, Ilja Bytschok, Walter Senn, Johannes Schemmel, Karlheinz Meier, and Mihai Petrovici, accepted in Scientific Reports, 2018.

Synaptic correlated of working memory and its capacity and Phenomenological model of information recall from long-term memory

Possible outcomes and implementation towards other SPs

In terms of integration of my results by other SPs, I could propose two possibilities. First, my model of working memory is based on neural network simulations with either rate neurons or point integrate and fire neurons with short-term synaptic plasticity in connections between pyramidal neurons. This mechanism fits organically into SP6 much more realistic simulations where network plasticity is a major focus (in particular, the project of Giuseppe Chindemi). I will discuss with him the possibility to implement my working memory model on his platform.

Second, my model of memory recall seems to be quite relevant for the SP3.3 project on episodic memory. In particular, my model is based on the assumption that recall of memory items from a

presented list is controlled by overlaps between distributed memory representations. This provides direct predictions that could be tested by imaging of neuronal activity upon presentation of the items, either using high-resolution fMRI or PET-fMRI as performed by SP3.3. I will establish the collaboration with SP3.3 in order to experimentally test the predictions from my model, by imaging the brain of human subjects performing recall experiments.

Balancing new against old information: the role of puzzlement surprise in learning

Possible outcomes and implementation towards other SPs

The model is potentially relevant for a collaboration with the cognitive neuroscience subproject SP3 as well as for neurorobotics SP10. A collaboration with Michael Herzog has been initiated and will continue in SGA2.

4.3 T4.3.3 Functional plasticity for multi-compartment neurons

Learning rules that can be implemented on the neuromorphic platforms and evolving the SpiNNaker neuromorphic platform to support Three-Factor learning rules

Possible outcomes and implementation towards other SPs

Activities of T433 have were only briefly reported in the SP4 part of the deliverable, because of their better thematic fit under CDP5, where they have been reported in a detailed way in Section 2.3.5.

In particular, we like to highlight the following outcomes/integration of results T433 wrt SP9: The supervised INST/FILT rule we developed utilises gradient descent on the likelihood of target spike frames and has only modest requirements for neuromorphic hardware compared to more biologically faithful approaches. More specifically, this rule only requires access to standard STDP traces, which, as of HICANN-DLS v2, are the only analogue hardware quantities that are accessible to the local plasticity processing unit (PPU). The implementation work on the HICANN-DLS v2 prototype has begun in SGA1 and will be carried over to SGA2 68) in a collaboration with U Heidelberg (WP9.2).

During SGA1, it became apparent that a more systematic approach to implementation of learning rules on neuromorphic platforms was needed, and we therefore set up a cross-SP4-SP9 working group within CDP5 to facilitate the extension of the SpiNNaker API and underlying code infrastructure such that various custom third-factor plasticity rules can easily be implemented by third parties on SpiNNaker. Within this work group we prioritised existing plasticity rules with respect to their estimated implementation complexity within SpiNNaker, and are using in this sense simpler rules as stepping stones to progress to more complex rules. These rules are:

- the Brader-Fusi-Senn Rule (Brader *et al.*, Neural Computation 2007),
- the Urbanczik-Senn Rule, in progress (see KR1.1-1.3).
- the INST/FILT rule, planned for SGA2

The Brader-Fusi-Senn Rule has been integrated into the SpiNNaker platform, currently in “Fusi_plasticity” branch of the official SpiNNaker software repository, and as such is available within and outside the HBP. Eventually this branch will be merged into “master” branch in WP9.3

5. WP 4.4 Models of cognitive processes

5.1 T4.4.1Models of spontaneous activity

Topological similarity to estimate functional connectivity

Possible outcomes and implementation towards other SPs

The present model was developed to provide an answer to a theoretical question, as a proof of concept. In principle, the model was not intended to serve as a comprehensive simulation of the brain activity. However, due to its computational efficiency, it can serve as a first proxy of expected functional connectivity from tractography data. In this sense, the model could easily be integrated within the workflows of tractography data retrieval from the Human Brain Atlas (SP5), to allow users for a quick estimation of functional connectivities. The model can be used either with human, mouse or macaque structural connectivities. Also, the model could be used to infer the impact of structural damage (e.g. stroke lesions) on the expected recurrent network flows. In this sense, it could serve as a first indicator in lesion research as performed in SP1 and SP3.

Macroscopic model of spontaneous human brain activity

Possible outcomes and implementation towards other SPs

The model captures realistic whole brain resting-state dynamics and contains both a global coupling parameter and a tunable parameter representing the working point of each brain region. The model is thus useful to characterise and investigate brain dynamics at different brain states (awake/sleep, anaesthesia, conscious/unconscious) which is an intense line of research of SP3, in relation with medical applications for SP8. Also, a runnable version of the model could be implemented in the HBP Platforms (probably via the Collab, involving SP6 maybe) that would allow external users to explore the behaviour of the model. Furthermore, if properly linked to the Human Brain Atlas, external users could choose structural and resting-state fMRI BOLD signals from the catalogue in the atlas and run the model after fitting the global and local parameters according to the dataset chosen.

Model of spontaneous activity in awake mouse primary auditory cortex based on large scale Ca2+ imaging data

Possible outcomes and implementation towards other SPs

Spiking network models of spontaneous activity were developed in SGA1, for different network states, from Up/Down state activity seen during sleep and anaesthesia, to asynchronous states typical of the awake brain (Zerlaut and Destexhe, Neuron 2017). These models were developed using data from HBP, and they were written in a formalism compatible with neuromorphic hardware (SP9). In SGA2, we plan to study the responsiveness and computational properties of such models, and this work will be done conjointly with hardware implementations in SP9. We also plan to use these models to study how “normal” network states develop into pathological states, such as epilepsy. Possible links with SP8 will be developed.

5.2 T4.4.2 Models of low-level vision

Model of retinal processing

Possible outcomes and implementation towards other SPs

The model described here can be used as a realistic input for any modelling of the thalamus or visual cortex. This is relevant for other tasks of SP4 like the 4.4.1 where thalamus models are considered. For other SPs, it is relevant for SP10 where visuomotor tasks will be explored. We have contacted several people in SP10 who are interested in using such a model. In particular, in the case of motion tracking, the model may give predictions that are quite different from a naïve linear model of the retina. Future work will be aimed at designing a version of our model that can be implemented in the framework used by SP10.

Model for high-level contributions to low level vision

Possible outcomes and implementation towards other SPs

A functional model showing the benefits of the contribution of high-level visual areas to lower level areas, with applications to Neurorobotics in SP10 for *in silico* models of behaviour, cognition and motor control, has been published. It shows that the combined bottom-up top-down model detects critical image features that are not detected by the purely feed-forward model, and performs successfully the task of producing full interpretation, by identifying all the internal parts within minimal images.

5.3 T4.4.3 Models of motor control

Basal Ganglia systems level model

Possible outcomes and implementation towards other SPs

KTH (Task 4.4.3): The basal ganglia system level model in Lindahl *et al.* [1] below is planned to be used as a framework for building hybrid basal ganglia models together with SP6, consisting of point neuron models modules linked with detailed microcircuit model modules of the striatum (the latter microcircuit model is being built in SP6 currently). Also through the use of this systems level model we have generated hypotheses regarding how oscillatory components (as seen in various basal ganglia disturbances) can spread throughout the basal ganglia system. These hypotheses will be verified in detailed models in SP6 during SGA2. Finally, we also have planned to link our SP4 system level model to a spinal cord neurorobotics model in SP10, also during SGA2.

5.4 T4.4.4 Models of spatial navigation

Modelling spatial navigation and memory

Possible outcomes and implementation towards other SPs

Our consideration of how environmental and self-motion information combine to drive grid cell firing patterns (Evans & Burgess, in prep; see Collaboratory) has been subject to a first test in experiments that we helped to design, in collaboration with SP3 Episense (Cacucci lab). This experiment has been submitted for publication, and a paper on the apparatus we designed to investigate this issue has been accepted for publication (Chen *et al.* 2018, eLife 7:e34789).

Furthermore, Evans and Bicanski are drafting a review article on the notion of simultaneous localization and mapping (SLAM) and how it relates to spatial cell firing as reported in rodent

electrophysiology experiments. The article will involve substantial interactions with SP3 Episense (Pearson lab, see below) and their expertise in SLAM.

Work on the comprehensive model of spatial and episodic memory (Bicanski and Burgess, in 2nd revision at eLife) connects our theoretical work to both experimental and robotic pillars of the HBP. First, it has led to fruitful exchange with SP3 Episense (Duzel lab), and has helped to design an experiment on human hippocampal pattern completion, see Grande *et al.* (2017). Second, at the same time Bicanski has provided documention for the model of spatial and episodic memory to SP3 Episense (Pearson lab), with a special focus on relating SLAM (a classical problem in robotics) to spatial cell firing in the hippocampal formation. This documentation was primarily intented outline possible parallels between the spatial and episodic memory model and SLAM systems employed in robotics. It also serves as a basis for the upcoming review article with Evans (see above). Third, in addition, code for the model of spatial and episodic memory was shared with SP3 Episense (Pearson lab). The codebase can serve as a basis for an implementation of egocentric to allocentric transformations of sensory inputs on a robot, paving the way for a possible implementation of the complete spatial and episodic memory model on a mobile robotic platform.

Chen G, King JA, Lu Y, Cacucci F, Burgess N. Spatial cell firing during virtual navigation of open arenas by head-restrained mice. eLife. 2018 Jun 18;7:e34789.

Grande X, Bisby JA, Berron D, Horner AJ, Duzel E, Burgess N (2017) Hippocampal Subfield Contributions to the Recollection of Multi-Element Events: Functional Evidence at 7 Tesla. Society for Neuroscience Abstract 167.04 / SS19

5.5 T4.4.5 Development of a large-scale, mean field model on sensorimotor integration

Large-scale model of visuo-motor integration

Possible outcomes and implementation towards other SPs

The model is an integral part of CDP4, which is born with the aim of integrating the models into virtual experiments run at the Neurorobotics Platform, SP10.

6. WP 4.5 Linking model activity and function to experimental data

6.1 T4.5.1 Comparing models with mouse and human brains

Comparison of experimental and simulated neural activity data

Possible outcomes and implementation towards other SPs

Component 418: 'Massively Parallel Electrophysiology data' uses tools developed in SP5 (Elephant, T5.7.1) and SP9 (Model simplification and validation, T9.1.5) and provides a statistical model to SP6 (Validation Framework, T6.4.4 [SGA1]). The results of component 418 are made available in the HBP Collaboratory using tools from SP7 (NEST, T7.5.5, and UNICORE, T7.5.6).

Component 1864: 'SP4 -SGA2 - Integrative Loop for Comparison of Experimental and Simulated Data using the Validation Framework (software)' uses tools developed in SP5 (Elephant, T5.7.1), SP9 (Model simplification and validation, T9.1.5) and SP6 (Validation Framework, T6.4.4 [SGA1])

to validate a model that is co-developed with T4.2.1. The experimental data are to be implemented in the Neural Activity Resource (SP5, T5.7.2). The results of component 1864 are made available in the HBP Collaboratory using tools from SP7 (NEST, T7.5.5, and UNICORE, T7.5.6).

Component 812: 'Workflow for comparison of electrophysiological and simulated data (service)' applies an example workflow using tools for quantitative comparison of neural network statistics in SP5 (Elephant, T5.7.1), SP9 (Model simplification and validation, T9.1.5) and SP6 (Validation Framework, T6.4.4 [SGA1]) to validate a model that is co-developed with T4.2.1. The workflow is made available in the HBP Collaboratory using tools from SP7 (NEST, T7.5.5, and UNICORE, T7.5.6).

6.2 T4.5.2 Mouse brain function from structure

Models of mouse brain function from (T4.5.1 & T4.5.2)

Possible outcomes and implementation towards other SPs

This model was integrated to the Neuroinformatics Platform through the model catalog with two separate models: “Mouse stroke Brain network model” and “The Virtual Mouse Brain". Both are linked towards the scripts in TVB for The Virtual Mouse Brain based on the Allen Connectome, which allow modelling brain resting state activity of the mouse, as well as stroke (work in progress, hence it is a private model). The model is done in a close collaboration with SP1 as part of CDP1. SP1 provides the empirical stroke data that is used for comparison and they are also responsible for the alignment of the experimental data with the Allen atlas. This cooperation will be continued in SGA2. For the future, the model is planned to be continued towards other platforms such as NEST, as well as towards the other platforms through the future integration of TVB in CDP8.